UNLV Theses, Dissertations, Professional Papers, and Capstones

5-1-2019

Early Contractional History of the Funeral Mountains and its Influence on the Formation of the Funeral Mountains Metamorphic Core Complex, Death Valley, CA

Taylor Douglas Craig
tcraig1992@gmail.com

Follow this and additional works at: https://digitalscholarship.unlv.edu/thesesdissertations

Part of the Geology Commons

EARLY CONTRACTIONAL HISTORY OF THE FUNERAL MOUNTAINS AND ITS

INFLUENCE ON THE FORMATION OF THE FUNERAL MOUNTAINS

METAMORPHIC CORE COMPLEX, DEATH VALLEY, CA

By

Taylor Douglas Craig

Bachelor of Science in Geology
Appalachian State University
2015

A thesis submitted in partial fulfillment
of the requirements for the

Master of Science - Geoscience

Department of Geoscience
College of Sciences
The Graduate College

University of Nevada, Las Vegas
May 2019

Thesis Approval

The Graduate College
The University of Nevada, Las Vegas

January 29, 2019

This thesis prepared by

Taylor Douglas Craig

entitled

Early Contractional History of the Funeral Mountains and Its Influence on the Formation of the Funeral Mountains Metamorphic Core Complex, Death Valley, CA

is approved in partial fulfillment of the requirements for the degree of

Master of Science - Geoscience
Department of Geoscience

Michael Wells, Ph.D.
Examination Committee Chair

Thomas Hoisch, Ph.D.
Examination Committee Member

Pamela Burnley, Ph.D.
Examination Committee Member

Dennis Bazylinski, Ph.D.
Graduate College Faculty Representative

Kathryn Hausbeck Korgan, Ph.D.
Graduate College Dean

ABSTRACT

Early contractional history of the Funeral Mountains and its influence on the formation of the Funeral Mountains Metamorphic core complex, Death Valley, CA

by

Taylor D. Craig

Dr. Michael L. Wells, Examination Committee Chair
Professor of Geoscience
University of Nevada, Las Vegas

Zones of localized crustal thickening in orogenic belts commonly host low-angle normal faults, which have been controversial since their recognition. The metamorphic core complexes of the Sevier hinterland are localized within a belt that is attributed with the highest degrees of crustal thickening during Sevier orogenesis. This association of deep-rooted detachment faulting and early contractional deformation indicates an important link between the two processes, however repeated tectonic episodes often overprint and obscure the earlier fabrics, making this link difficult to study. The Funeral Mountains metamorphic core complex, located in Death Valley, CA, has a complex history of protracted SE-contraction and tectonic burial of Late Jurassic age that has since been overprinting by two periods of NW-directed detachment faulting during Late Cretaceous and Miocene time. Exposure of a Barrovian-style metamorphic field gradient and a thick stratigraphic section with large rheologic contrasts has provided a unique opportunity to investigate the apparent genetic link between contractional structures and the development of low-angle normal faults. Detailed mapping at 1:10000 scale has revealed evidence of four separate fabric forming events. Evidence for early burial was found within the Kingston Peak diamictite, which contains a well-developed bedding-parallel foliation with asymmetric strained clasts with SE-vergence. This early foliation was subsequently folded during a second period of

contraction of Early Cretaceous(?) age. This event produced NNE-SSW mesoscopic to map-scale folds with SE-vergence. A new U-Pb zircon age of 95.63 ± 0.95 Ma, from a peraluminous granite intrusion that preserves no contractional fabrics, may provide lower constraints on the age of contraction. Two periods of top-NW shear overprint the earlier top-SE fabrics during the Late Cretaceous and Miocene, which produced two intracore shear zones, the Monarch Canyon shear zone and the Eastern shear zone, and the primary dome forming fault, the Boundary Canyon Detachment fault. The contractional fabrics are subparallel with extensional structures of opposite kinematics, indicating deformation generated by structures of similar orientations. These observations, in conjunction with the absence of an enigmatic thrust fault responsible for the deep burial of the Funeral Mountains, has led us to hypothesize that tectonic reactivation of a Late Jurassic thrust fault was the primary mechanism behind detachment faulting within this complex.

ACKNOWLEDGMENTS

To say that the road to completing this thesis was a character-building experience would be quite the understatement, however saying that it was not one of the best experiences of my life thus far would be a total lie. There are many people I need to thank for making this experience happen, but none come close to the thanks I owe my advisor, Dr. Michael Wells. From the moment I emailed Michael with interest in pursuing a master's degree under his advisement, he was nothing but kind and enthusiastic. His willingness to entrust this project, and his constant support throughout this whole process has made this entire experience an enjoyable. Michael has been so much more than an advisor, he has been a mentor, and above all else a friend. I look forward to keeping in touch with him for the rest of my life.

I also would like to thank my committee members, Dr. Thomas Hoisch, Dr. Pamela Burnley, and Dr. Dennis Bazylinski, for their support and feedback throughout my graduate career. I would like to thank the UNLV Geoscience office staff, Cinch Irwin, Maria Roja, Liz Smith, and the many student workers who have worked during my time here. I also want to thank John the Janitor. John would always pop his head in my office when I was working late to check up on me or stop me in the hallway during beers on the balcony (B.O.B.) to ask about what the seminar was about this week. John would always put a smile on my face and renew my motivation to keep working hard. On that note I would also like to thank B.O.B., I think for reasons that are clear.

I want to thank those who acted as field assistants to me during my field seasons. Lee Hess, you came out with me on my first outing and gave me valuable advice that stuck with me and helped me get through my hardest days in the field. Stewart Williams, you spent a solid two weeks in the field with me and never once complained, not even during those grueling overnight

trips and through all the strenuous climbs. Kevin Rafferty, you came out with me towards the end of my field work, but your constant excitement for all the incredible geology gave me new insight and renewed my drive to get this project done.

I want to thank all the friends that I made in the Geoscience Department. The long nights and stressful assignments were always balanced by the great times spent hanging out, hiking, climbing, and yes, also occasionally going to Oddfellows. I have formed lifelong relationships with many people, and I cannot wait to see where all our lives take us.

Lastly, I would like to thank my incredible family. Moving across the country was by no means an easy process, but my family has provided constant support for me throughout all my ups and downs out here. Whenever I began doubting myself, they were always there to tell me I could do it and that I would do an amazing job. I consider myself blessed to have the family that I have, and I could not have done any of this without their constant support.

TABLE OF CONTENTS

LIST OF FIGURES

INTRODUCTION

Metamorphic core complexes (mccs) are relics of large magnitude extension that, through substantial exhumation, provide a window into the processes occurring within the middle crust; these rocks largely preserve a record of the extensional processes that strongly overprint earlier contractional fabrics. In the Western U.S., a N-S trending string of Cordilleran mccs occur within the hinterland of the Sevier fold-and-thrust-belt, with a second population within Mesozoic contractile belts (i.e., Maria Tectonic Belt) of California, Arizona, and Mexico (Figure 1; Armstrong, 1982; Coney and Harms, 1984). The importance of prior crustal thickening in regions where mccs have developed has been recognized (e.g. Armstrong, 1982; Coney and Harms, 1984; Spencer and Reynolds, 1990), but more detailed studies on the role of previous contractional deformation in the localization, resulting geometry, and development of extensional systems are few. This is in large part due to the tendency for repeated episodes of deformation, through reactivation, to obscure and overprint earlier fabrics, thus making it difficult to recognize structures from the earliest deformational history in a region. In some instances, however, the earliest fabrics can be preserved in the up-dip portions of detachment fault footwalls if there is a strain gradient in the shear direction and/or if detachment faulting exhumes a large metamorphic field gradient. Exposure of metamorphic field gradients can provide an opportunity to observe the earlier fabrics as regions of lower metamorphic grades often experience the least amount of overprinting. The Funeral Mountains metamorphic core complex (FMCC), located in Death Valley, CA, have a complex history of NW-directed extension that is predated by a large-magnitude tectonic burial event for which the fabrics are highly overprinted (Figure 2; Hoisch and Simpson, 1993; Applegate and Hodges, 1995).

Exposed within the FMCC is a large metamorphic field gradient that increases in grade to the NW and reaches maximum metamorphic grade in the Monarch Canyon region. Petrologic analyses to determine peak metamorphic conditions prior to exhumation have found an increase of metamorphic grade from lower greenschist to upper amphibolite facies, from SE to NW through the FMCC (Labotka, 1980; Hoisch and Simpson 1993). Monarch Canyon, which is the northwesternmost extent of the FMCC, reached peak conditions of $700°$ C at a depth of ~32 km (Labotka, 1980; Hoisch and Simpson, 1993; Applegate and Hodges, 1995; Mattinson et al., 2007). Seventeen km southeast of Monarch Canyon at Indian Pass, peak conditions reached a temperature of $490°$ C at a depth of ~19 km (Hoisch and Simpson, 1993; Hoisch et al., 2014). Eleven kilometers further south, in Echo Canyon, chlorite-bearing slates and phyllites are of lower greenschist facies metamorphic grade (Hoisch and Simpson, 1993). Exhumation of the FMCC was accomplished by two periods of extension, one during the Late Cretaceous and the second during the Miocene due to slip along the Boundary Canyon detachment fault (BCD); both events are characterized by NW-vergent kinematics (e.g., Holm and Dokka, 1991; Applegate et al., 1992; Hoisch and Simpson, 1993; Beyene, 2011). Another exhumation event, of early Cretaceous age, was also documented by Hoisch et al. (2014) using garnet growth P-T modeling and $^{40}Ar/^{39}Ar$ thermochronology. Extension and exhumation of FMCC has been well documented, but investigation of earlier burial fabrics in this region is lacking, although large scale burial has been proposed in several studies (i.e. Applegate and Hodges, 1995; Hoisch et al., 2014) A need for burial is primarily based on the observation that peak metamorphic conditions requires a large amount of overburden, which cannot be explained by the ~13 km of stratigraphic burial alone, requiring an earlier tectonic burial event to accommodate this load.

The metamorphic grade and degree of development of top-NW fabrics decrease SE of Monarch Canyon. In the Chloride Cliff region, a large section of the regional stratigraphy is exposed with significant variation in lithologies and associated rheologies. Due to the lower metamorphic grade and the contrasting rheologies of the stratigraphy, much of the extensional strain has been localized within the weaker lithologies and along regional shear zones, preserving the earliest contractional fabrics associated with burial of the FMCC between these shear zones.

This study is focused on the structural and kinematic analysis of fabrics that developed associated with the contractional and burial history of the FMCC in the Chloride Cliff region. Additionally, we present new geochronologic and thermochronologic data to aid in better understanding the evolution of the FMCC. Field work conducted within the Chloride Cliff region has revealed evidence for two periods of SE-vergent deformation prior to the overprinting by NW-vergent extensional deformation. Orientations of stretching lineations and fold hinges of the SE-vergent fabrics show similar to subparallel orientations with structures associated with NW-vergent fabrics. This similarity in orientation provides evidence that supports inheritance from the kinematics and geometry of the contractional history during subsequent extension of the region. The timing of this early contraction has been constrained by a prograde Lu-Hf garnet growth age of 158.2 ± 2.6 Ma from the lower Johnnie Formation schist and post-metamorphic muscovite $^{40}Ar/^{39}Ar$ cooling ages of 146-152 Ma, nearby in Indian Pass, providing the first definitive evidence for tectonic burial during the Late Jurassic (Hoisch et al., 2014). One problem that remains is the recognition of a structure or structures of this age that could be responsible for this burial magnitude. It has been previously hypothesized that the thrust responsible for burial of the FMCC strata was cut out by detachment faulting and transported to the NW (Applegate and Hodges, 1995), however no thrusts with sufficiently large throw have been mapped within this

region of Late Jurassic age, including within the hanging wall of the BCD to the NW (Neimi, 2002). Due to the apparently missing thrust, and the marked similarity in transport azimuths (ca. 180° from apart) between NW and SE-vergent fabrics, we hypothesize that the BCD is the current expression of a Late Jurassic thrust that was reactivated during the Late Cretaceous and the Miocene, leading to the exhumation of the FMCC (Figure 3).

GEOLOGIC SETTING OF THE FUNERAL MOUNTAINS

Death Valley Fold-Thrust Belt

Contractional deformation during the Permian to Triassic led to the formation of the Death Valley fold-thrust belt (Snow, 1992). The structures associated with this event exposed in the Cottonwood Mountains include the Lemoigne thrust, Marble Canyon thrust, White Top backfold, Racetrack duplex zone, and the Last Chance thrust, going from structurally lowest to structurally highest (Snow and Wernicke, 1989; Snow, 1992). These structures generally trend north-northeast and are interpreted to record east-southeast vergence associated with the deformation (Snow and Wernicke, 1989). The offset of these structures by the Neogene to present day, right-lateral Furnace Creek and northern Death Valley Fault Zones, is the basis for several attempts to reconstruct Cenozoic to present day extensional and transtensional deformation (Snow and Wernicke, 2000; Renik and Christie-Blick, 2013).

Correlations of Death Valley Fold-Thrust Belt structures

The southern Funeral Mountains have several structures that have been correlated to structures in the Cottonwood Mountains, namely the Lees Camp anticline (Winters Peak anticline), and the Schwaub Peak thrust (Snow and Wernicke, 1989, 2000; Renik and Christie-Blick, 2013). The White Top Mountain backfold, a west-vergent anticline and the east-vergent Marble Canyon thrust in the Cottonwood Mountains were originally correlated with the Winters Peak anticline and Schwaub Peak thrust by Snow and Wernicke (1989, 2000), based on their having similar geometries, overall vergence, and similar offsets. These correlations, along with correlations of several other structures found in neighboring ranges, led to the interpretation of approximately 68

5

± 4 km of Tertiary offset between the Funeral Mountains and Cottonwood Mountains (Snow and Wernicke, 1989).

The west-vergence of the Winters Peak anticline noted in the Snow and Wernicke (1989) study has been questioned by Czajkowski (2002) and disagrees with mapping of Wright and Troxel (1993), which both note a SE-vergence to the structure (Renik and Christie-Blick, 2013). Czajkowski (2002) has also argued for a Cretaceous age of the Winters Peak/Lees Camp anticline, which would be overall inconsistent with the inferred age of the White Top Mountain backfold (Renik and Christie-Blick, 2013). This has led to correlations of the Schwaub Peak thrust with the Panamint Thrust located in Tucki Mountain and of the Marble Canyon thrust with the Grapevine thrust in the Grapevine Mountains (Czajkowski, 2002; Renik and Christie-Blick, 2013). East of the Marble Canyon thrust is the Dry Bone syncline, which Renik and Christie-Blick (2013) have correlated with a broad syncline in the Indian Pass region of the northern-central Funeral Mountains. These correlations, along with correlations from around the Death Valley region and to the southeast in the Resting Spring-Nopah Ranges, have led to the interpretation of approximately 68 ± 14 km of dextral strike-slip offset between the Cottonwood Mountains and the Resting Spring-Nopah Ranges during the Neogene (Renik and Christie-Blick, 2013).

East Sierran Thrust System

Adjacent to and partially contained within the Death Valley region is deformation associated with the Early Jurassic to Early Cretaceous East Sierran thrust system (ESTS). Present along a ~150 km long ~N-S trend, from the Cronese Hills and Lane Mountain to the south and to the southern Inyo Mountains to the north, are a system of contractional faults and folds, and associated mylonitic to cataclastic fault rocks, associated with the East Sierra Thrust system. These faults are believed to have been active as early as 190 Ma and persisted until 148 Ma

6

(Walker et al., 1990; Dunne and Walker, 1993; Coleman et al., 2003; Dunne and Walker, 2004). The system is composed of a series of thrust faults that have a general NW strike, and hanging-wall motion is NE-vergent (Coleman et al., 2003). Folding associated with this event has N-NW trends and are typically upright to slightly overturned and may represent two generations of folding (Coleman et al., 2003; Dunne and Walker, 2004). In the southern portion of the ESTS, in the region in and adjacent to the Cronese Hills, thrust faults typically have a N-NE trend and are associated with folding that has a SE-vergence (Walker et al., 1990).

Sevier-Laramide Orogeny

The Sevier-Laramide Orogeny began in the Late Jurassic due to the onset of continuous Andean-style eastward subduction of the Farallon slab beneath the North American Plate (DeCelles, 2004; Yonkee and Weil, 2015). Protracted subduction began in the Late Jurassic and persisted until the Oligocene-Miocene when the plate margin underwent a switch from a convergent margin to the present-day San Andreas transform system (e.g., Atwater and Stock, 1998). During this period, two distinct styles of orogenesis occurred within the North American Cordillera: the "thin-skinned" Sevier style and the "thick-skinned" Laramide style (DeCelles, 2004; Yonkee and Weil, 2015). Although these two orogenies are distinct in their style, they overlap both spatially and temporally within the eastern portions of the Sevier-Laramide deformational corridor (e.g., Yonkee and Weil, 2015). Sevier orogenesis is linked to the continuous Andean-style subduction along the western margin of Laurentia and is strongly controlled by preexisting crustal anisotropies (DeCelles, 2004; Yonkee and Weil, 2015). Laramide style orogenesis is linked to a shallowing of the subduction angle of the Farallon slab in the Late Cretaceous (~90-80 Ma), due to a combination of increased plate convergence rates and the subduction of the conjugate Shatsky Rise (CSR), a young and buoyant oceanic plateau embedded

within the Farallon plate (Coney and Reynolds, 1977; Henderson et al., 1984; Saleeby, 2003; Liu et al., 2010). A decrease in relative plate convergence rates and subsequent slab rollback led to the cessation of the Sevier-Laramide orogeny in the Paleocene, although active subduction persisted until the Oligocene-Miocene (e.g. Engebretson et al., 1985; Copeland et al., 2017).

The structural style of Sevier orogenesis has been described as "thin-skinned" with deformation occurring within the upper portions of the crust in a system dominated by eastward propagating folds and thrusts and a regional decollement (DeCelles, 2004). One of the largest controls of the style and distribution of the Sevier orogeny is attributed to the geographic extent of the passive margin sequence (DeCelles, 2004), a westward-thickening sequence of clastic and carbonate rocks deposited along the western margin of Laurentia during the progressive rift to drift phases associated with the Neoproterozoic rifting of Rodinia (e.g., Stewart, 1972, 1976; Bond et al., 1985). The relative strength contrasts between this thick and weak sedimentary package and the strong and resistant underlying crystalline basement created a zone favorable for the formation of a large regional decollement (DeCelles, 2004). Stratigraphic variations across the span of the fold and thrust belt control the style of thrusting (DeCelles, 2004; Yonkee and Weil, 2015). Thrusts associated with Sevier deformation, which localized within the fine-grained passive margin strata, exhibit two primary styles based on their location in the westward thickening wedge, 1) large widely spaced thrust sheets to the west where the passive margin is thick, and 2) thinly spaced and imbricate thrust sheets to the east where the passive margin is thin (DeCelles, 2004). As the leading edge of the fold-thrust belt migrated eastward and reached the shelf to slope transition, the style of thrusting changed to widely spaced thrusts with large amounts of displacement (>50 km) along large flats above thick quartzite Precambrian rocks (Camilleri et al., 1997; Mitra, 1997; DeCelles, 2004; Yonkee and Weil, 2015). Although the

8

typical style of the Sevier is considered to have a continuous eastward migrating fold and thrust belt, the presence of out-of-sequence faulting (DeCelles and Mitra, 1995; DeCelles and Graham, 2015) and synconvergent extension have been noted within the Sevier hinterland (e.g., Wells et al., 2005). Evidence for synconvergent extension has largely been noted within the exposures of metamorphic rocks in mccs (Wells et al., 2005; Wells and Hoisch, 2008; Wells, et al., 2012). The presence of surface breaking normal faults during the Late Cretaceous further support this observation (Druschke et al., 2009).

The flattening of the Farallon slab ultimately led to the onset of the "thick-skinned" Laramide-style deformation during the Late Cretaceous (e.g., Saleeby 2003; Liu et al., 2010). A period of quiescence in the magmatic arc that began approximately ca. 80 Ma is thought to be due to the emplacement of the flat slab beneath the arc and the shutting off of asthenospheric input into the system, which further supports the timing of slab flattening (DeCelles et al., 2009). The subducting flat slab drove deformation far to the east to regions as far inboard as present-day North Dakota by ~60 Ma (Dickinson et al., 1988; Liu et al., 2011). Typical deformation styles associated with the Laramide orogeny are high-angle reverse faults that sole into underlying basement, termed basement-cored uplifts, and their associated fault propagation folds (Dickinson and Snyder, 1978; Yonkee and Weil, 2015). Beginning around 55 Ma the slab began to retreat, potentially due to a change in relative convergence rates leading to rollback of the Farallon slab (e.g., Humphreys, 1995; Smith et al., 2014; Copeland et al., 2017).

Cenozoic Basin and Range Extension

The earliest record of Cenozoic extension in the North American Cordillera is preserved in mccs in the Sevier hinterland (Coney, 1987). One reigning hypothesis on the initiation of extension and mcc formation is due to failure of the Farallon slab and subsequent slab rollback (Coney, 1987;

Humphreys, 1995; Copeland et al., 2017). Plutons and volcanic rocks are found closely associated with most Cordilleran mccs, which has led researchers to posit that magmatism may play a significant role in the formation of mccs (e.g. Coney and Harms; 1984; Coney, 1987; Lister and Baldwin 1993). Two sweeps of volcanism, one beginning in the north in present day Montana at approximately 55 Ma, and another beginning in the south in present day Arizona/Mexico at approximately 35 Ma, are found closely linked both spatially and temporally with the age of extension recorded within core complexes of the North American Cordillera (Dickinson, 2009; Ricketts et al., 2015). The two oppositely directed sweeps in magmatism and extension converged to the latitude of Las Vegas at approximately 16 Ma (Wernicke et al., 1988; Dickinson, 2009; Ricketts et al., 2015). Although extension within mccs tend to show temporal spatial trends, it has been observed that these regions will often experience multiple episodes of extension (e.g., Wells et al., 2000). It has been noted that the location of these metamorphic core complexes occurs within a belt associated with the highest degree of crustal thickening (Coney and Harms, 1984; Coney, 1987).

Brittle extension of the upper crust through the formation of ~N-S trending horst and graben sequences, forming the modern Basin and Range physiography, preserves an overall younger extensional history (Stewart, 1971). Block faulting during the Cenozoic was driven by predominately east-west directed extension with NNE-SSW-striking high-angle normal faults (Stewart, 1971; Wernicke et al., 1988). This deformation dismembered many of the Mesozoic thrust sheets in the hinterland and western part of the foreland thrust belt, providing excellent exposures of the deformed passive margin strata during uplift and tilting of the ranges.

Eastern California Shear Zone

Present day deformation in the Death Valley region is due to the Eastern California shear zone (ECSZ), a zone largely dominated by dextral strike-slip faulting (Dokka and Travis, 1990a,b; Reheis and Dixon, 1996). The ECSZ formed approximately 10-6 Mya as a zone of accommodation for the dextral shear between the North American and Pacific plates (Dokka and Travis, 1990a,b; Frankel et al., 2007). This zone is defined by a series of discontinuous, NW-striking right-lateral strike-slip faults, that span the area of the eastern California Mojave Desert and Death Valley regions, and is also believed to be kinematically linked to the Walker Lane belt to the north (Dokka and Travis, 1990a,b; Reheis and Dixon, 1996; Frankel et al., 2007). In the Death Valley region, the main components of this system are the Northern Death Valley fault zone (NDVFZ), Furnace Creek fault zone (FCFZ) and the Southern Death Valley fault zone (SDVFZ) (Burchfiel and Stewart, 1966; Dokka and Travis, 1990a,b; Frankel et al, 2007). The origin of the central segment of Death Valley is believed to be due to transtensional "pull apart" style basin formation due to the relative motions on the FCFZ and the SDVFZ (Burchfiel and Stewart, 1966).

GEOLOGY OF THE FUNERAL MOUNTAINS

Exhumation during slip along the BCD has exposed a thick succession of Mesoproterozoic to Neoproterozoic metasedimentary rocks (e.g., Labotka, 1980; Holm and Dokka, 1991; Hoisch and Simpson, 1993; Wright and Troxel, 1993; Applegate and Hodges, 1995; Wolfman et al., 2017). The oldest units within the complex belong to the Proterozoic Pahrump Group, which consists of the Mesoproterozoic Crystal Springs Formation, and the Neoproterozoic Horse Thief Springs Formation, Beck Springs Dolomite, and Kingston Peak Formation. This sequence is unconformably overlain by the Neoproterozoic Noonday Dolomite, Johnnie Formation, and Stirling Quartzite, and the Neoproterozoic to Cambrian Wood Canyon Formation (Hunt and Mabey, 1966; Applegate and Hodges, 1995; Wright and Troxel, 1993; Mahon et al., 2014; Wolfman et al., 2017). The oldest units are found within the deepest exposed portions of a dome in the NW-region of the complex, with younger rocks to the SE, dominated by Stirling Quartzite (Wright and Troxel, 1993). Units within the footwall have undergone Barrovian metamorphism with grade increasing from lower greenschist in Echo Canyon to upper amphibolite facies in the NW at Monarch Canyon (Labotka, 1980; Hodges and Walker, 1990; Hoisch and Simpson, 1993; Applegate and Hodges, 1995; Mattinson et al., 2007; Hoisch et al., 2014). The age of metamorphism was recently reported by Hoisch et al. (2014) to be of Late Jurassic age, determined by a Lu-Hf garnet growth age (158.2 $\pm$ 2.6 Ma) in Johnnie Formation schist associated with a compressional PT path from the Indian Pass area.

The complex forms an elongate NW-SE trending antiform, which formed through isostatic rebound during Miocene exhumation (Hoisch and Simpson, 1993). The primary dome forming fault, the BCD, is presently exposed along the northeastern flank of the dome and has a shallow dip to the NE (Wright and Troxel, 1993). Flanking the dome to the SW is the Keane Wonder Fault,

which some researchers have speculated is a continuation of the BCD (Hamilton, 1988; Hoisch and Simpson, 1993), although others believe it is a younger dextral fault (e.g., Reynolds, 1976; Wright and Troxel, 1993; Applegate and Hodges, 1995; Mattinson et al., 2007). Kinematics associated with movement along the Keane Wonder show a pervasive SW-dipping foliation, NW-trending lineation, and kinematic indicators showing NW motion of the hanging wall (Wright and Troxel, 1993; Hoisch and Simpson, 1993), which is consistent with the slip orientation for the BCD. Several intracore shear zones, oriented subparallel to the BCD, have been mapped within the core of the dome; the Monarch Canyon shear zone (MCSZ) of Applegate et al. (1992) and Applegate and Hodges (1995), named the Chloride Cliff fault by Wright and Troxel (1993) and the Eastern shear zone (ESZ) (Applegate et al., 1992). In the Applegate et al. (1992) study they proposed a third intracore shear zone, which they named the Chloride Cliff shear zone, which they interpreted to omit the Beck Springs Dolomite, placing the Kingston Peak Formation on the Crystal Spring Formation. Due to observations that support a continuous Beck Springs Dolomite throughout the region, we do not recognize this shear zone in this study, but rather recognize strain localization in the dedolomitized Beck Springs Formation. Far to the SE in the Funeral Mountains is the Lees Camp anticline, a SE-vergent anticline, which has been correlated with the White Top Mountain backfold (Snow and Wernicke, 1989; 2000). To the SE of the Lees Camp anticline is the SE-vergent Schwaub Peak thrust, interpreted to be of Permian age (Snow, 1992), which places Cambrian on Ordovician strata (Wright and Troxel, 1993). Deformation in the core consists of a network of brittle normal faults that cut the regional mylonitic foliation, and locally cut the BCD (Wright and Troxel, 1993), likely of an age consistent with the opening of the Death Valley basin. This study has documented two new fabrics present within the FMCC: a bedding-parallel shear fabric with highly asymmetric clasts and SE-vergence, and open to close overturned folds within

the Chloride Cliff region with SE-vergence and NNE-SSW trending fold axes that deform this earlier shear fabric.

Footwall rocks throughout the northern section of the core have undergone mylonitization associated with extensional deformation. In Monarch Canyon, the earliest fabrics have been overprinted and the fabrics reflect NW-shearing from deformation associated with the Late Cretaceous and Miocene extensional events (Holm and Dokka, 1991; Hoisch and Simpson, 1993; Applegate and Hodges, 1995; Mattinson et al., 2007). To the SE, beginning in the Chloride Cliff region, extensional overprinting becomes less pervasive and the dominant fabric reflects SE-vergent kinematics, interpreted here to be associated with Late Jurassic burial and contraction. The Late Cretaceous to Paleocene muscovite granite dikes that are pervasive in the NW part of the range decrease in abundance to the SE (Applegate et al., 1992; Hoisch and Simpson, 1993; Mattinson et al., 2007; Sauer, 2014).

MAPPING AND STRUCTURAL ANALYSIS

Detailed structural mapping at 1:10,000 scale within the Chloride Cliff area (Figure 4), along with interpretations based on prior studies (e.g., Hoisch and Simpson, 1993; Applegate and Hodges, 1995; Hoisch et al., 2014), documents the presence of five deformational events (D_1 to D_5) and three associated folding events. D_1 and D_2 are associated with SE-directed burial and contraction, whereas D_3 and D_4 are associated with two periods of NW-directed extension. D_5 deformation is related to post-doming brittle extensional deformation. We associate deformation temperatures to deformational events through the analysis of dynamically recrystallized quartz fabrics associated with structural fabrics and constraints on the thermal history of the Chloride Cliff region based on previously published work (Figure 5; Hoisch and Simpson, 1993; Beyene, 2011; Sauer, 2014; Craddock et al., 2018). Understanding the timing, geometry, and kinematics of these events has important implications for the evolution of the FMCC.

D_1: Late Jurassic Top-Southeast Shear

Due to the extensive overprinting by D_2 fabrics, D_1 fabrics that have little to no overprinting and are exposed in the kinematic plane (XZ) have only been found within several outcrops of the Kingston Peak diamictite; these occurrences preserve a strong bedding-parallel foliation with highly asymmetric strained clasts (Figure 6A). Quartzite, vein quartz, and dolomite are the primary clast types within the diamictite and show differing amounts of strain. Quartzite clasts typically have aspect ratios over a range of 2:1 and 6:1, whereas the dolomite clasts have aspect ratios as low as 3:1 ranging to aspect ratios that exceed 16:1. Asymmetry of clasts shows a consistent top-SE sense of shear. Stretching lineations measured on foliation surfaces in these regions show a slight variation in orientation but have an overall SE plunge with an average orientation of 21°, 148° (Figure 6A inset).

In the Chloride Cliff region, peak conditions reached depths of approximately 19-27 km and temperatures of 575-600° C based on thermobarometry of metamorphic rocks (Hoisch and Simpson, 1993). Deformation fabrics associated with the highest temperatures of deformation in these rocks are likely associated with this burial event. Microstructural analysis of samples containing abundant quartz supports the estimated peak temperature conditions. Quartz is typically coarse grained and has amoeboid and interlocking grain boundaries (Figure 6B). Grains typically have well formed subgrain boundaries, and commonly exhibit undulose extinction. Pinning of quartz at grain boundaries with mica and migration of quartz over mica is prevalent in most samples. These textures are consistent with dynamic recrystallization by fast grain boundary migration (GBM) (Urai et al., 1986; Stipp et al., 2002) and a lower-temperature overprint. These textures provide peak temperature estimates exceeding 500 °C, and the lack of chessboard extinction brackets the upper limit at ~650 °C (Hirth and Tullis, 1992; Stipp et al., 2002). Current constraints on the timing of D_1 are primarily based on the 158.2 ± 2.6 prograde garnet growth age and post-metamorphic cooling muscovite $^{40}Ar/^{39}Ar$ cooling ages of 146-152 Ma from the Indian Pass region (Hoisch et al., 2014). It is important to note that this garnet grew at peak metamorphic conditions and overgrows a crenulation fabric, which may support garnet growth near the late stages of burial. Muscovite $^{40}Ar/^{39}Ar$ cooling ages in the Chloride Cliff region of 77 to 86 Ma (Sauer, 2014) provide a lower limit for D_1 deformation, as the estimated deformation temperatures of ~500° C exceed the closure temperature of argon diffusion in muscovite (Harrison et al., 2009)

D_2/F_1: Early Cretaceous(?) Contraction

The Kingston Peak diamictite and the Johnnie Formation schist exhibit pervasive folding of the D_1-foliation (F_1) (Figure 7A, B). Stereonet projections of fold hinge orientations from folded diamictite clasts and schist layers, along with intersection lineation orientations from the Kingston

16

Peak diamictite, show an overall NNE-SSW trend of fold axes with an average fold axis trend of 197° (Figure 7D). These folds show a vergence towards the SE, indicating SE-directed shear. F_1 is also defined by the presence of open to close, overturned, outcrop to map scale folds within the Kingston Peak Formation, Noonday Dolomite, and the Johnnie Formation (Figure 8). Fold analysis from two of these overturned synclines within the region provide fold axis orientations of 03°, 205° and 07°, 005°, which are consistent with the orientations of bedding-scale folds; both structures show a similar ESE-vergence (Figure 8A,B).

Deformation associated with D_2 is also present as a bedding-parallel mylonitic foliation that shows well developed S-C fabrics, asymmetric clasts, and shear bands that show top-SE kinematics. D_2 fabrics are differentiated from D_1 fabrics primarily through the presence of folded clasts, crenulations, and through the orientation of the stretching lineation as there is an ~30° variation in D_1 and D_2 orientations. D_1 fabrics within the Kingston Peak diamictite can only be confidently identified in zones we believe may have been shielded from D_2 deformation due to strain localization along small and discrete shear zones just above these domains. D_1 fabrics elsewhere have been extensively overprinted by D_2. D_2 fabrics can occasionally be found preserved within the NW part of our map area but become stronger and more pervasive to the SE. Stretching lineations measured on foliation surfaces typically plunge to the SE and have an average orientation of 19°, 112° (Figure 7C), which is consistent with the expected shearing directions from fold orientations. The timing of D_2 is currently unconstrained and may even be related to protracted deformation associated with D_1, but due to differing styles of deformation and a minor difference in kinematics (~30°) we keep them separate here.

D3/F2 and D4/F3: Late Cretaceous and Miocene Extension

Although SE-vergent fabrics are the most pervasive fabric within the SE part of our map area, evidence for NW-directed deformation can be found throughout the entire area, where it appears to be more prevalent in weaker lithologies, such as carbonates and schists. The dominant kinematics for both extensional events is NW-directed shearing, with mylonitic fabrics becoming pervasive in the Monarch Canyon area to the NW. Similar to areas to the NW where the extensional fabrics dominate, within our map area, differentiation of D_3 and D_4 is difficult as the kinematics are virtually identical. It may be possible, however, to assign F_2 to D_3 and F_3 (passive doming of the complex) to D_4. Due to the similarity in these deformational events, structural data for D_3 and D_4 will be combined in this study.

Carbonate-rich rocks of the Beck Springs Dolomite, Horsethief Springs, and Crystal Spring formations typically have well developed stretching lineations, which can be used to determine the direction of shearing during fabric formation. Stretching lineations measured on foliation surfaces of rocks with NW dominated shear sense show an overall SE plunge and have an average stretching lineation of 18°, 111° (Figure 9B). The dominant SE plunge of stretching lineations are due to the doming and back rotation of this portion of the FMCC. The top-NW extensional deformation typically presents itself within the weaker lithologies of the region and is commonly evidenced by S-C fabrics in schists, and bedding-scale folding within carbonates (Figure 9). Fold hinge and intersection lineation orientations, measured from bedding-scale folds in the Beck Springs Dolomite and the Horse Thief Spring Formation, show a general NNE to SSW trend with an average trend of ~20°-220°. The timing of these two extensional events comes from previous studies of the FMCC (Holm and Dokka, 1991; Applegate et al., 1992; Applegate and Hodges, 1995; Beyene, 2011).

Microstructural analysis of samples with a dominant NW-directed fabric and abundant quartz allow for analysis of deformation conditions associated with extension. Quartz in these samples are commonly coarse and exhibit small, strain-free quartz grains, with similar optical orientations, that mantle the host grain (Figure 10). These fabrics are consistent with low temperature grain boundary migration, or bulging recrystallization (BLG) (Stipp et al. (2002). Some samples also exhibit quartz textures with elongate quartz grains with well-developed subgrain boundaries consistent with subgrain rotation recrystallization (SGR), however the dominant fabric appears to be BLG. These samples occasionally preserve evidence for GBM recrystallization, but always show overprinting by the lower temperature regimes. The deformation temperatures inferred from these microstructures are consistent with greenschist facies conditions and likely record deformation during progressive cooling. It is interpreted here that these fabrics record conditions associated with D_3 as these deformation temperatures are consistent with cooling through $^{40}Ar/^{39}Ar$ muscovite closure in this region, which was one the main lines of evidence from the Beyene (2011) study for exhumation of the FMCC during the Late Cretaceous.

Intracore Shear Zones

Slip along the BCD, the primary dome bounding detachment fault, is currently thought to be associated with slip during the D_4 Miocene extensional event. Structurally beneath the BCD are two mapped "intracore shear zones" (Figure 11), the Eastern shear zone (ESZ), and the Monarch Canyon shear zone (MCSZ), which have been interpreted to be Late Cretaceous (Applegate et al., 1992; Wright and Troxel, 1993). The ESZ is mapped within the eastern portion of our map area where it separates the Stirling Quartzite from the Johnnie Formation, progressively truncating the upper and middle members of the Johnnie Formation to the north, resulting in the Stirling juxtaposed directly above the lower Johnnie Formation. Towards the northern portion of the

mapped area (Figure 4) the ESZ truncates against, or merges with, the BCD. Due to poor exposure in this area, the exact nature of the interaction between the BCD and the ESZ is unclear, however two likely relationships exist: 1) the ESZ is cut by the BCD, and the ESZ was active during D_3 but inactive during D_4 and, 2) the ESZ merges upwards into the BCD, and both were active simultaneously during D_3 and D_4. The presence of Tertiary deposits in the hanging wall of the BCD and the young zircon (U-Th)/He ages from the Johnnie Formation (Beyene, 2011) suggest that it is unlikely that the ESZ cuts the BCD. The MCSZ as expressed by the contact between the Johnnie Formation and the underlying Noonday Dolomite, begins in the center of our map area, NW of the region dominated by SE-vergent folds that deform this stratigraphic level. In this zone, the MCSZ has a bedding-parallel orientation and it may locally omit portions of the Kington Peak diamictite and Noonday Dolomite (Figure 11A), although stratigraphic thickness variations as seen elsewhere in Death Valley within the Kingston Peak (Miller, 1985; Prave, 2001; MacDonald et al., 2014) may account for these observations. Diabase dikes, with a K-Ar biotite age of 34.4 ± 0.9 Ma (Wright and Troxel, 1993) and the target of hornblende $^{40}Ar/^{39}Ar$ analysis in this study, cut the MCSZ in the central portion of the map area. These diabase dikes lack a mylonitic foliation and still preserves an igneous texture.

D_5: Brittle Extension

Since the end of detachment faulting in the Funerals, the range has been deformed by a network of brittle normal faults (Figure 12). Everywhere the brittle faults are found they cut the regional metamorphic and mylonitic foliations attributed to D_1 to D_4 deformation. Brittle faults mapped in this study tend to have a range of orientations, but the most prominent faults have NW-SE or WSW-ESE strikes. These faults typically exhibit normal-sense offset, but some faults occasionally display some component of normal and strike-slip offset. In the NW portion of the

map area, a large normal fault referred to as the Big Bell fault (Applegate, 1995), strikes NW-SE and drops stratigraphy to the SW. Several smaller faults with similar kinematics are present in the hanging wall and footwall of the Big Bell fault. Another significant normal fault located to the SE has a WSW-ENE trend and down drops stratigraphy to the SE. Based on interpretations from cross sections (Figure 4) this normal fault cuts several of the large SE-vergent folds associated with D_2. To the SE of the Chloride Cliff region Wright and Troxel (1993) have mapped a large network of NE-SW striking normal faults that predominately drop stratigraphy to the NW. Where these faults intersect the BCD, they appear to be cut, indicating they predate slip along the BCD. Slip on the Big Bell fault has kinematics consistent with extension described by Fridrich and Thompson (2011) in their '~4.5 - ~3 Ma tectonic reorganization', which well postdates current constraints of slip on the BCD. Brittle extension may have predated D_4 extension in regions further to the SE, but in the Chloride Cliff region it appears brittle faulting is post-dome formation.

GEOCHRONOLOGY AND THERMOCHRONOLOGY

Hornblende $^{40}Ar/^{39}Ar$

$^{40}Ar/^{39}Ar$ Analytical Methods

Several hornblende-rich lithologies were chosen for $^{40}Ar/^{39}Ar$ analysis, including amphibolite layers within the Johnnie and the Kingston Peak formations, to better constrain the timing of cooling; additionally, one sample from a prominent diabase dike in the central part of the map region was analyzed to constrain the intrusion age. Samples were crushed and sieved to a 250-88 μm size fraction, and density separated using iterative density fractions using methylene iodide (MEI), diluted with acetone. Density fractions were analyzed and selected for further processing based on the quality of the minerals contained within the separate. The selected density fractions were then sieved to 149-125 μm or 125-105 μm size fractions, followed by handpicking to concentrate inclusion-free hornblende.

Samples selected for analysis were packaged in Al foil and stacked within a fused silica tube. Every 5-10 mm within these tubes were packages of GA-1550 biotite, which was used as a neutron fluence monitor. Also added to the packages were synthetic K-glass and optical grade CaF_2 to monitor neutron induced argon interferences from K and Ca. Packages were sent the TRIGA Reactor at the U.S. Geological Survey in Denver, CO. Samples were in the 1 MW TRIGA type reactor for a total of 28 hours. Measured $(^{40}Ar/^{39}Ar)_K$ values were 4.00 ($\pm$ 2.03%) x 10^{-2}. Ca correction factors were $(^{36}Ar/^{37}Ar)_{Ca}$ = 2.43 ($\pm$ 0.51%) x 10^{-4} and $(^{39}Ar/^{37}Ar)_{Ca}$ = 5.55 ($\pm$ 0.58%) x 10^{-4}. Individual J-factors were determined through fusion of 4-8 crystals of GA-1550 biotite and are commonly within a range of ~5.30-5.65 x 10^{-3}.

Following irradiation, samples were analyzed at the Nevada Isotope Geochronology Lab (NIGL) at UNLV, using a MAP215-50 Single Collector Mass Spectrometer. Samples underwent a detailed heating schedule with 19 to 21 steps, from 800 °C to 1400 °C. Interfering gases produced during each step were removed using two SAES GP-50 getters prior to analysis of ^{36}Ar-^{40}Ar isotopic ratios. The data was collected and processed using LabSPEC software. Data was then exported and processed using the Microsoft Excel macro Isoplot (Ludwig, 2003), where the age was calculated, and plots were generated.

Thermochronology

A total of four amphibolite samples, spanning ~9 km along the transport direction of extension, were selected and processed for hornblende $^{40}Ar/^{39}Ar$ thermochronology to supplement existing muscovite ages to better constrain the thermal history. Three of the four samples analyzed yielded discordant age spectra suggesting variable incorporation of excess argon (Figure 13). The fourth sample, SCFM315-16B, an amphibolite within the Horsethief Springs Formation, contained no definable plateau but exhibited a flattish segment, with ages between 118-108 Ma that allowed a preferred age to be interpreted from the data (Figure 14). Although the data are not well behaved, we use the steps with consistent ages to generally reflect the age of the sample. This age range overlaps with a previously published $^{40}Ar/^{39}Ar$ hornblende age of 112.9 ± 0.8 Ma from a garnet amphibolite from Chloride Cliff (Hoisch and Simpson, 1993). This age is consistent with the currently known timing of contraction and may reflect denudational cooling prior to detachment faulting in the region.

Geochronology

A prominent network of NE-striking diabase dikes in the region was sampled and analyzed for ^{40}Ar/^{39}Ar hornblende geochronology. One of these dikes has a previously published K-Ar biotite age of 34.4 ± 0.9 Ma (Wright and Troxel, 1993), however due to the now recognized limitations of the K-Ar dating system, we sought to improve the age. Although sample TC17FM-16 did not generate a definable plateau, several steps have broadly similar ages and a preferred age range was determined. Similar to sample SCFM315-16B, heating steps tended to concentrate throughout a span of ~6 Ma, providing an age range of intrusion of ~42-36 Ma (Figure 14) Although these data are not well behaved, the analysis is consistent with the previously published biotite K-Ar age, supporting a Late Eocene-Early Oligocene age for the emplacement of these diabase dikes.

U/Pb Zircon Geochronology

U/Pb Analytical Methods

U/Pb zircon analysis was conducted on a single garnet-bearing granitic intrusion found in the central region of the map area. The sample was crushed and sieved to a 250-53 μm size fraction prior to being run on the Wilfley table. Further density separations were performed using MEI and the densest fraction was magnetically separated using a Frantz. The remaining separate was handpicked for clear euhedral zircon grains. Zircons were mounted in epoxy and analyzed for U/Pb on a Thermo Element 2 single-collector ICP-MS at the University of Arizona LaserChron center. Isotope data was processed using Microsoft Excel and ages were generated using the TuffZirc tool and Concordia plots in Isoplot.

Igneous Zircon

Data collected from 37 zircons separated from sample TC17FM-45 showed two main populations of zircon ages, an older population of inherited zircons and a younger population of magmatic grains. The young population of grains provided a weighted mean age of 95.63 ± 0.95 Ma, generated using TuffZirc from a coherent group of 17 zircons (Figure 15A). A conventional Concordia plot had an upper intercept of 1705 ± 48 Ma (Figure 15B), which is consistent with detrital zircon populations of the regional basement and the Crystal Springs Formation (Iriondo et al., 2004; Barth et al., 2009; Maclean et al., 2009; Mahon et al., 2014). This body intrudes into the Kingston Peak diamictite and truncates the D_1 foliation. This unit also possesses a strong solid-state foliation that has a subparallel orientation to the surrounding D_1 foliation. Petrographic analysis of this sample shows a mylonitic fabric with top-to-the NW kinematics, consistent with D_3 and D_4 kinematics (Figure 16). The field and petrographic structural relationships show that this intrusion postdates D_1, providing a lower constraint on the timing of D_1 contraction in the region. Quartz microstructures in this sample provide evidence that dynamic recrystallization occurred at temperatures consistent with GBM in quartz. As $^{40}Ar/^{39}Ar$ muscovite cooling ages in and adjacent to this region range from ~75-86 Ma (Beyene, 2011; Sauer, 2014), estimated temperatures of deformation, from quartz microstructures in this sample, exceed the expected ambient temperatures during this time and may provide evidence that shearing took place during or shortly after emplacement, leading to elevated temperatures in relation to the surrounding country rock.

DISCUSSION

Extension in The Funeral Mountains

The FMCC has been the subject of study for the past four decades and its extensional history has been well documented. Extensional unroofing during both the Late Cretaceous and the Miocene led to the progressive exhumation of Neoproterozoic-Cambrian strata, exposing rocks in the NW part of the range that had been buried to peak depths of ~35 km. The primary dome-bounding fault, the BCD, has been attributed to extension during the Miocene event, however it has been suggested that the BCD may have captured a Late Cretaceous shear zone, leading to the rapid cooling signature along the trace of the BCD during this time (Beyene, 2011; Sauer, 2014). Extensional fabrics from both extensional events are co-planar and co-linear with the same kinematics. This observation leads to the interpretation that these events may have occurred from slip along the same structure or a structure of similar orientation.

Miocene extension is currently believed to have begun around 12-11 Ma (Holm and Dokka, 1991; Hoisch et al., 1997; Beyene, 2011) and the current lower constraints on the timing of Late Cretaceous extension are ~70 Ma (Applegate et al., 1992), which requires a period of quiescence of approximately 60 Ma between unroofing events. During this time there was some igneous activity within the Funerals, namely the intrusion of the diabase dike in the central portion of the map area, which in a few places cuts the MCSZ, and some Paleocene leucogranite and pegmatite dikes and sills in the deepest levels of Monarch Canyon (Mattinson et al., 2007; Sauer, 2014). This hiatus and the cross-cutting nature of extensional structures allows for some differentiation of extensional fabrics to be made.

Two intracore shear zones within the FMCC, the deeper MCSZ and the shallower ESZ, may provide some insight into variations between the Late Cretaceous and Miocene extensional events. As stated earlier, it is very difficult to differentiate fabrics of both events as they share similar kinematics and geometry, however the relationship of the MCSZ and the diabase dikes may allow us to speculate on the intensity and extent of deformation associated with these two events.

Eastern Shear Zone and The Monarch Canyon Shear Zone

The MCSZ and the ESZ represent two zones that accommodated high degrees of strain during extension in the Funeral Mountains, and both are currently interpreted to have been active during the Late Cretaceous extensional event (Applegate et al., 1992). New evidence from structural mapping, new $^{40}Ar/^{39}Ar$ geochronology, and preexisting K-Ar geochronology may provide evidence for a lack of motion along the MCSZ, or at least a portion of the MCSZ, during the Miocene extensional event. The MCSZ is localized along the contact of Johnnie Formation and the Noonday Dolomite, although high attenuation of the Noonday locally places the Johnnie Formation against the upper Kingston Peak Formation. In the central portion of the map area a diabase dike cuts the MCSZ in several places. In all localities of the diabase dike, including those where it intersects the MCSZ, the intrusion shows a lack of structural foliation preserving a strong igneous texture, and has no discernible offset. As this intrusion predates the Miocene extensional event, the lack of offset indicates that the MCSZ, in the Chloride Cliff area, was inactive during the Miocene and is a probable Late Cretaceous structure. The inactivity of this rheologically weak shear zone during the Miocene may provide evidence for shallow levels of strain penetration in the Chloride Cliff region, during Miocene extension. This allows the interpretation that most, if not all, top-NW fabrics structurally below the MCSZ can be treated as Late Cretaceous fabrics

lacking a Miocene overprint. Thin section analysis of quartz-rich samples within the MCSZ and from the stratigraphically lowest samples show well preserved NW-directed shear sense and are associated with dynamically recrystallized quartz consistent with the SGR to BLG regimes. These observations require that this portion of the FMCC had cooled below 400 °C by the end of the Late Cretaceous extension event if we follow the interpretation that Miocene strain did not penetrate this deep into the core of the dome. These deformation temperatures are consistent with cooling below the $^{40}Ar/^{39}Ar$ muscovite closure temperature during the Late Cretaceous, which is one of the thermochronometers that has been used to constrain unroofing and cooling during this period.

The ESZ separates the Stirling Quartzite from the upper Johnnie Formation in the SE portion of the map area, and progressively truncates the upper and middle members towards the NW where the Stirling Quartzite is juxtaposed with the lower Johnnie Formation. To the NW in a region with poor exposure, the ESZ eventually intersects the BCD. The nature of the contact between the ESZ and the BCD is uncertain, with two alternatives: 1) the ESZ merges with the BCD and represents slip during both the Late Cretaceous and the Miocene, and 2) the ESZ is cut by the BCD and slip on the ESZ occurred exclusively during the Late Cretaceous, like the CSZ. The continuation of the BCD follows the same stratigraphic and structural horizon as the NW portion of the ESZ and may provide evidence that the two faults/shear zones were active at the same time, however this remains speculative.

Comparison of Late Cretaceous and Miocene Fabrics

Because it is likely that the NW-fabrics below and within the MCSZ are Late Cretaceous, these fabrics can be used to compare to the definitive Miocene fabrics. Stretching lineation orientations measured at outcrops showing strong NW sense of shear collected from both above and below the MCSZ are indistinguishable when compared using stereographic projections. NW-

vergent bedding-scale folds found in weaker lithologies, such as schists and carbonates, also show sub-parallel to parallel orientations of fold hinges measured throughout the region. To the SW of Chloride Cliff, along a 5 km trace of the BCD south and north of Monarch Canyon, a highly strained marble tectonite with an extremely fine grain size (9 to 3 microns) was extensively measured for kinematics. Estimated deformation temperatures from this unit based on grain size (e.g., Ebert et al., 2008) are in the range of 230 to 280° C, placing deformation within the Miocene based on the age of $^{40}Ar/^{39}Ar$ muscovite closure in this region (82-75 Ma; Beyene, 2011; Sauer, 2014) and U-Th-He zircon ages (9-8 Ma; Beyene, 2011). The average stretching lineation from this calcmylonite is 06°, 109° (Figure 17), and it can be argued that these kinematics reflect the slip direction during the Miocene time. These measurements are co-linear to all extensional lineations from the Chloride Cliff Region (18°, 111°; Figure 9B). This strong parallelism between both events indicates a similar geometry and kinematics is responsible for the formation of these fabrics. It has been interpreted that the BCD captured a Late Cretaceous shear zone (ESZ; Beyene, 2011; Sauer 2014), which was responsible for Late Cretaceous extension in the FMCC, however we interpret that the BCD may be the fault responsible for both the Late Cretaceous and Miocene unroofing.

Contractional Fabrics in an Extensional Complex

Repeated episodes of tectonism often obscure and overprint earlier fabrics, making it difficult to recognize the earliest structures. In the North American Cordillera there is a strong spatial correlation between the regions of maximum crustal thickening during Sevier orogenesis and the mccs found within the Sevier hinterland. This spatial link provides evidence in support of the notion that contractional deformation within a region plays a strong role in later gravitational collapse. To overcome the difficulty in studying this link due to overprinting, we studied the

Chloride Cliff region which offered: (1) a well exposed sequence of the regional stratigraphy from the Stirling Quartzite down to the lower Crystal Springs Formation, and (2) an intermediate position along the field metamorphic gradient. These factors, along with the contrasting strength of lithologies in the region and strain localization along the intracore shear zones during the D_3 and D_4 extensional events, led to the preservation of SE-vergent contractional fabrics. This preservation of the earlier deformation has provided a unique opportunity to understand how the contractional history of an orogen can affect, and possibly have some control, on the style and kinematics of later crustal extension.

Previous studies of the FMCC have documented a Barrovian metamorphism that decreases in grade to the SE (e.g., Labotka, 1980; Hoisch et al., 2014), and peak burial depths that cannot be explained by stratigraphic thickness alone (Applegate and Hodges, 1995); this has led to the interpretation that the region was buried by a large SE-directed thrust sheet prior to extension in the Late Cretaceous (Applegate and Hodges, 1995; Hoisch et al., 2014). Prior to this study, SE-vergent fabrics had not been identified. Constraints on the timing of this burial are primarily based on a Lu-Hf prograde garnet growth age of 158.2 ± 2.6 Ma (Hoisch et al., 2014). Microstructural study of these rocks show that these garnets overgrow a crenulation cleavage and may reflect growth near the end of burial. Timing of D_1 can be estimated by the garnet growth age but determining the timing of D_2 is challenging. Based on the U/Pb age from the granodiorite, which does not show evidence for SE kinematics, we know that D_1 was over by the Late Cretaceous. One question that remains is whether there was a gap between D_1 and D_2, or if the event is protracted and represents a phase of shearing followed by folding during continued contraction.

Late Jurassic Thrust Faulting in Death Valley

Late Paleozoic to early Mesozoic contraction associated with the Death Valley fold and thrust belt and the Last Chance thrust system are believed to be responsible for much of the contractional deformation in the Death Valley region. The presence of significant Late Jurassic burial and metamorphism in the Funeral Mountains brings into question how pervasive thrusting of this age may have been in the Death Valley region. Currently most contractional structures within the Death Valley region are interpreted to be of Early Jurassic age or older. Just to the west of southern Death Valley, in the southern Panamint Range and in the Slate Range, are two thrust faults that have been interpreted as Jurassic in age (Wrucke et al., 1995). Similarly, Andrew (2002) noted the presence of Late Jurassic aged deformation in the central Panamint Range.

The Layton Well thrust is a shallowly west dipping thrust fault with ~7 km of exposure in the southern Slate Range (Smith et al., 1968; Wrucke et al., 1995). On the east side of the range, a sequence of small-scale folds with east-vergence are present within the footwall of the thrust. Contained within this section is a thick sequence of volcanics rocks, a few of which have U-Pb ages of 150 and 148 Ma (Wrucke et al., 1995). These ages are consistent with a ~152 Ma pluton with synkinematic textures and a ~151 Ma pluton that is deformed along the thrust (Dunne and Walker, 2004). U-Pb ages from plutonic rocks within the hanging wall of the thrust have yielded an age of 148 Ma and a pluton that seals the thrust has an age of 147 Ma indicating motion had ceased along the thrust by this time (Wrucke et al., 1995, and references therein), however a deformed >145 Ma intrusion may provide evidence for protracted movement along the thrust or renewed motion during this time (Dunne and Walker, 2004). These constraints provide a Late Jurassic age of faulting.

The Butte Valley thrust is a curved and presently non-planar fault that is exposed across most of the southeastern Panamint Range (Wrucke et al., 1995). Juxtaposition of Proterozoic strata in the hanging wall with volcanic rocks as young as the Late Jurassic in the footwall have led to interpretations that offset along this structure is no less than 10 km (Wrucke et al., 1995). These Late Jurassic volcanic rocks do not have any direct dates but have been correlated to a 170-148 Ma volcanic sequence located in the Inyo Mountains, Alabama Hills, and Slate Range (Dunne and Walker, 1993; Wrucke et al., 1995). In the hanging wall of the Butte Valley thrust is a range scale anticline that is cut by the 148 ± 3 Ma Independence dike swarm (Chen and Moore, 1979; James, 1989; Glazner et al., 1999; Andrew, 2002) and the 145 ± 2 Ma Manly Peak pluton (Andrew, 2002). Wrucke et al. (1995) have interpreted the arcuate shape of the thrust as due to folding following thrust faulting. Alternatively, the structure has been interpreted as due to 'caldron subsidence' during the Late Jurassic, based on the absence of deformation and associated faults and shear zones throughout Butte Valley (Davis and Burchfiel, 1997). Accordingly, failure of a Jurassic plutonic complex roof led to the down dropping of younger rocks relative to the surrounding Proterozoic basement, leading to the stratigraphic juxtaposition noted by Wrucke et al. (1995) (Davis and Burchfiel, 1997).

Andrew (2002) noted seven separate deformation events in the Panamint Mountains, the earliest of which (D_1) he interprets as east-directed contraction and burial during the Late Jurassic. Development of east-vergent microfolds in rheologically weak layers, and shear zones developed within metamorphic and igneous rocks are the primary evidence for kinematics (Andrew, 2002). Fold axes typically exhibit a N to NNW trend and have associated E to ENE-directed shearing and trends of stretching lineations (Andrew, 2002). Complex north-trending folds in the Tucki Mountain region documented by Hodges et al. (1987) have been correlated to this Late Jurassic

deformation, however this region has been significantly overprinted by later deformation (Andrew, 2002). Deformation timing is constrained by a sheared hornblende diorite with a U-Pb zircon age of 175.6 ± 1.2 Ma, which are subsequently cut by dikes of Independence dike swarm affinity, with crystallization ages of ~148 Ma (Chen and Moore, 1979; James, 1989; Glazner et al., 1999; Andrew, 2002). This brackets the D_1 deformation in the Panamint range between ~176 and 148 Ma, consistent with the timing of peak metamorphism in this region (Labotka, 1985; Andrew, 2002).

The kinematics and timing of the deformation in the Slate Range and Panamint Mountains (Wrucke et al., 1995, Dunn and Walker, 2004; Andrew, 2002) seem consistent with the proposed thrust faulting that led to burial in the FMCC and may record regional contraction during this period, however, the location precludes any direct cause and effect. Beyond these structures noted above, there is a lack of evidence for Late Jurassic thrust faulting in the Death Valley region, which is at odds with the degree of Late Jurassic burial indicated by peak burial depths from the FMCC.

Paradox of Low-Angle Normal Faulting

Since the recognition of low-angle faults that record normal sense motion, many hypotheses have been presented to explain this phenomenon. Early arguments opposing these structures centered around the problem that a normal fault slipping at low angle defied Andersons theory of faulting. In the case of normal faulting, or gravity faulting in Andersons classification of faults, the primary compressive stress, σ_1, is vertical (Anderson, 1951). Slip is predicted to occur on 60° dipping faults for a rock with frictional properties that follow Byerlees Law. Another commonly cited argument against low-angle slip is the lack of seismicity that is associated with faults dipping <30° (Jackson, 1987; Collettini, 2011). This contradiction with classic rock mechanics has caused researchers to hypothesize that low-angle normal faults did not originally

slip at low angles but were rotated into a low angle following slip at a high angle. Alternatively, it is argued that there are mechanisms that could allow for normal faults to slip at low angles. In this section we will look at some of these opposing hypotheses and how they may pertain to observations in the Funeral Mountains (Figure 18).

Slip Cannot Occur at a Low-Angle

Several hypotheses have been presented to explain low-angle normal faults without the need for slip at a low angle including the rolling-hinge model and planar-rotational (domino) faulting (Proffett, 1977; Axen, 1988; Wernicke and Axen, 1988; Axen and Bartley, 1997; Lavier et al., 1999). Both models work by the progressive rotation of initially high-angle faults to low angles, with all slip occurring during the high-angle phase but differing slightly in their mechanisms.

Planar rotational (domino) faulting. Block faulting is one of the most common styles of faulting found throughout the Basin and Range province. Domino faulting is a type of block faulting where both the fault plane and fault block rotate during slip. The occurrence of these faults in association with detachment faulting have been observed within the Cordillera (e.g., Wernicke and Burchfiel, 1982; Axen, 1988; Lister and Davis, 1989). The process of domino faulting involves closely spaced synthetic normal faults that progressively rotate during slip (Figure 18A). As the fault plane rotates, slip eventually ceases as slip is no longer favorable along this plane, and a new fault set develops. This leads to a relationship where the youngest faults exhibit the steepest dips in the array of domino faults (Proffett, 1977; Lister and Davis, 1989). This relationship has been documented in studies within the Snake Range, where the highest angle faults are all of the youngest generation and cut the older, shallowly-dipping faults (Gans et. al., 1985). Domino-

bounding faults root into an underlying shallowly dipping decollement that need not accommodate major slip.

Rolling hinge model. Arguably one of the most popular models for the formation of mccs is the rolling hinge model (Figure 18B). Similar to domino block faulting, this proposed evolutionary model involves the sequential rotation of an array of initially listric high-angle normal faults that sole into a larger detachment (Axen and Bartley, 1997; Lavier et al., 1999). When large amounts of displacement occur along a normal fault it creates a negative load on the footwall leading to an isostatic response, progressive uplift and the formation of an antiformal footwall (Spencer, 1984; Wernicke and Axen, 1988; Axen and Bartley, 1997). In this hypothesis, an initially high-angle fault, that soles relatively deep into the crust, slips and begins to exhume the footwall causing isostatic rebound to occur. This rebound causes a hinge to form where the inactive rotated faults begin to transition to the active high-angle faults (Axen and Bartley, 1997; Lavier et al., 1999). As new faults begin to form the hinge migrates, or 'rolls', in the direction of slip. The 'rolling' of this hinge eventually leads to an older back-rotated, inactive portion of the detachment, a relatively horizontal portion of the detachment, and the younger high-angle section, which is overall represented by an antiformal dome (Axen and Bartley, 1997). This process allows for slip to occur exclusively along the high-angle portion of the detachment fault while the previously rotated sections are inactive and are at low angles (Axen and Bartley, 1997).

Slip Can Occur at a Low-Angle

Despite the apparent issues surrounding the contradiction of low-angle normal faulting with traditional rock mechanics, others propose that low-angle faults can slip while at angles of $<30°$. Some of these hypotheses, which will be outlined below, include elevated levels of pore fluid pressure, rotation of principle stresses, the recently published Keystone fault hypothesis, and

tectonic reactivation and inheritance (e.g. Melosh, 1990; Axen, 1992; Axen, 1993; Fletcher et al., 2016; Swanson and Wernicke, 2017).

Rotation of principle stresses. One of the main problems with low-angle normal faults is the unfavorable orientation of the fault plane in relation to the orientation of σ_1. One way to resolve this issue is if rotation of the principle stresses occurs leading to an orientation of σ_1 favorable for normal slip on a low-angle fault plane. Stress rotation is a commonly cited hypothesis and has been suggested to be what controls the formation of large bedding-parallel decollements confined within rheologically weak layers during orogenic events (Bradshaw and Zoback, 1988; Melosh, 1990). Within the earth's crust, stress refraction commonly occurs when a fault reaches a boundary where there is a large viscosity contrast between lithologic layers, which can lead to rotation of the principle stress orientations up to an angle of 45° (Bradshaw and Zoback, 1988). If this observation is applied to a larger scale, then the rheological boundaries within the crust could help drive regional scale stress rotation and the formation of low-angle normal faults at depth (Melosh, 1990). Stress rotations have also been noted in relation to fault weakening due to a damage induced-change in the elastic properties during faulting (Faulkner et al., 2006). This may provide a mechanism that can explain low angle slip at higher structural levels where deformation is predicted to be dominated by brittle structures.

Pore fluid pressure. An alternative proposed explanation is that high pore fluid pressure along fault zones could promote slip at low angles in both the ductile and brittle regimes (Reynolds and Lister, 1987; Axen, 1992; Healy, 2009). Increases in pore fluid pressure are known to cause faulting at lower shear stresses than typically expected for a given medium by decreasing the overall confining pressure of the system (e.g. Terzaghi, 1936; Tullis and Yund, 1980). The elevated pore fluid pressure would decrease the frictional component of the fault zone and would require a

lower effective shear stress to promote slip (Healy, 2009). It has been noted, however, that rotation of the principle stress orientations is still required in order for slip to occur (Axen, 1992; Healy, 2009).

Keystone fault hypothesis. A more recent hypothesis to explain slip on faults, such as low-angle normal faults, that are misoriented in relation to the maximum compressive stresses of a region is the Keystone fault hypothesis. A study by Fletcher et al. (2016) focused on the magnitude 7.2 El Mayor-Cucapah earthquake, an earthquake that initiated slip along an entire network of faults. Fault orientations ranged from optimally oriented to severely misoriented faults, but slip occurred throughout the whole range of fault orientations (Fletcher et al., 2016). If a misoriented fault, the keystone fault, in a network of faults pins the optimally oriented faults and causes movement to be locked, then the network may remain undisturbed until critical stress is reached on the keystone fault, causing the whole network to fail (Fletcher et al., 2016).

Tectonic reactivation and inheritance. In the debate on the mechanics of low-angle normal faulting, the idea of tectonic reactivation or inheritance is often underappreciated. It has been recognized that high-angle normal faults will commonly reactivate during contraction as high-angle reverse faults and that thrust faults will reactivate as low-angle normal faults, leading to angles of 60º between σ_1 and the fault plane (Sibson, 1985). Bruhn et al. (1982) even found instances of slip reactivating along low-angle joints, such that the angle between the regional σ_1 and the fault plane would have been 70-80º. Collentini (2009) demonstrated that slip will preferentially occur along weak foliation planes, and that foliated natural samples typically have lower frictional coefficients (0.45-0.20) than powdered samples (0.60) that lack these anisotropies. Below are brief syntheses on areas where the reigning hypothesis on low-angle fault slip is due to reactivation and inheritance, listed in order of increasing scale of the reactivation phenomenon.

Mormon peak detachment. The frontal thrust of the Sevier fold and thrust belt is in the Mormon Mountains. The Mormon thrust cuts up section from lower Paleozoic to Jurassic strata and is commonly associated with a footwall syncline (Burchfiel et al., 1982; Bohannon, 1983; Swanson and Wernicke, 2017). The trace of the Mormon thrust is continuous and commonly linear except where it has been disturbed by Miocene normal faults, which in this region is related to the Mormon peak detachment fault (Swanson and Wernicke, 2017). The Mormon Mountains form a structural dome punctuated by klippen of the Mormon Peak detachment hanging wall (Swanson and Wernicke, 2017). The Mormon Peak detachment appears to localize itself along the frontal ramp of the Sevier belt, formed by the Mormon thrust, cutting down section along the ramp and through the thrust flat into Proterozoic basement (Swanson and Wernicke, 2017). The present orientation of the detachment has been altered since initiation due to flexure during detachment faulting and rotation related to later extension in the region (Swanson and Wernicke, 2017). Estimates from this study indicate initial fault dips along the detachment ranged from 20-25° in the southern exposures, steepening to dips of ~40° to the north (Swanson and Wernicke, 2017). Also located in this region is the younger Tule Springs detachment system, which cuts the Mormon peak detachment (Axen, 1993; Swanson and Wernicke, 2017). The Tule Springs detachment has also been interpreted to have formed due to reactivation of the Sevier frontal thrust ramp during the Miocene (Axen, 1993). This fault is interpreted to have slipped at extremely low-angles ranging from 3°-15°, with limits on dip no greater then 36° (Axen, 1993). Both structures provide evidence that structural reactivation can play a significant role in accommodating slip at low-angles and that low-angle slip was occurring at shallow depths well above the brittle-ductile transition where mccs are believed to form.

Pequop fault. The East Humboldt Range, Wood Hills, and Pequop mountains of NE Nevada preserve a complex history of contraction followed by exhumation of metamorphic rocks through detachment faulting (Camilleri and Chamberlain, 1997; Camilleri et al., 1997). Two periods of contractional deformation along the inferred Windermere thrust and the Independence thrust are bracketed between the Late Jurassic and the Late Cretaceous (Camilleri and Chamberlain, 1997; Camilleri et al., 1997; Camilleri, 1998). Contraction in the area caused Barrovian metamorphism and thermal weakening of the footwall strata, which led to progressive footwall collapse and the formation of bedding parallel to subparallel structural foliation and shallow dip of the strata to the NW (Camilleri et al., 1997; Camilleri, 1998). There is no exposure of the Windemere thrust, but evidence for its existence is due in large part to the requirement for large amounts of burial to accommodate peak metamorphism and formation of the large barometric gradient observed in this region and the repetition of the Paleozoic-Mesozoic aged strata along the low-angle normal faults (Camilleri and Chamberlain, 1997). Cross sections and structural interpretations from Camilleri and Chamberlain (1997) place the Pequop fault largely along the subsurface trace of the Windermere thrust and at an orientation similar to, but structurally higher than the Independence thrust. This structural relationship could indicate a component of reactivation of the Windemere thrust, which would lead to obscuring of its presence, and potentially some component of inheritance of the weak structural foliation that was formed during early contraction and footwall collapse. Furthermore, it shows the tendency for normal-sense slip along inclined crustal panels.

Caledonian backsliding. Reactivation on a significantly larger scale than either of the previous two examples is the instance of the classic Caledonian backslide. In the Ordovician-Upper Silurian, SE-convergence between Laurentia and Baltica led to the formation of the

Caledonian nappe, which was emplaced upon the Baltic shield (Morley, 1986; Fossen, 1992). In the Devonian, following contractional deformation, the orogen began to collapse, however extension was not confined to the orogenic wedge (Fossen and Rykkelid, 1992). The basal decollement of the orogen underwent significant reactivation during this period leading to approximately 30 km of 'backsliding' (Fossen, 1992; Fossen and Rykkelid, 1992). The backsliding was first recognized due to the large-scale overprinting of NW-vergent fabrics upon the contractional SE-vergent fabrics (Fossen and Rykkelid, 1992). These overprinted fabrics are subparallel to parallel to one another and differ in their opposing asymmetry (Fossen and Rykkelid, 1992; Rykkelid and Fossen, 1992).

Evidence for Reactivation/Inheritance in The Funeral Mountains

In the Funeral Mountains, estimated burial depths, a NW-increasing Barrovian-style metamorphic field gradient, and the recognition of pervasive SE-shear fabrics and contractional structures that clearly predate extension, all provide evidence for extensive tectonic burial due to crustal shortening. Metamorphic isograds in the region crosscut the regional stratigraphy indicating an initial NW-inclination of the rocks during burial (Hoisch and Simpson, 1993). This dip of the footwall rocks can be explained by thermal weakening of the footwall during burial and progressive footwall collapse, similar to what is seen in the East Humbolt-Wood Hills-Pequop ranges (e.g. Camilleri and Chamberlain, 1997). Underthrusting of the footwall led to inclination of the footwall strata and the development of a strong and shallowly NW-dipping bedding-parallel foliation. This burial is accomplished by an enigmatic thrust fault of Late Jurassic age, which presently has not been recognized. It has been proposed that detachment faulting excised the thrust and transported it to the NW (Hodges and Walker, 1990; Applegate and Hodges, 1995). The Grapevine Mountains, which have been interpreted as having an initial position over the

metamorphic rocks of the Funeral Mountains (e.g., Snow and Wernicke, 1989; Hoisch and Simpson, 1993), do not have any recognized structures of the proper age or with enough associated shortening to accomplish the depths of burial recorded in the FMCC. We believe that a more likely explanation is that the thrust fault was reactivated during regional detachment faulting and is currently expressed as the BCD (Figure 2). This would not be the first-time reactivation of thrust faults has been proposed in the Funeral Mountains. Cemen and Wright (1990) have proposed a series of reactivated reverse faults in the southern Funeral Mountains, namely the Clery thrust and a portion of the Schwaub Peak thrust.

Thrust Reactivation

In zones of reactivation, overprinting often obscures earlier fabrics making them difficult to identify. In Monarch Canyon, the deepest structural levels of the FMCC, most of the early contractional history has been erased by strong overprinting during extensional exhumation of the dome. To the SE, beginning in the Chloride Cliff region, there begins to be a progressive change from NW-dominated to SE-dominated kinematics. The preservation of both contractional and the extensional fabrics provides a unique opportunity to compare the fabrics and structures of all documented deformational events. The primary fabrics compared in this study are: stretching lineations associated with kinematics determined in the field or through thin section analysis, intersection lineations, and fold hinge orientations of folded clasts and larger scale folds (Figure 19).

In the Chloride Cliff region, stretching lineation orientations dominantly possess a SE-plunge due to the back rotation of the FMCC caused by isostatic rebound and footwall flexure during extensional exhumation of the complex. Comparison of stretching lineation orientations on a stereonet (Figure 19A) reveal parallelism of the D_2-D_4 fabrics. D_1 differs slightly from D_2-D_4

with an average slip vector of ~148° as compared to the slip vectors of 292° and 291° for D_2 and D_3/D_4 respectively. Determination of shear sense in the field was not always possible as some lithologies did not show shear sense well, and as such there are a large collection of lineation measurements with indeterminate kinematics that all fall within a similar range to the D_2-D_4 lineations. These indeterminate lineations were collected across the entire map area and likely represent fabrics from all deformational events.

Intersection lineation and fold hinge orientations typically exhibit low plunges (<30°) and are usually measured in weak clasts in heterogenous rock types or within weak lithologies such as carbonates. Several of the fold hinge measurements were also determined using cylindrical best fit analyses on Stereonet 9 (Allmendinger, 2013) from bedding measurements collected from outcrop-scale folds defined by the Johnnie Formation, Noonday Dolomite, and Kingston Peak Formation. A stereonet comparison of these fabrics shows striking parallelism (Figure 19B). The trend of fold axes typically varies within a 30-40° range and there are no obvious differences between D2 and D3/D4. The trend of contractional and extensional folds in this region is consistent with the expected orientations assuming standard fold vergence (transport perpendicular to hingeline) based on the direction of shearing from measured stretching lineations. This observation further supports the notion that folding in this region is related to contractional and extensional shear.

As noted above, both contractional and extensional fabrics show similarity in their orientations indicating they were formed by shear associated with a structure with a similar geometry. One way to explain this is to have different structures that have similar orientations but possess opposite kinematics, which formed the early contractional fabrics and the later extensional fabrics. The alternative explanation is that the structure responsible for burial reactivated during

extension and is responsible for the formation of the D_1-D_4 fabrics. Both scenarios are certainly viable, however when considering that reactivation plays a significant role in crustal deformation and has been a widely recognized and accepted mechanism (e.g. Donath, 1962; White et al., 1986; Holdsworth et al., 1997), it seems likely that if a structure existed at an orientation favorable to generate the fabrics observed during D3 and D4, then reactivation would preferentially take place in lieu of forming a new structure.

Inheritance of the Regional Structural Foliation

An alternative hypothesis to the genesis of the BCD still requires a strong genetic link to the early contraction in the Funeral Mountains. As mentioned previously, evidence from the metamorphic isograds indicates an initial dip of the regional stratigraphy of 30-40° to the NW (Hoisch and Simpson, 1993). The regional foliations generated during both contraction and extension of the FMCC tends to be subparallel to one another, at least in the region from Chloride Cliff to Monarch Canyon. Intracore shear zones and the BCD also possess a parallel to subparallel relationship to the regional stratigraphy, commonly localizing at stratigraphic contacts where a stronger lithology is in direct contact with a weak lithology; for example, the BCD localizes itself along the contact of the Stirling Quartzite and lower Johnnie schist from the northern portion of Chloride Cliff all the way to Monarch Canyon. The stratigraphic control of the BCD, and the reconstruction from metamorphic petrology of a 30-40° NW-inclination of bedding following burial of the Funeral Mountains (Hoisch and Simpson, 1993), requires slip on the BCD to have initiated at a low-angle. If this low-angle slip was not accommodated due to reactivation of a pre-existing fault, then it seems likely that contrasting rheologies and weaknesses generated by the regional foliation, together with the regional NW dip, may have influenced the geometry and kinematics of the BCD. The idea of structural and stratigraphic anisotropies governing the

orientation of faults and fractures is not new. Donath (1962) demonstrated that fractures forming in a slate typically formed parallel to the cleavage out to orientations of 60º from σ_1.

Regional Thrust Correlations

To generate enough burial to reach the peak conditions seen in the Funeral Mountains, a large regionally significant thrust would be required. Several studies have addressed the timing, geometry, and kinematics of regional thrust sheets within this region (e.g., Snow and Wernicke, 1989; Caskey and Schweickert, 1992; Andrew and Walker, 2009; Pavlis et al., 2014; Giallorenzo et al., 2018), however none of these currently recognized thrust sheets provide a particularly satisfying fit to the story. The proposed timing of Late Jurassic thrust burial fits well with the timing of exhumation of the Wheeler Pass thrust sheet as revealed by low-temperature thermochronometers, however stratigraphic correlations and geographic positioning make correlating these two structures unlikely (Giallorenzo et al., 2018). Given these conditions, the hypothesis of thrust reactivation would require the addition of a new thrust sheet, which is currently expressed by the BCD.

The BCD has been correlated with the Fluorspar Canyon fault system at Bare Mountain and the Bullfrog Hills detachment fault system, two separate detachment systems to the north of the Funeral Mountains (Hamilton, 1988; Maldonado, 1990, and references therein). Similar to the FMCC, there appears to be a trend of increasing grade to the NW within the core of the Bare Mountains. These kinematic similarities and the relative position of the ranges has led to a hypothesis that the detachment faulting responsible for exhumation of all three ranges are connected and a part of the same system (Hamilton, 1988; Maldonado, 1990; Hoisch et al., 1997). If this hypothesis is correct, and the BCD does extend as far north as the Bullfrog Hills, then this could represent the northern extension of the proposed thrust sheet. This would also require this

structure to be responsible for peak metamorphic grades in these ranges and to have originally been the thrust responsible for burial.

Correlating this structure to the south and the west of the Funeral Mountains becomes significantly more difficult. Right-lateral translation due to the NDVFZ, FCFZ, and the SDVFZ have offset the east and west sides of Death Valley and made a direct correlation of structures difficult. Reconstructions of these of Cenozoic dextral strike-slip faulting through the comparison of correlative structures that possess similar geometries, kinematics, and broadly consistent ages, have given similar estimates of offset ranging from 68 ± 4 km (Snow and Wernicke, 1989) and 68 ± 14 km (Renik and Christie-Blick, 2013). Given these estimates, any correlation of the BCD across these fault zones would place a correlative structure within the central portion of the Last Chance Range. The Last Chance thrust, a significant regional thrust fault with slip estimates of 30-32 km (Stewart et al., 1966; Stevens and Stone, 2005), is present in this range and is a tempting candidate for correlations with burial in the Funerals, however studies have determined a likely Permian age of slip, which significantly predates the timing of burial in the Funerals (Stevens and Stone, 2005). Although a correlative structure should exist elsewhere in the Death Valley region, at this time there are no satisfying correlations that can be made.

The interpretation of the BCD as a reactivated thrust sheet would place a new thrust between the currently mapped Grapevine/Ubehebe thrust, which has been correlated with the Last Chance thrust by Snow and Wernicke (1989), and the Marble Canyon/Schwaub Peak thrust. As stated earlier, the Last Chance thrust is interpreted as a Permian structure; the Marble Canyon/Schwaub Peak thrust has a similar interpreted age with broad constraints between the Late Permian and Middle Triassic (Snow et al., 1991; Snow, 1992). This would place a Jurassic aged thrust in between two Permo-Triassic thrust faults. It is important to note that the Late Jurassic

garnets from Indian Pass (Hoisch et al., 2014) overgrow a crenulation cleavage and likely reflects garnet growth near the end of burial. This proposed thrust sheet is associated with contractional deformation within the Cordillera and may have developed just prior to, and may slightly overlap in time with, the Late Jurassic Wheeler Pass thrust sheet.

CONCLUSIONS

New geologic mapping, structural analysis, and geochronology, coupled with prior studies, has refined the Jurassic to Miocene tectonic history of the Funeral Mountains and elucidated a history of tectonic reactivation. During the Middle to Late Jurassic, thrust development, NW underthrusting of footwall strata, and associated burial led to peak metamorphism and development of a regional foliation. Following this burial, continued contraction led to folding of this regional foliation at the bedding scale and the development of map-scale folds. Major contractional deformation in this region ended prior to intrusion of a 95 Ma peraluminous granitic intrusion that cross-cuts contractional fabrics. Following contractional deformation, a period of NW-directed shear during the Late Cretaceous led to rapid cooling and partial exhumation of the FMCC rocks and imparted a mylonitic fabric on the 95 Ma granite. A second period of NW-shear associated with detachment faulting during the Miocene led to the final exhumation of the FMCC, exposing rocks in the Monarch Canyon region that had been buried to depths of ~32-35 km in the Late Jurassic. This final exhumation of the FMCC was accomplished through slip along the BCD, a regionally significant detachment fault that may be correlative to detachment faults at both Bare Mountain and the Bullfrog Hills to the north.

Present orientations of the BCD with respect to regional stratigraphy, and reconstructions of a 30-40° dip of stratigraphy interpreted from regional metamorphic isograds, provide evidence that slip initiated and continued at low-angles. Mapped traces of major Late Jurassic thrust faults in the Funeral Mountains region are absent, but structural and kinematic evidence from the Chloride Cliff region may provide evidence for reactivation of an early thrust fault as a mechanism for detachment faulting during both the Late Cretaceous and Miocene extensional events. Mylonitic and fold fabrics associated with both earlier contractional (D_2) and later extensional

47

deformation events (D_3 and D_4) recorded in this region possess a sub-parallel relationship and are typically parallel to sub-parallel to the orientation of regional foliations generated during initial burial (D_1) of the FMCC. Recognition of this large-scale burial may require the addition of another regionally significant thrust that currently lacks a surface trace and has been previously undocumented due to large scale reactivation, which has overprinted and obscured evidence of the original nature of the fault zone. The unique geology of the FMMCC, in particular its metamorphic field gradient and the concentration of extensional strain at the deeper NW end of the complex, provides an opportunity to examine the importance of tectonic reactivation and inheritance as a major mechanism for facilitating detachment faulting within the Earth's crust.

Appendix A: Figures
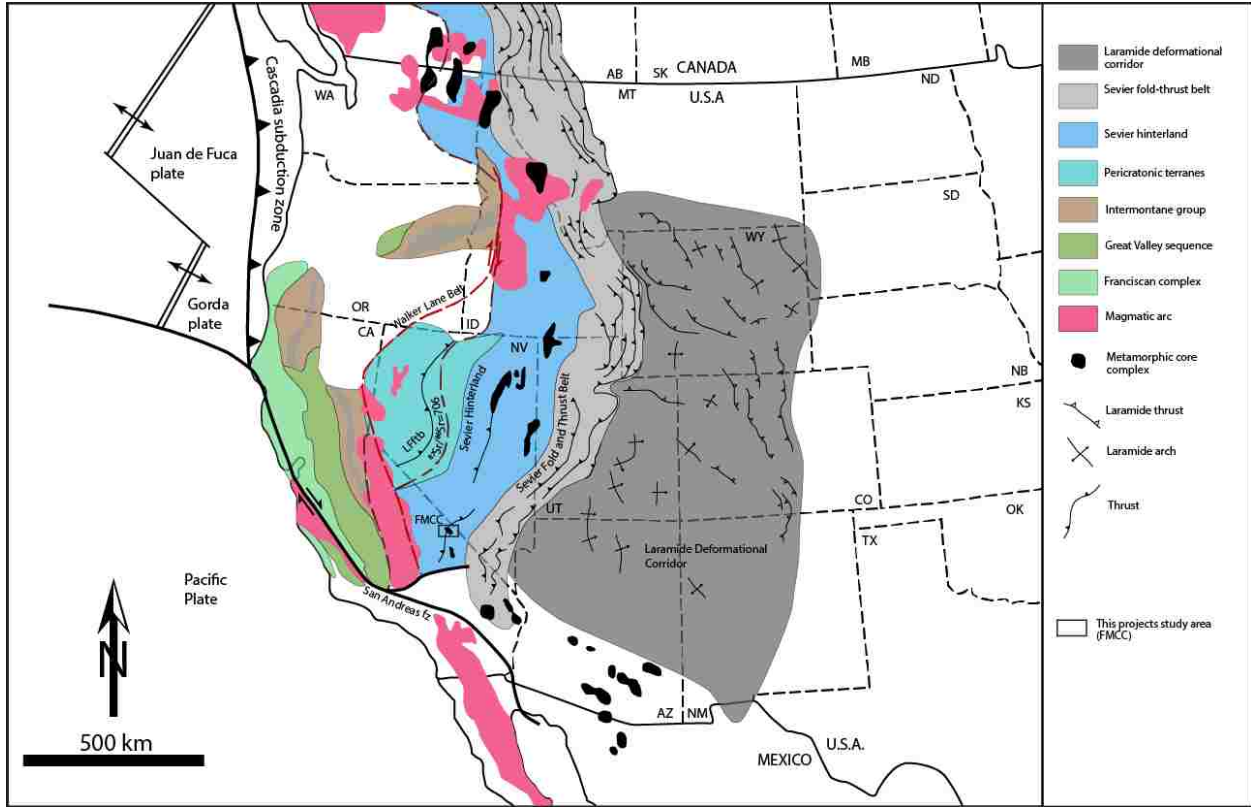
Figure 1: Regional geology of the western U.S. Cordillera: Simplified tectonic map of the US Cordillera, which highlights specific Paleozoic to present day structural domains and structures. Black box outlines the FMCC. Modified after Hoisch et al., 2014 and Yonkee and Weil, 2015.
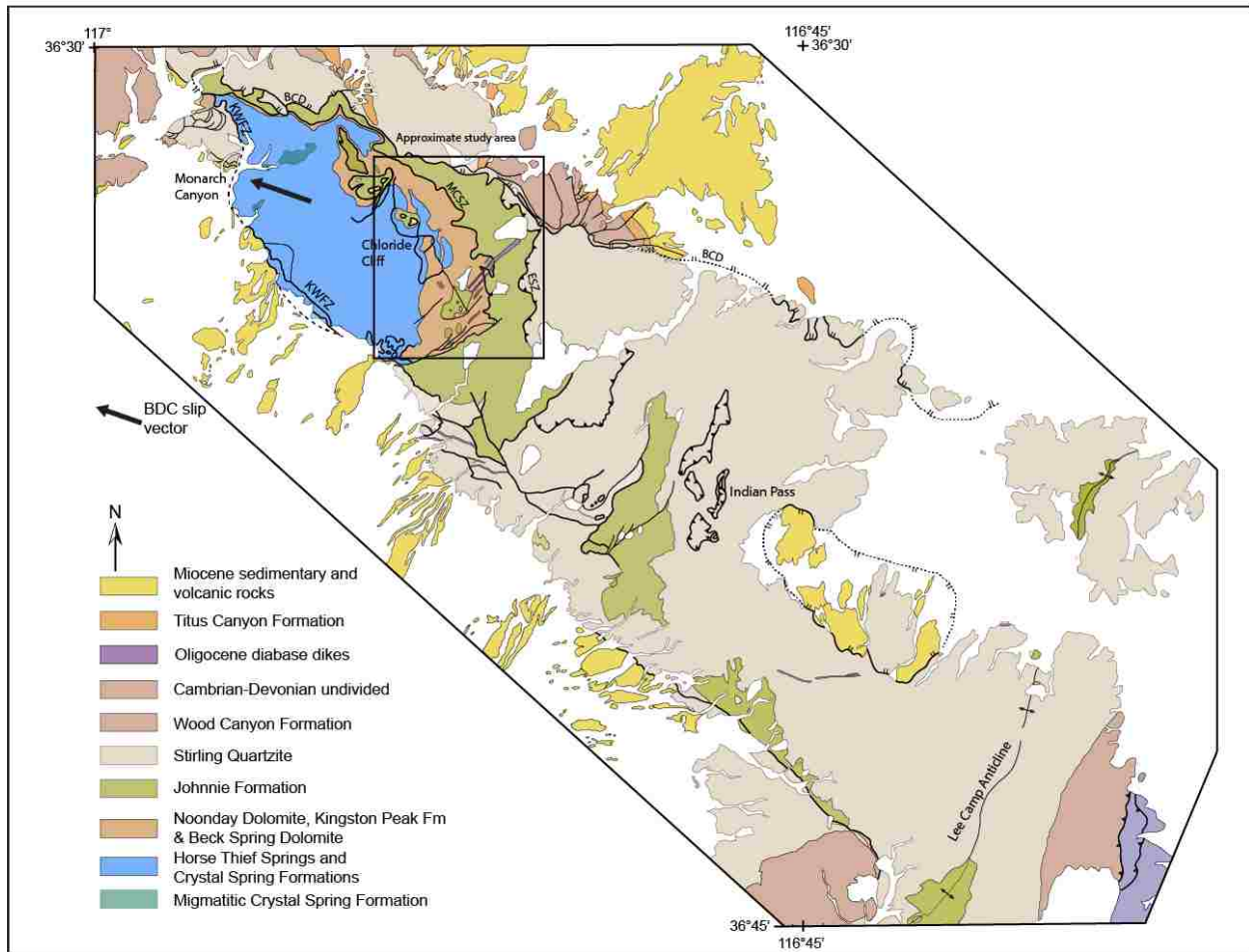
Figure 2: Generalized map of the Northern and Central Funeral Mountains. Black box denotes the approximate map area for this study.
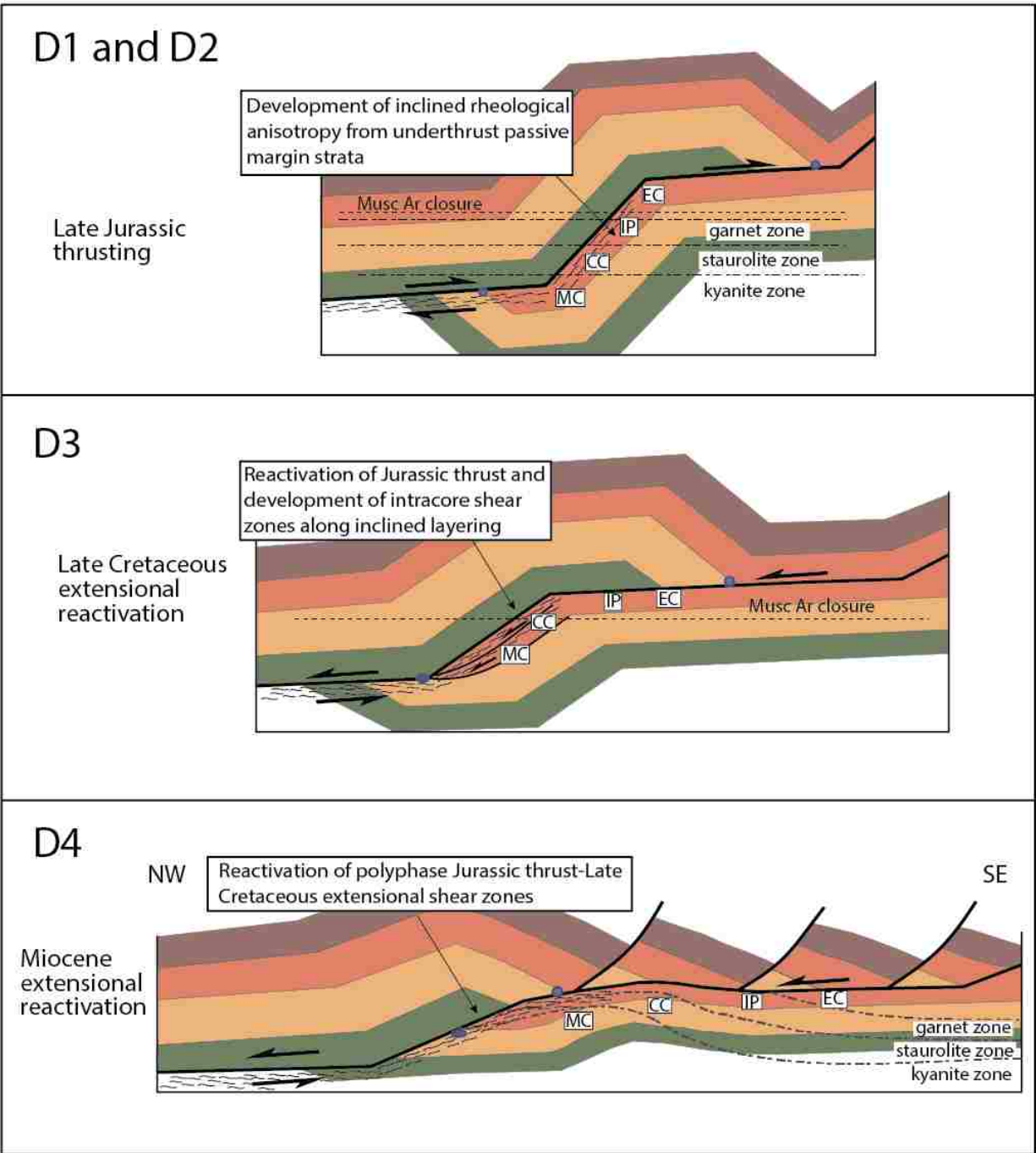
Figure 3: Schematic diagram of proposed reactivation hypothesis: Geologic history of the Funeral Mountains illustrating our hypothesis of tectonic reactivation as the mechanism for low angle normal faulting. EC: Echo Canyon, IP: Indian Pass, CC: Chloride Cliff, MC: Monarch Canyon.
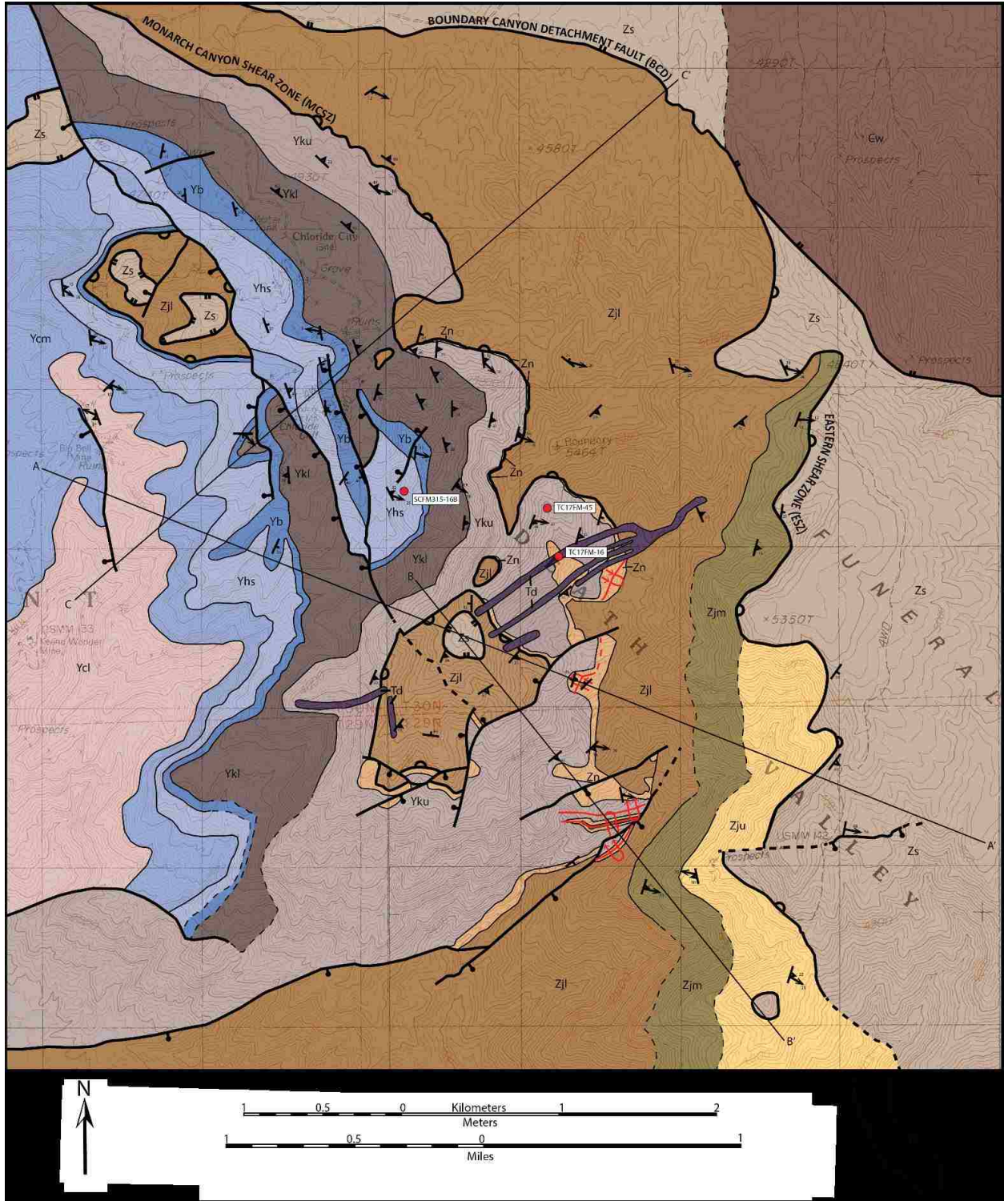
Figure 4: Map, Legend, and Cross sections of the mapping area: Map was constructed at 1:10000 scale.

Figure 4 (continued)
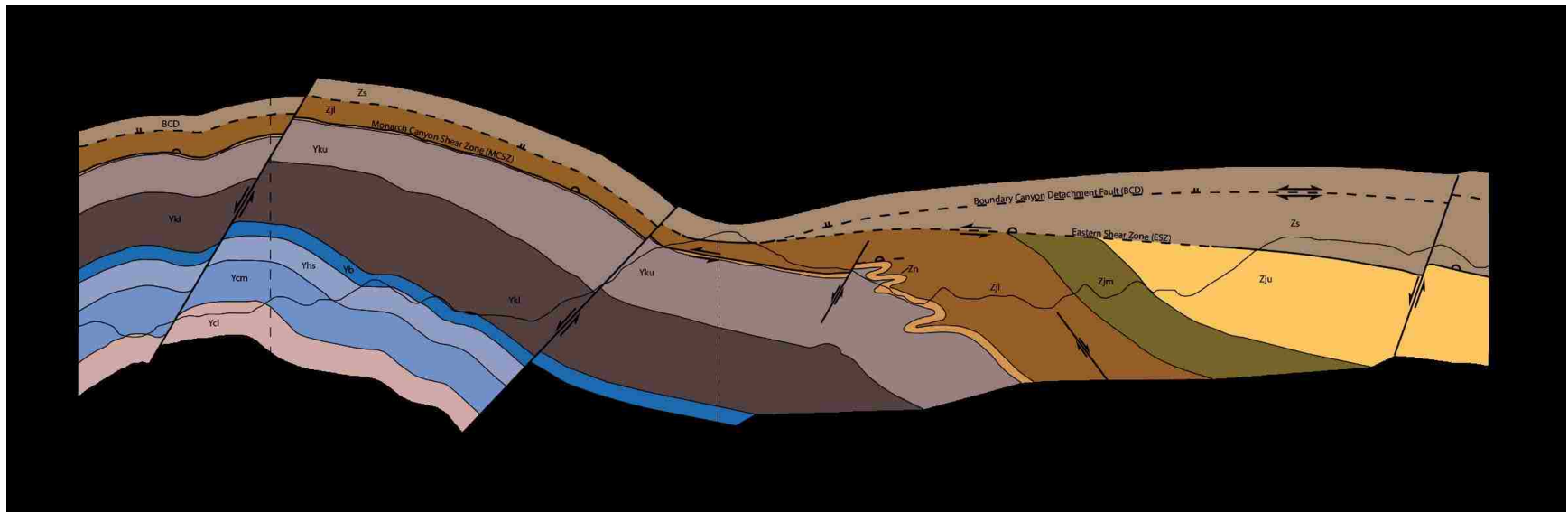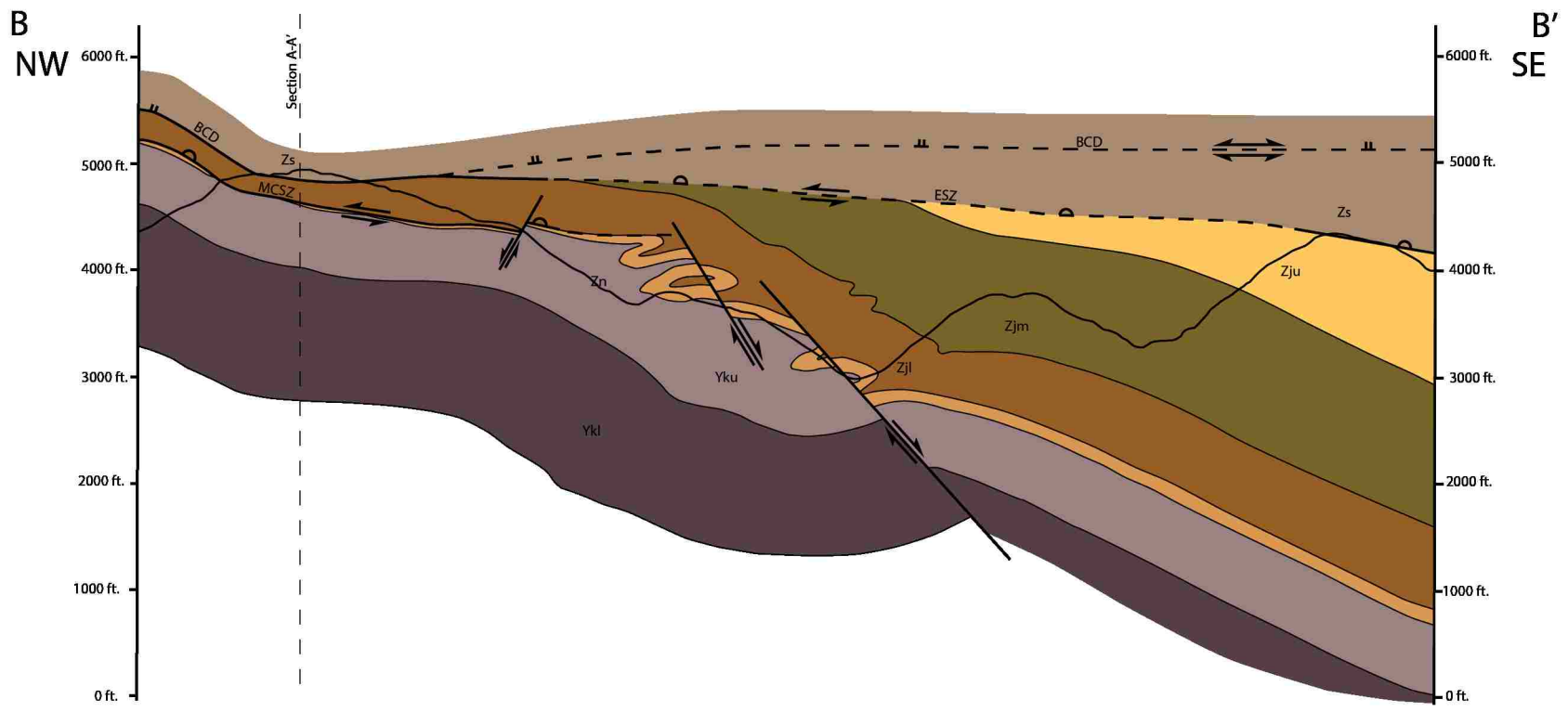
Figure 4 (continued)
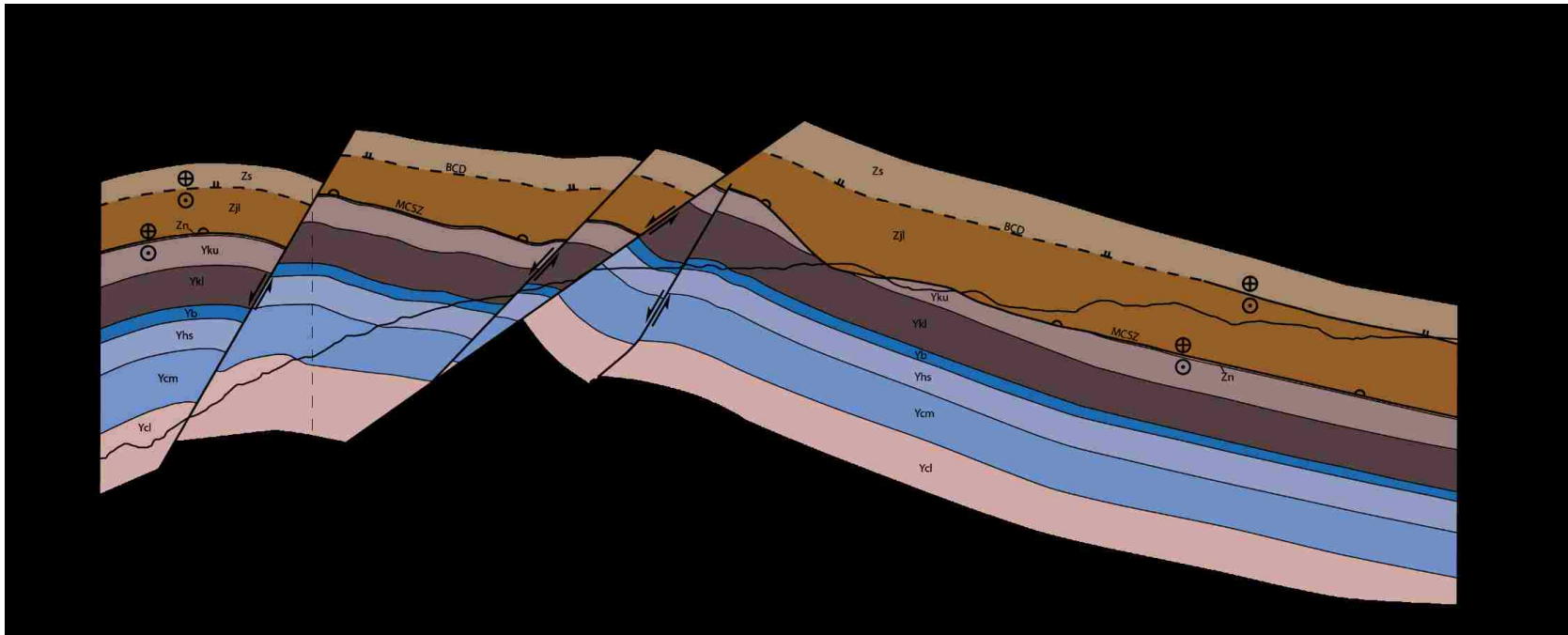
Figure 4 (continued)

Figure 4 (continued)
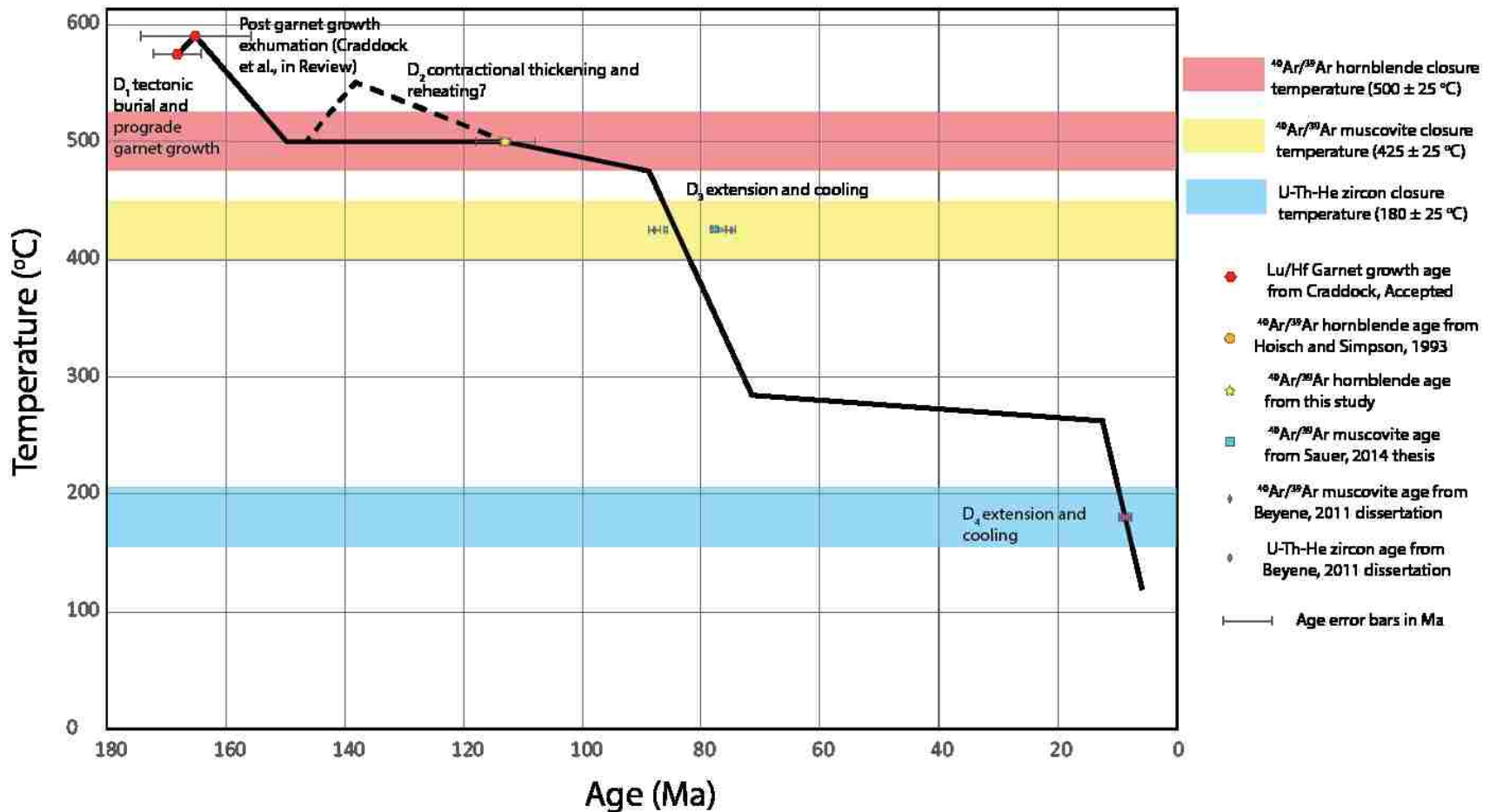
Figure 5: Generalized cooling history of the Chloride Cliff region: Thermal history of the Chloride Cliff region based on thermochronology from other studies and a single $^{40}Ar/^{39}Ar$ amphibole age from this study. Dashed line indicates interpretations based on field relationships but have no hard constraints. Temperature drop following garnet growth is based on observations from Hoisch et al., 2014 where they observed a large temperature drop following garnet growth in the Indian Pass region.
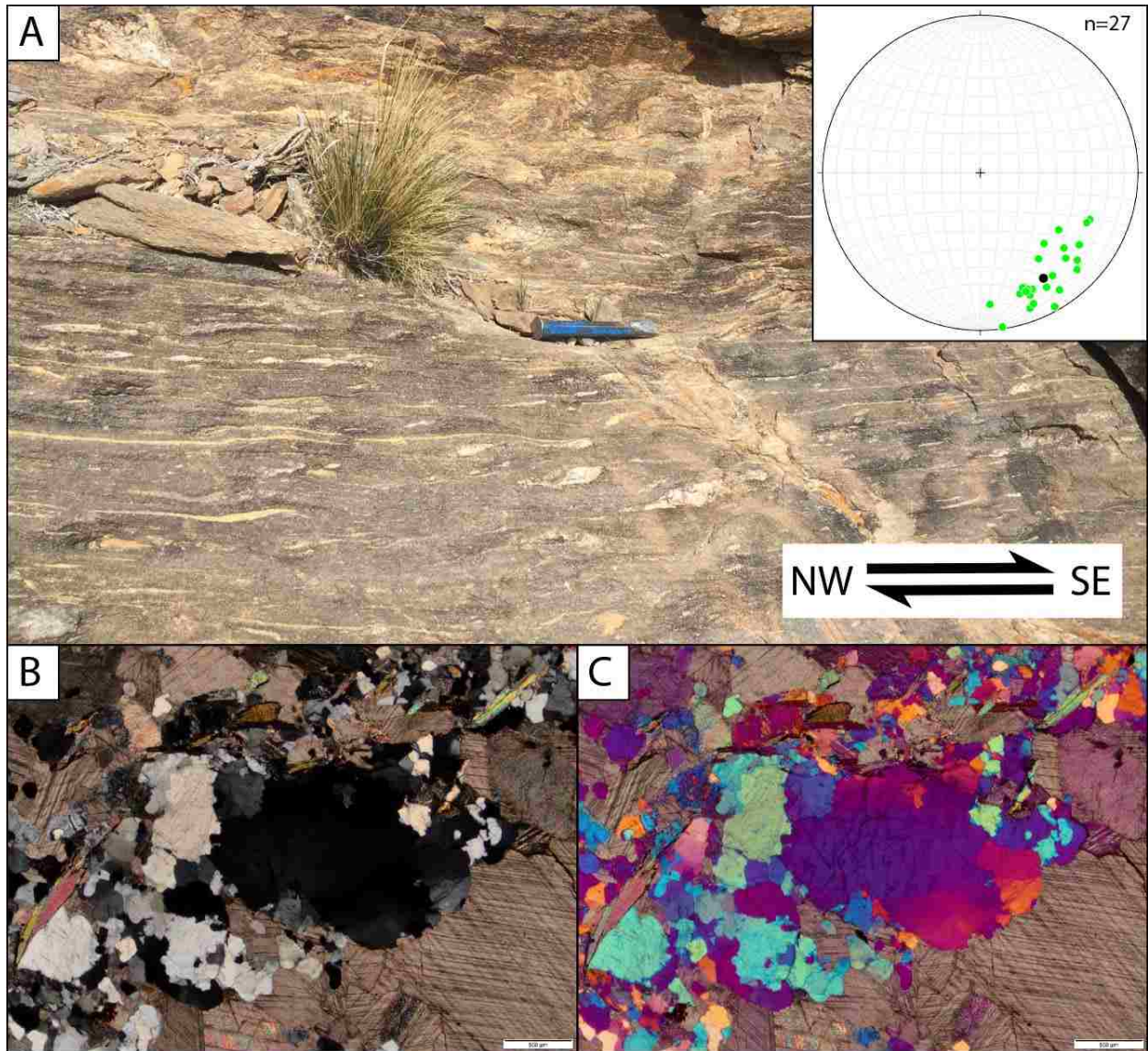
Figure 6: D₁ deformation figure: A) Field photo of the Kingston Peak Diamictite where the D_1 foliation is preserved and unaffected by D_2. Diamictite contains long, strung out dolomite clasts and highly asymmetric quartzite clasts that provide shear sense. Inset is a stereogram of stretching lineations measured in locations that preserve D_1 deformation with average stretching lineation (black circle) of 21, 148. B) Photomicrograph in cross polarized light from sample TC17FM-46, collected just SE of field photo, displaying quartz GBM textures. C) Photomicrograph from B with inserted gypsum plate.
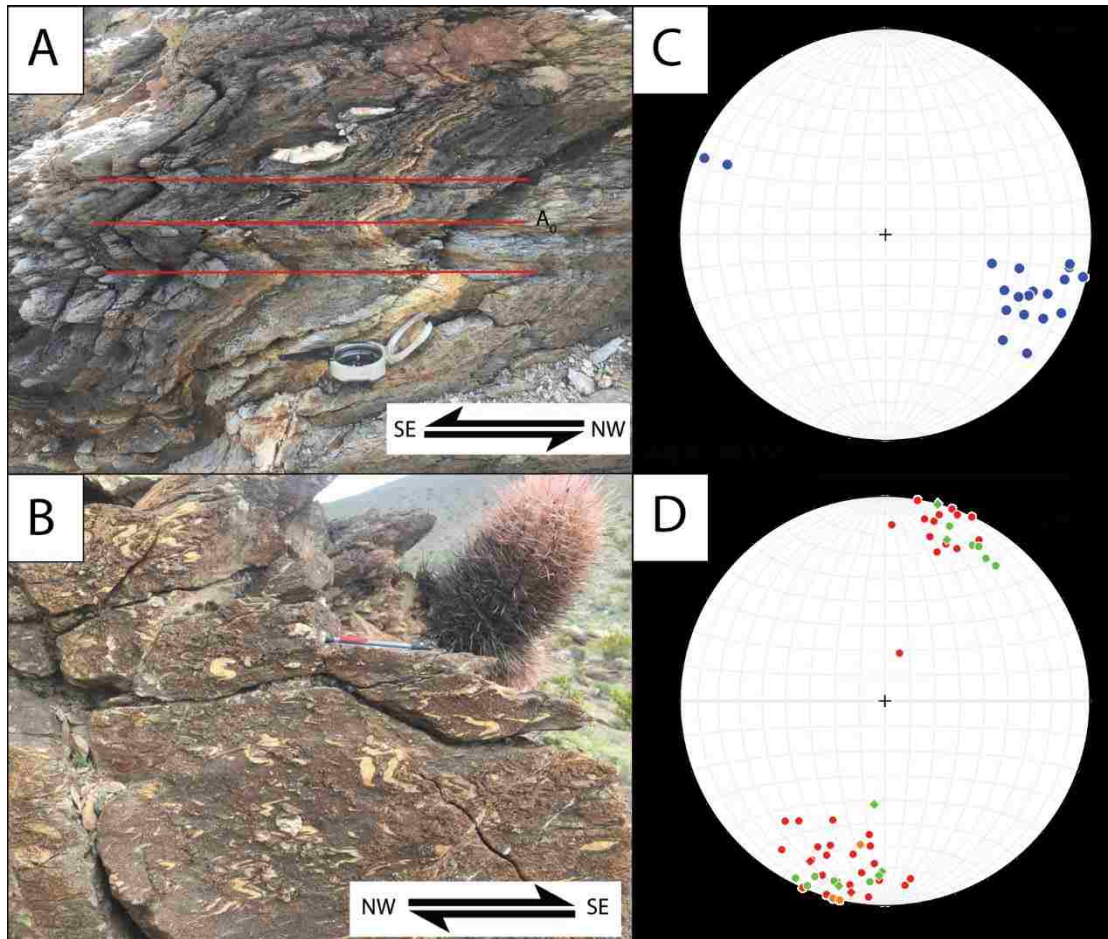
Figure 7: D₂ deformation figure: Fabrics associated with D_2 deformation A) Photo of lower Johnnie schist with folded D_1 foliation. Red lines define axial surfaces of bedding-scale SE-vergent folds. B) Photo of Kingston Peak diamictite with asymmetrically folded clasts with SE-vergence. C) Stereogram of stretching lineations measured in locations associated with D_2 deformation. D) Stereogram of intersection lineations and fold hinges. Diamonds: intersection lineations, Circles: hinge lines, Red: Kingston Peak, Orange: Johnnie Fm., Green: Noonday.
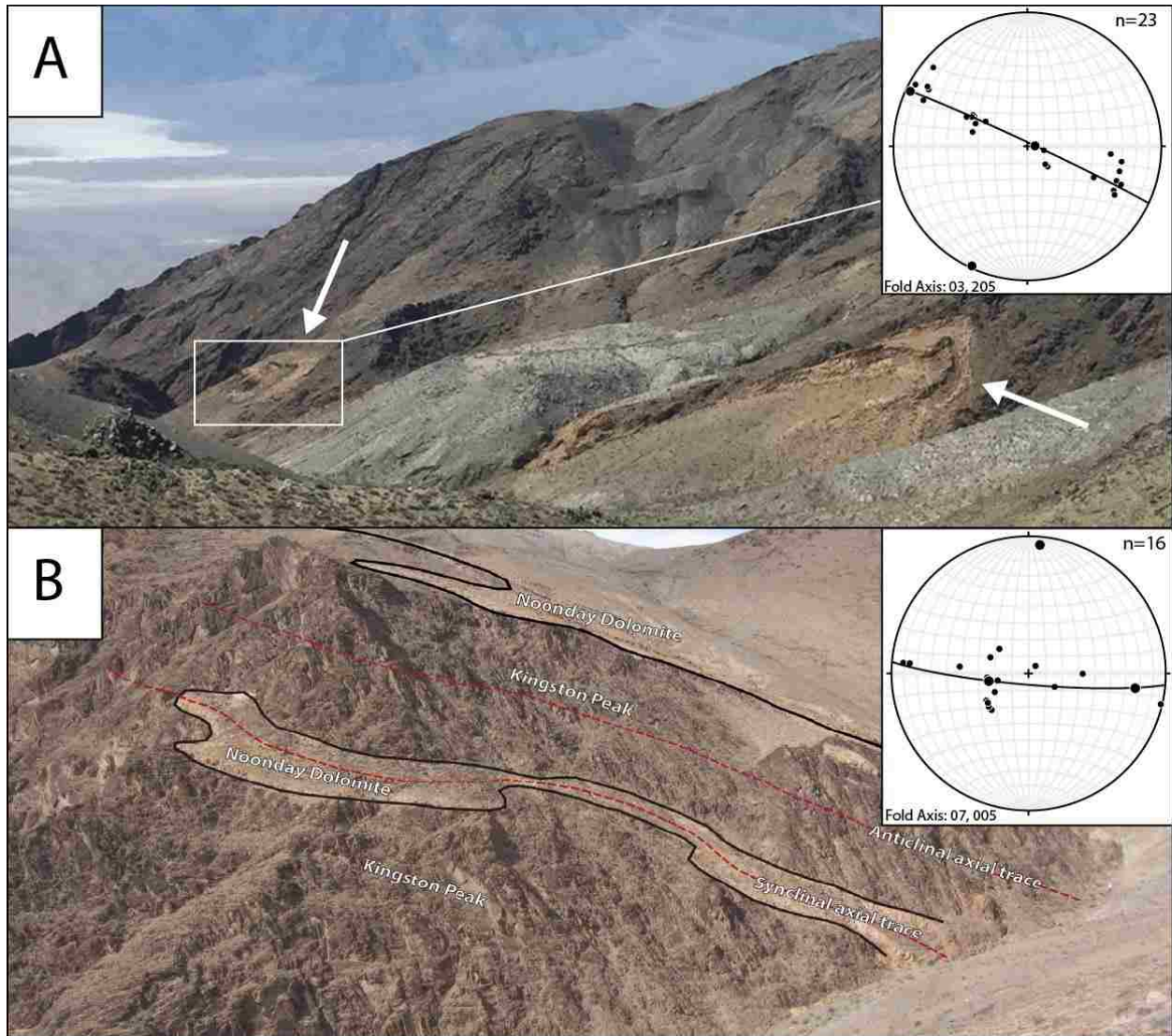
Figure 8: D₂ Outcrop scale folding: A) Photo looking W with white arrows pointing to two folds defined by folded Kingston Peak Formation and Noonday Dolomite, cored by Johnnie Formation (too small to label). Inset shows a Pi diagram of folded noonday surrounded by the white box indicating a fold axis of 03°, 205°. B) Anticline-syncline fold pair defined by the Noonday Dolomite and Kingston Peak Formation. Inset shows Pi diagram with measurements from the syncline with a fold axis of 07°, 005°.
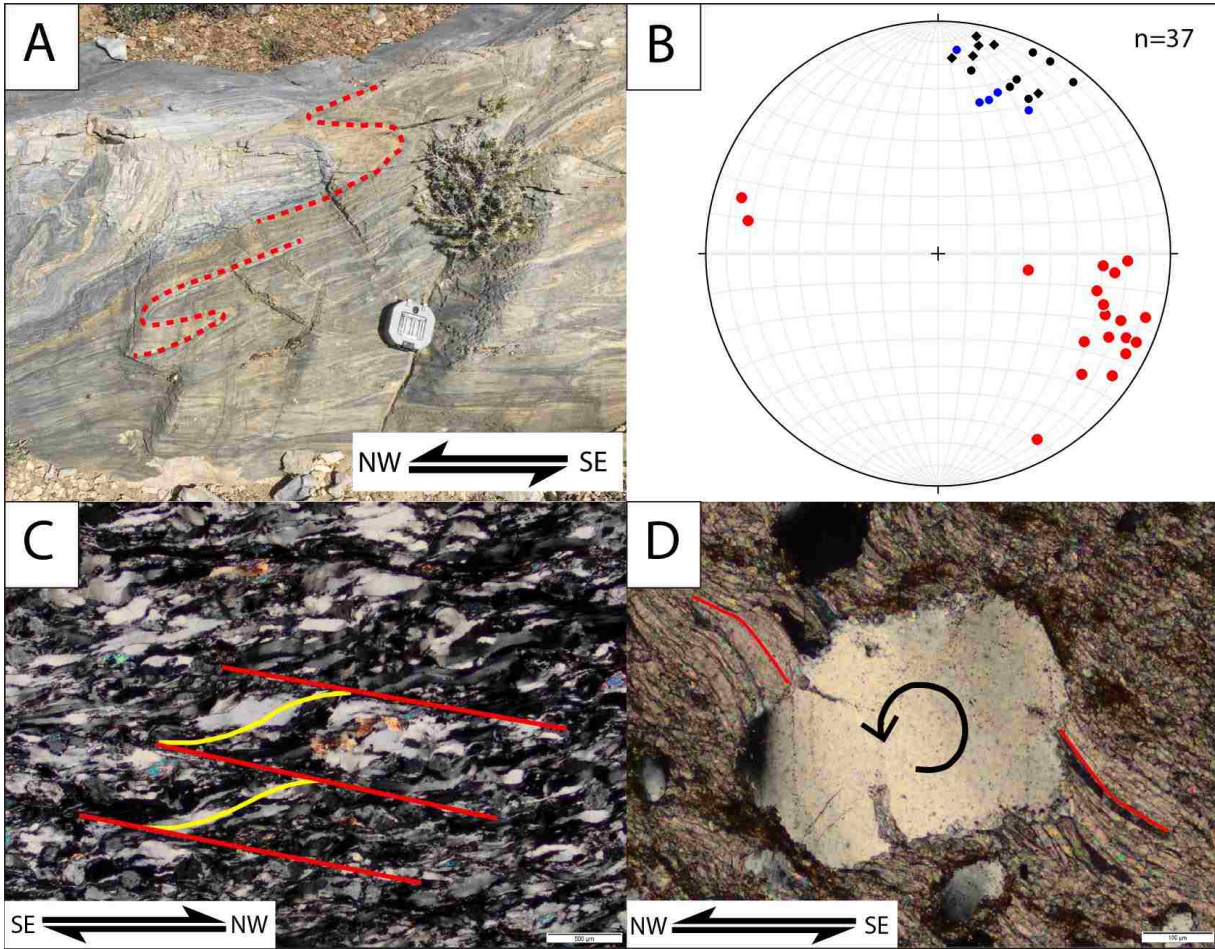
Figure 9: D₃ and D₄ deformation style: A) Photo of Beck Springs Dolomite with NW-vergent bedding scale folds. B) Stereogram of stretching lineations (Red), intersection lineations (Diamonds), and fold hinges (black and blue circles). Blue: Beck Springs Dolomite, Black: Crystal Springs Fm. C) photomicrograph of quartzite in the Johnnie Fm. (Sample TC17FM-43) at the CSZ, which displays strong C'-bands (red) and S-foliation (yellow). D) Calcite strain fringe from the noonday dolomite showing NW-directed kinematics (Sample MW13FM-17) .
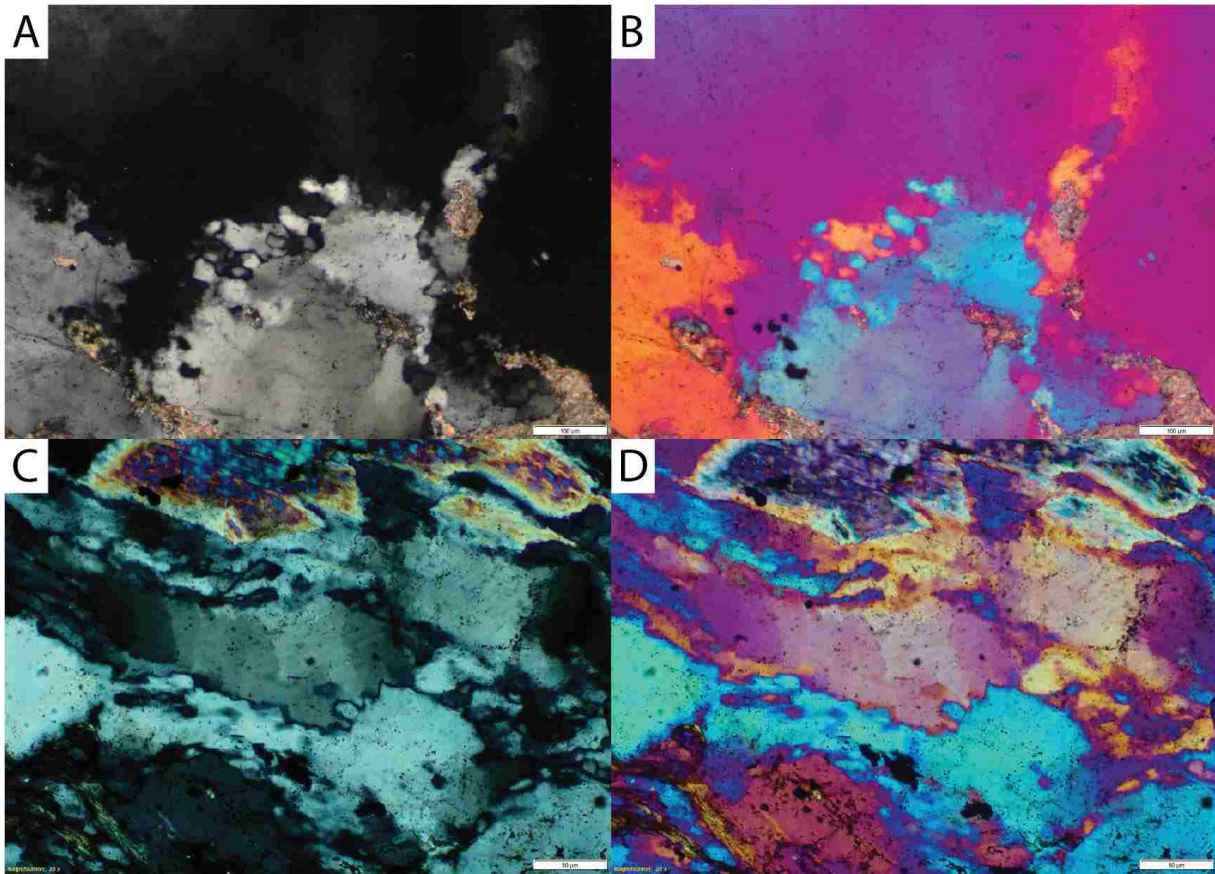
Figure 10: D₃ and D₄ deformation conditions: Photomicrographs of dynamically recrystallized quartz from samples with NW-directed kinematics. A) Photomicrograph from the Crystal Springs Fm. (Sample TC17FM-40) that displays BLG recrystallization in quartz. B) Same photomicrograph from A with gypsum plate inserted. C) Photomicrograph from quartzite in the Johnnie Fm. at the MCSZ (Sample TC17FM-43) that displays BLG recrystallization in qtz. D) Same photomicrograph from C with gypsum plate inserted.
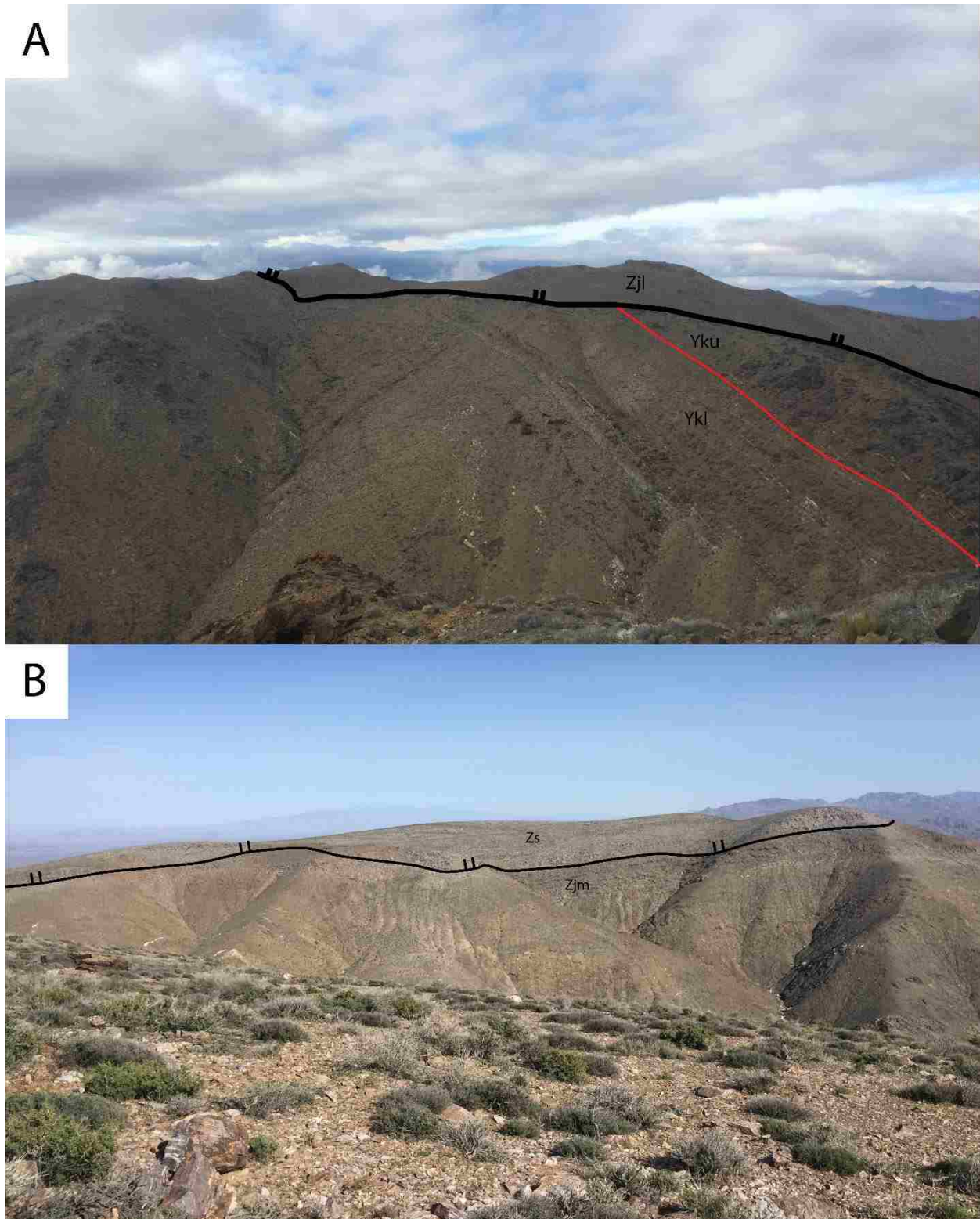
Figure 11: Eastern Shear Zone and Monarch Canyon Shear Zone: Annotated field photos of the Monarch Canyon shear zone (A) and the Eastern shear zone (B). Hatch marks are on the hanging wall side of the shear zone.
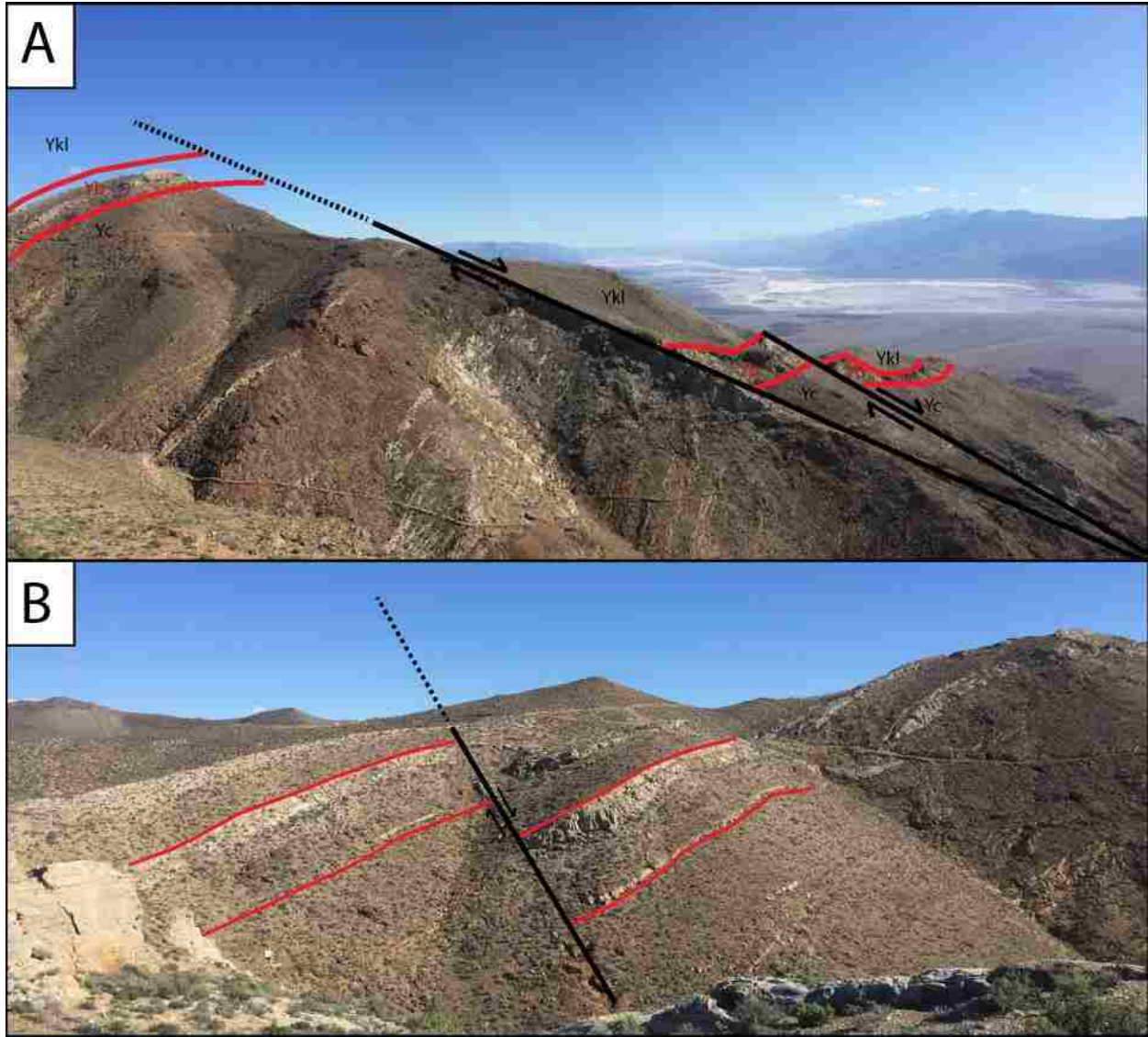
Figure 12: Brittle extensional faulting: Field photo of brittle faults near Chloride Cliff proper. A) Photo facing S of the Big Bell fault and a related splay down dropping the Crystal Springs, Beck Springs, and Kingston Peak to the W. B) Small brittle fault to the east of the Big Bell fault with similar kinematics.
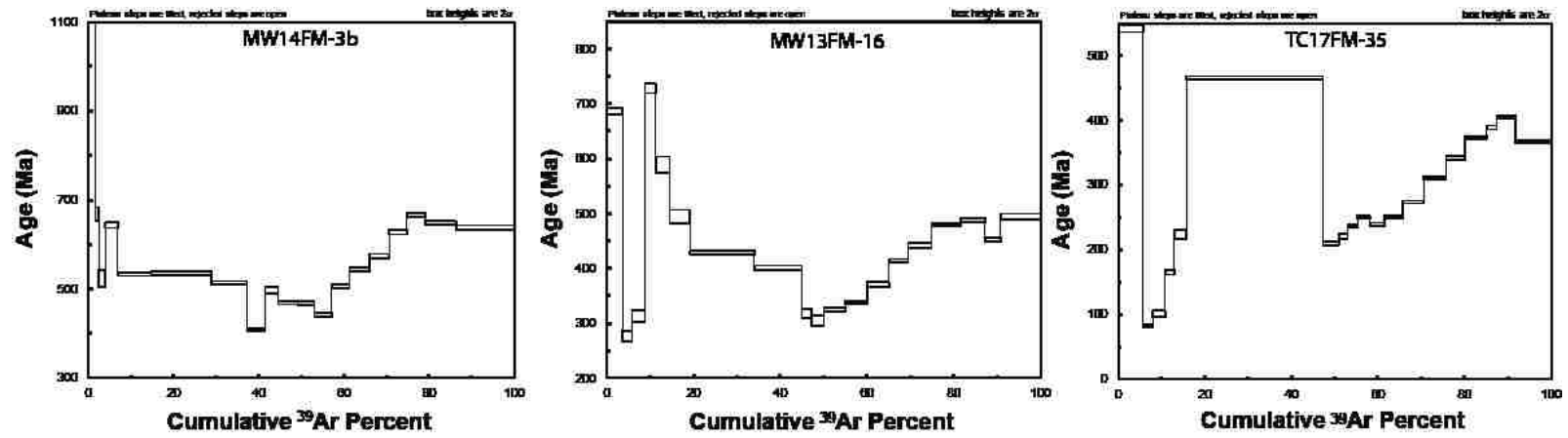
Figure 13: ^{40}Ar/^{39}Ar hornblende spectra of failed analyses: ^{40}Ar/^{39}Ar hornblende age of the 3 samples interpreted to have variable incorporation of excess argon.
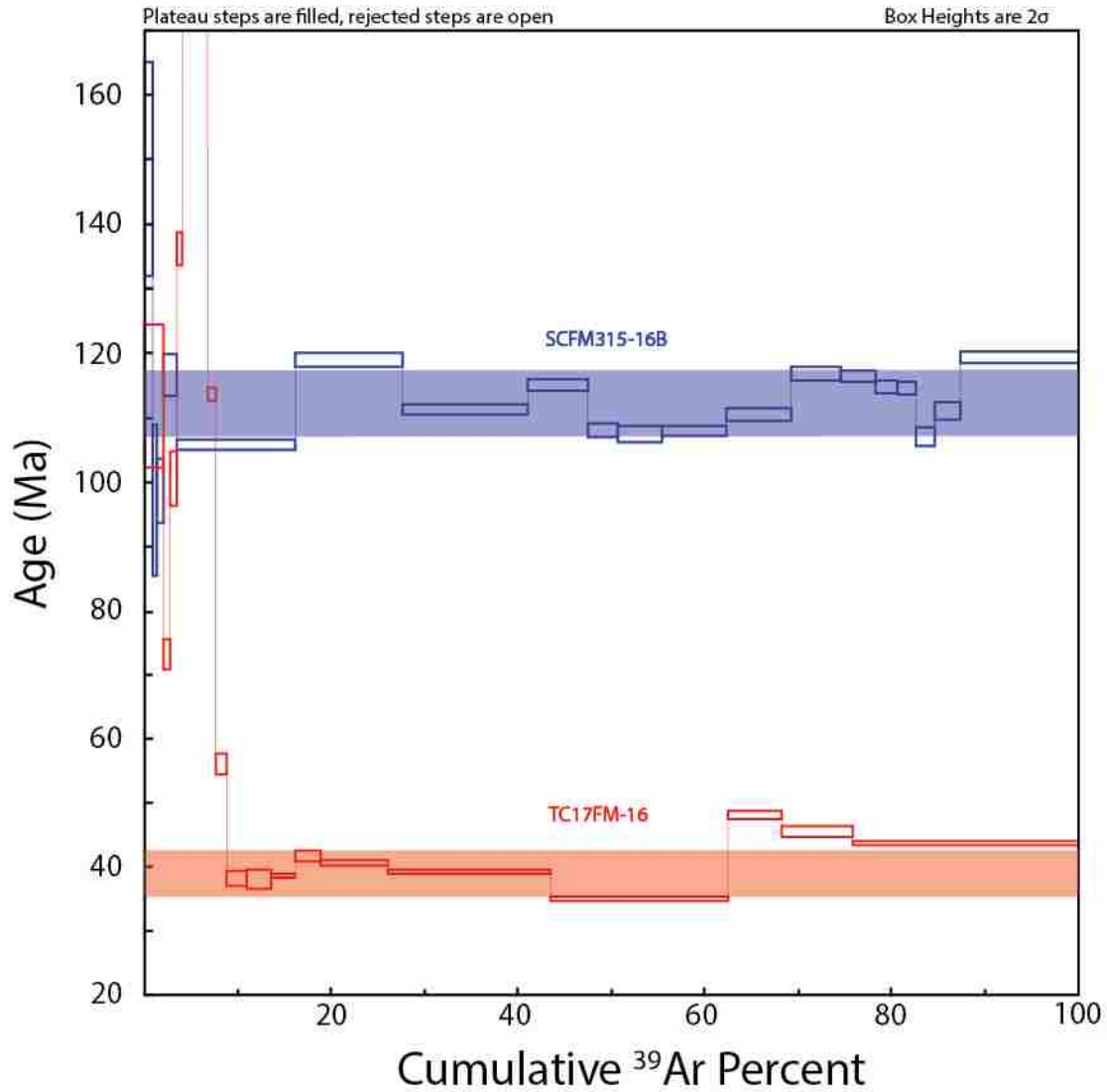
Figure 14: ^{40}Ar/^{39}Ar hornblende spectra of accepted analyses: ^{40}Ar/^{39}Ar spectrum for samples TC17FM-16 (Red) and SCFM315-16B (Blue). Colored boxes indicate range of ages that a majority of the gas steps cover for each sample. SCFM315-16B has a range of ~118-108 Ma and TC17FM-16 has a range of ~42-36 Ma.
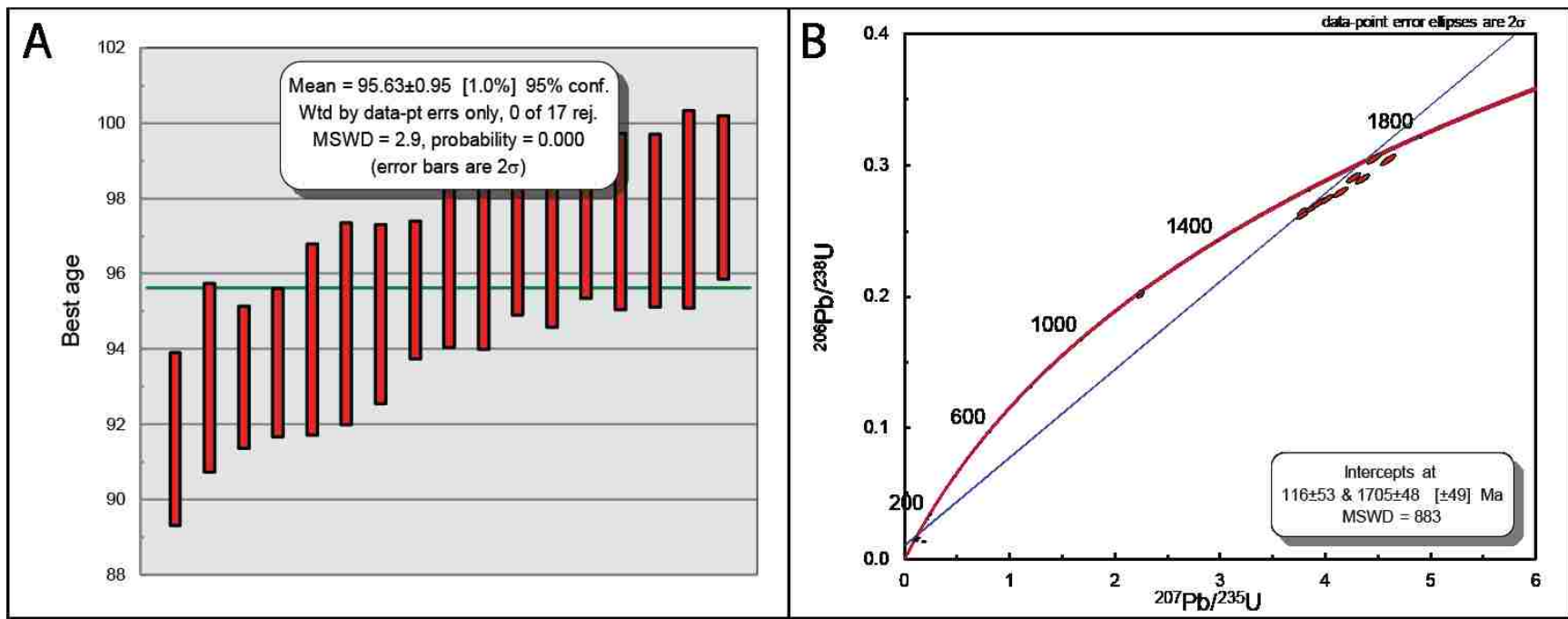
Figure 15: U-Pb mean weighted age and Concordia plot: A) Mean weighted U-Pb age from a coherent set of 17 igneous zircon grains generated using tuffzirc. B) Conventional Concordia plot of 37 inherited and igneous zircon grains.

67
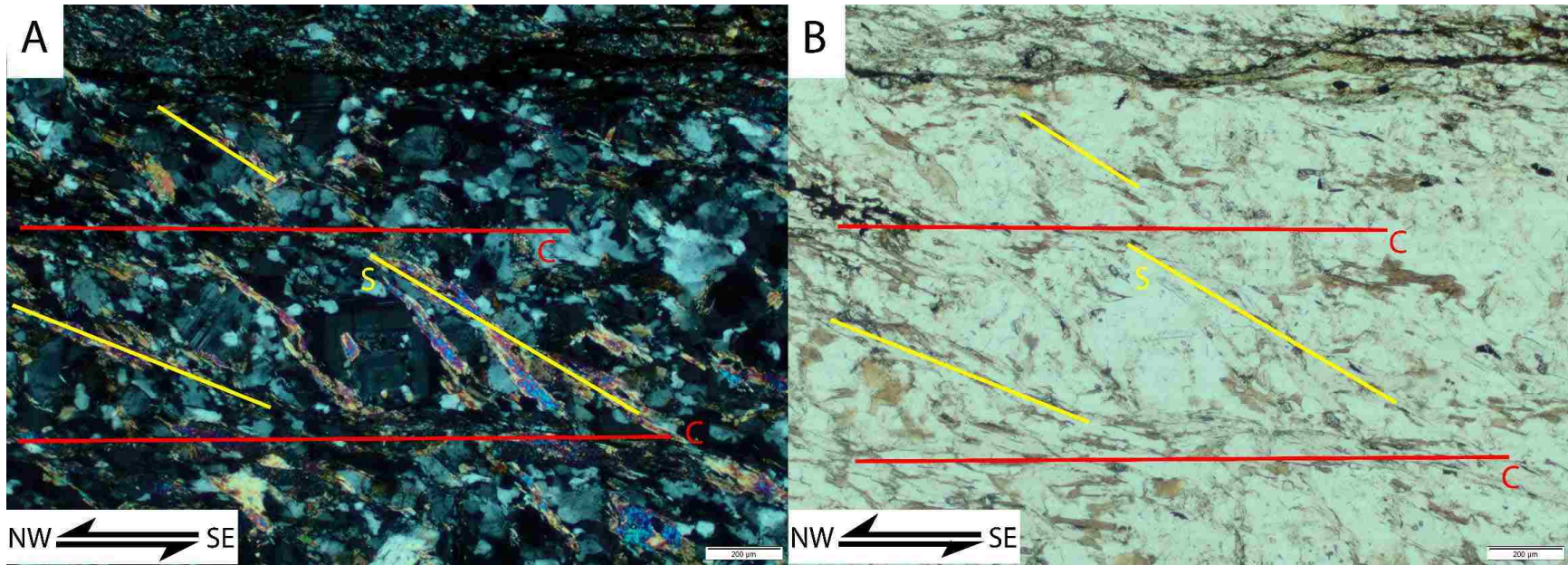
Figure 16: Microdiorite photomicrographs: Photomicrograph of microdiorite intrusion in A) cross polarized light and B) plane light (sample TC17FM-45). Red lines indicate C-foliations and yellow lines indicate S-foliations. These fabrics provide evidence for top to the NW sense of shear.
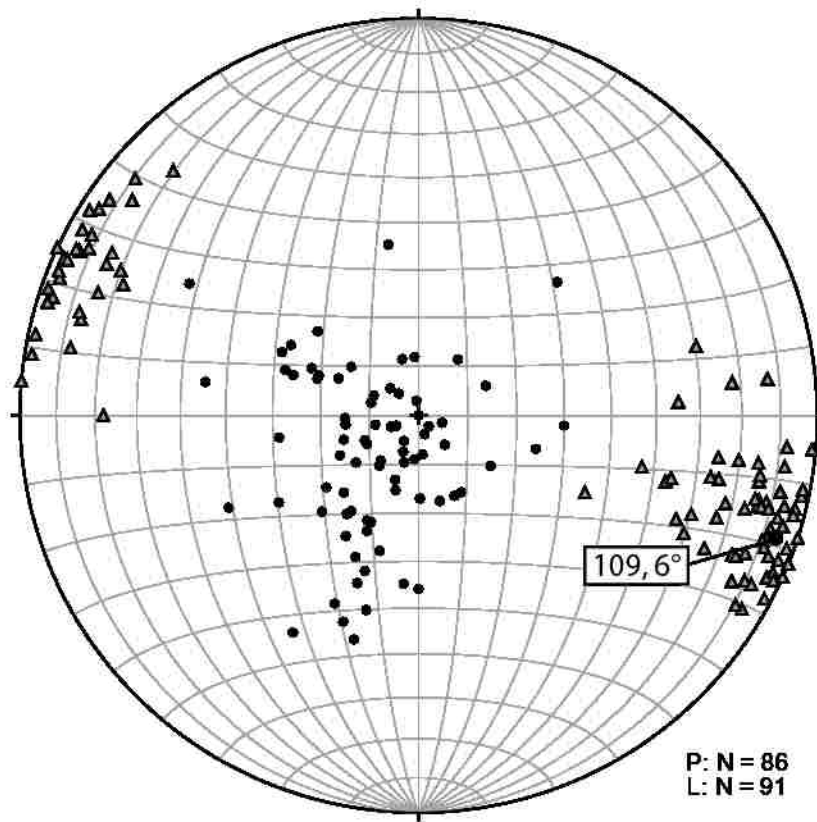
Figure 17: D4 stretching lineation stereogram: Stereogram of poles (P) to foliation (circles) and stretching lineations (L; triangles) from the highly strained marble tectonite in Earl Canyon. Average stretching lineation marked by large black circle (109, 6°).
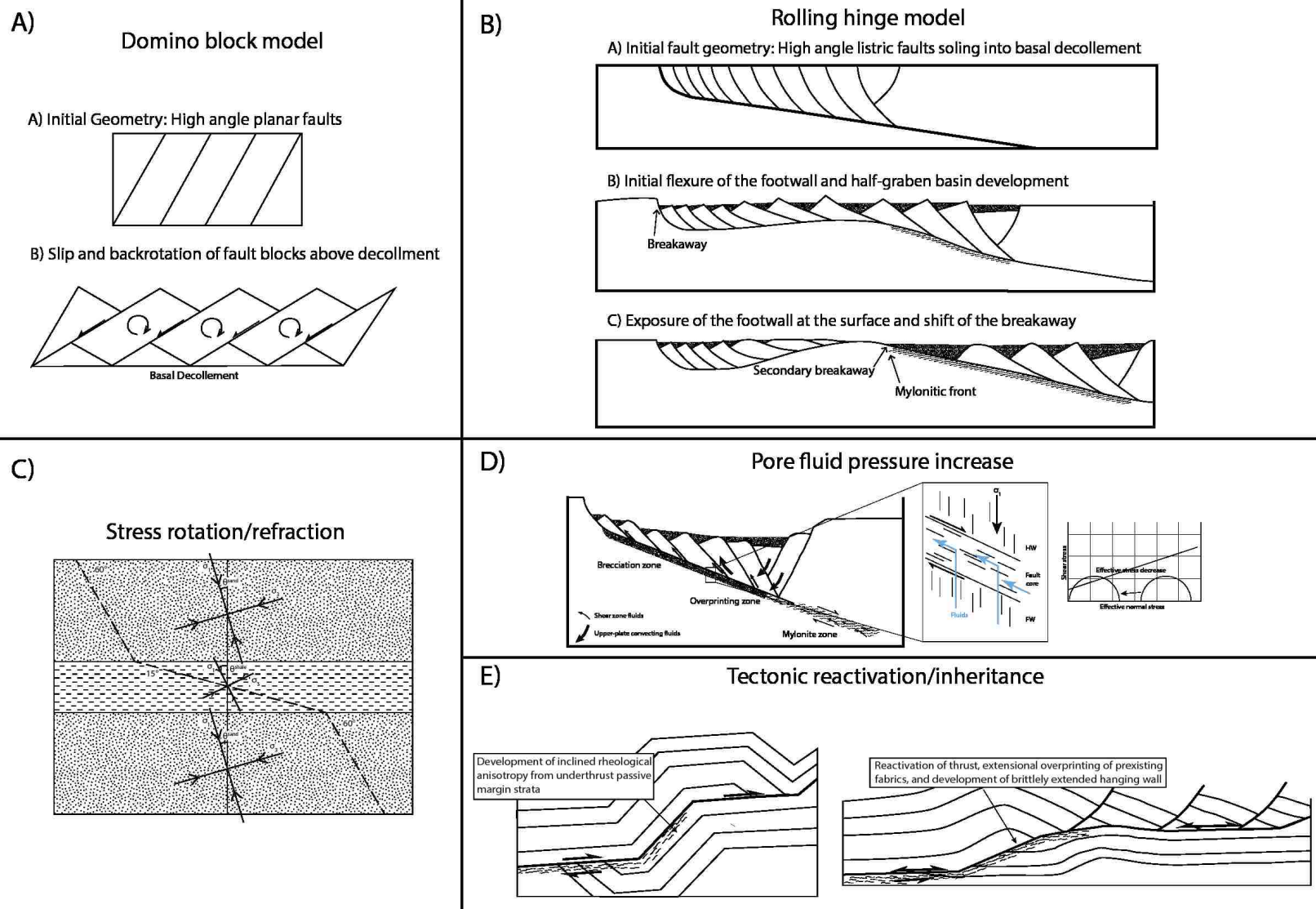
Figure 18: Low angle normal faulting models' diagram: A) Modified after Axen, 1988. B) Modified after Axen et al., 1997. C) Modified after Bradshaw and Zoback, 1988. D) Modified after Reynolds and Lister, 1987 and Healy, 2008. E) Reactivation model that incorporates footwall collapse during initial thrusting based on our model for the Funerals.
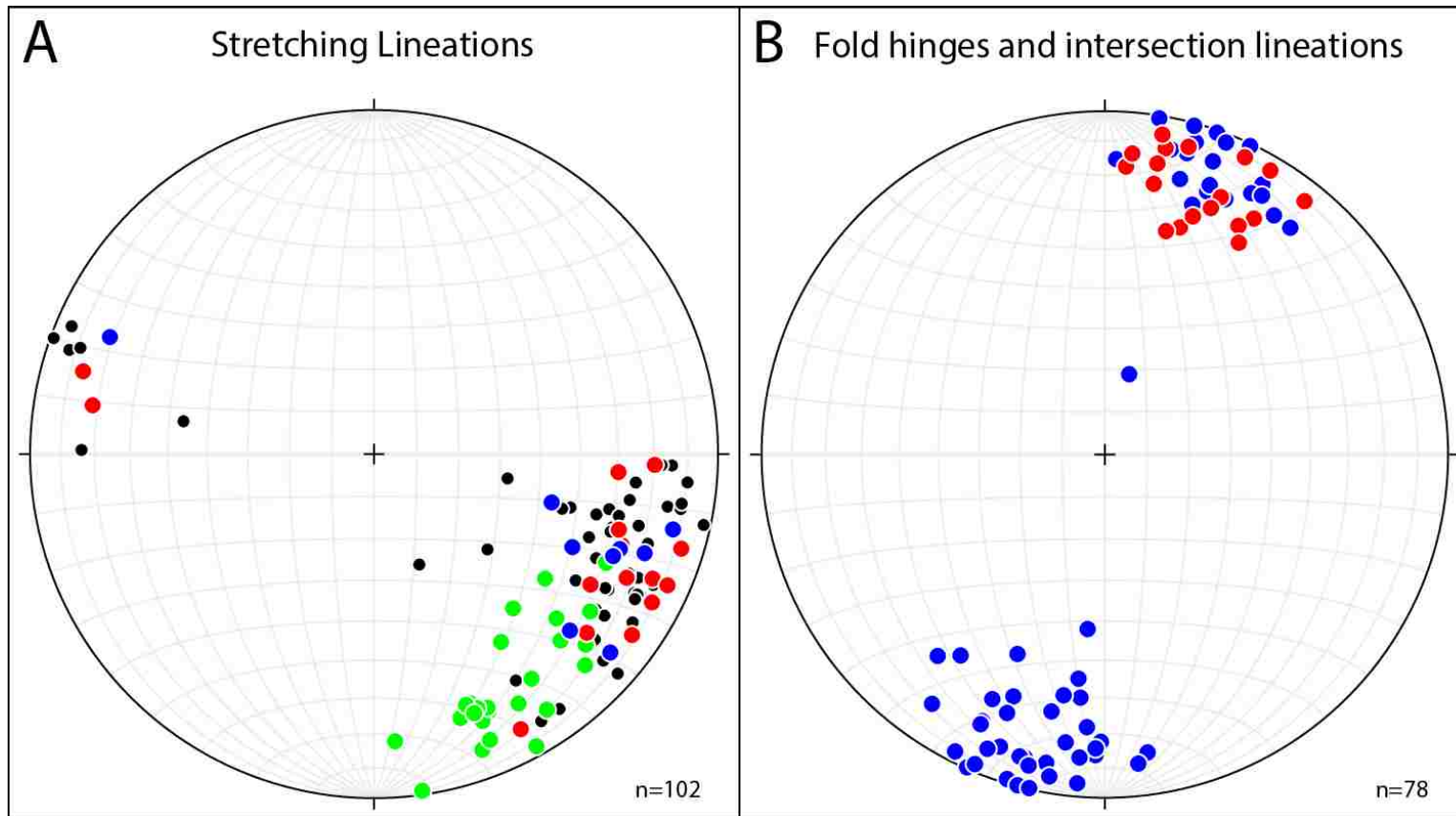
Figure 19: D₁-D₄ fabric comparison stereograms: Stereograms generated in Stereonet 9 of A) Stretching lineations from D1-D4 and B) Fold hinge and intersection lineation orientations from D2 and D3/D4. Green = D1, Blue = D2, Red = D3/D4, Black = indeterminate shear sense.

Appendix B: $^{40}Ar/^{39}Ar$ Data

Craig-University of Nevada, Las Vegas, TC17FM-16, Amphibole, 32.77 mg, J = 0.00529 ± 0.34%

4 amu discrimination = 0.5837 ± 0.06%, 40/39K = 0.040 ± 2.03%, 36/37Ca = 0.000243 ± 0.51%, 39/37Ca = 0.000555 ± 0.58%

step	T (C)	t (min.)	36Ar	37Ar	38Ar	39Ar	40Ar	%40Ar*	% 39Ar rlsd	Ca/K	40Ar*/39ArK	Age (Ma)	1s.d.
1	800	12	3.048	6.687	1.306	13.124	1726.57	11.0	2.0	8.86111008	12.248459	113.26	5.53
2	830	12	0.099	1.336	0.108	4.804	91.903	51.3	0.7	4.83175518	7.818871	73.12	1.15
3	860	12	0.078	1.865	0.136	4.549	94.643	65.2	0.7	7.12696369	10.832926	100.53	2.16
4	890	12	0.064	3.745	0.128	4.539	107.266	77.7	0.7	14.3677956	14.812170	136.10	1.27
5	910	12	0.067	4.930	0.123	3.489	115.640	81.6	0.5	24.6671364	21.376823	193.28	1.46
6	930	12	0.084	7.257	0.135	3.002	133.000	78.5	0.5	42.3799638	27.904663	248.40	1.98
7	950	12	0.095	10.753	0.178	3.324	180.861	82.5	0.5	56.9098504	36.845542	321.26	3.70
8	970	12	0.094	11.869	0.197	3.745	185.498	83.7	0.6	55.739116	34.035018	298.67	2.52
9	990	12	0.098	10.202	0.244	4.189	148.705	77.2	0.6	42.6994465	22.143203	199.84	2.08
10	1010	12	0.082	8.613	0.323	5.437	111.879	75.8	0.8	27.6745835	12.301686	113.74	0.54
11	1030	12	0.083	9.725	0.448	7.687	87.226	68.4	1.2	22.0716622	5.962765	56.03	0.83
12	1050	12	0.079	16.473	0.916	14.804	97.606	78.9	2.2	19.4007008	4.043768	38.19	0.62
13	1060	12	0.070	17.416	0.996	16.858	102.176	85.4	2.5	18.0061421	4.037668	38.13	0.73
14	1070	12	0.068	18.056	0.982	17.569	105.294	87.3	2.6	17.9119547	4.093541	38.65	0.17
15	1080	12	0.069	18.146	0.985	18.568	117.868	88.3	2.8	17.0291169	4.426866	41.76	0.43
16	1100	12	0.172	48.722	2.384	47.801	296.957	85.5	7.2	17.7640165	4.299725	40.58	0.18
17	1120	12	0.315	112.681	5.218	116.399	657.152	88.4	17.4	16.867898	4.155962	39.23	0.18
18	1150	12	0.389	125.142	5.461	126.865	670.595	84.1	19.0	17.1891467	3.704159	35.01	0.14
19	1190	12	0.152	38.812	1.928	38.373	281.441	86.1	5.8	17.6270248	5.102130	48.05	0.30
20	1240	12	0.191	52.933	2.412	50.247	347.299	85.6	7.5	18.3625022	4.827594	45.49	0.40
21	1400	12	0.484	158.476	7.726	161.714	1023.890	89.4	24.2	17.0764334	4.625355	43.61	0.17

Craig-University of Nevada, Las Vegas, SCFM315-16B, Amphibole, 16.81 mg, J = 0.00550 ± 0.35%

4 amu discrimination = 0.5837 ± 0.06%, 40/39K = 0.040 ± 2.03%, 36/37Ca = 0.000243 ± 0.51%, 39/37Ca = 0.000555 ± 0.58%

step	T (C)	t (min.)	36Ar	37Ar	38Ar	39Ar	40Ar	%40Ar*	% 39Ar rlsd	Ca/K	40Ar*/39ArK	Age (Ma)	1s.d.
1	800	12	0.899	1.821	0.404	3.321	513.10	12.0	0.9	9.71910369	15.597341	148.48	8.27
2	850	12	0.063	0.652	0.064	1.395	46.231	40.7	0.4	8.28148466	10.074902	97.30	5.87
3	900	12	0.068	2.236	0.105	2.993	66.011	61.7	0.8	13.2531637	10.230792	98.76	2.48
4	950	12	0.074	4.899	0.185	5.778	114.359	77.9	1.5	15.0477585	12.147931	116.68	1.64
5	1000	12	0.205	46.292	1.035	48.781	702.184	90.8	12.6	16.8494311	10.991836	105.90	0.39
6	1030	12	0.177	40.911	0.854	44.557	710.594	92.4	11.5	16.3003465	12.399249	119.02	0.53
7	1050	12	0.137	46.274	0.887	52.250	748.321	96.0	13.5	15.7203744	11.569609	111.29	0.40
8	1070	12	0.090	29.290	0.579	24.939	516.647	96.8	6.4	20.8732515	11.976949	115.09	0.42
9	1090	12	0.066	11.175	0.222	12.206	184.904	91.3	3.1	16.2533145	11.228280	108.11	0.56
10	1110	12	0.077	18.119	0.321	18.623	270.255	95.5	4.8	17.2766352	11.164302	107.51	0.66
11	1120	12	0.087	24.618	0.445	26.545	376.900	96.5	6.8	16.4649304	11.219506	108.03	0.41
12	1130	12	0.086	24.235	0.438	26.801	378.736	96.6	6.9	16.0523574	11.486444	110.52	0.46
13	1140	12	0.060	18.176	0.362	20.658	313.010	99.0	5.3	15.6174972	12.175887	116.94	0.53
14	1150	12	0.060	14.597	0.242	14.415	224.661	97.6	3.7	17.9844602	12.117506	116.40	0.45
15	1160	12	0.060	8.840	0.159	9.170	150.294	94.7	2.4	17.1175224	11.942363	114.77	0.51
16	1180	12	0.057	7.897	0.140	7.784	131.261	93.4	2.0	18.0181947	11.927112	114.63	0.49
17	1200	12	0.065	7.738	0.137	7.520	124.647	89.2	1.9	18.2763635	11.126973	107.16	0.70
18	1240	12	0.084	11.022	0.199	10.747	179.745	88.2	2.8	18.2156944	11.554495	111.15	0.71
19	1400	12	0.202	42.337	0.847	49.263	793.175	95.7	12.7	15.2532571	12.434886	119.35	0.46

Craig-University of Nevada, Las Vegas, TC17FM-35, Amphibole, 40.70 mg, J = 0.00538 ± 0.27%

4 amu discrimination = 0.5837 ± 0.06%, 40/39K = 0.040 ± 2.03%, 36/37Ca = 0.000243 ± 0.51%, 39/37Ca = 0.000555 ± 0.58%

step	T (C)	t (min.)	36Ar	37Ar	38Ar	39Ar	40Ar	%40Ar*	% 39Ar rlsd	Ca/K	40Ar*/39ArK	Age (Ma)	1s.d.
1	800	12	2.683	4.210	1.658	12.588	2317.27	41.7	5.7	5.86221747	65.018648	541.15	2.63
2	850	12	0.145	2.340	0.190	4.907	120.291	43.6	2.2	8.36369258	8.662037	82.17	0.96
3	900	12	0.161	9.741	0.315	6.205	150.441	54.7	2.8	27.6613653	10.683082	100.82	2.33
4	950	12	0.165	10.288	0.278	4.705	172.089	59.7	2.1	38.6298955	17.786433	164.87	1.58
5	1000	12	0.261	16.428	0.343	6.222	296.734	61.7	2.8	46.7355853	24.519772	223.55	3.70
6	1050	12	1.524	251.499	3.109	69.063	4995.060	88.0	31.5	64.7358973	54.771713	465.92	1.28
7	1080	12	0.144	28.546	0.232	8.141	268.132	83.3	3.7	62.2974355	22.891429	209.53	1.16
8	1090	12	0.103	14.900	0.152	4.270	159.410	79.2	1.9	61.9911123	24.204316	220.84	2.16
9	1100	12	0.105	19.389	0.192	5.184	195.369	86.5	2.4	66.5163554	26.048017	236.60	1.00
10	1110	12	0.106	22.511	0.200	6.214	236.452	89.7	2.8	64.3935791	27.629607	250.02	0.95
11	1120	12	0.136	27.799	0.250	7.431	275.833	86.8	3.4	66.5305951	26.323071	238.94	1.16
12	1130	12	0.152	35.675	0.295	9.250	348.811	88.8	4.2	68.6242536	27.689380	250.52	0.90
13	1140	12	0.185	41.676	0.365	10.684	442.247	88.2	4.9	69.4208047	30.493657	274.06	1.00
14	1150	12	0.193	43.985	0.380	11.138	518.119	89.5	5.1	70.2950882	34.943799	310.79	0.89
15	1160	12	0.184	38.549	0.373	9.828	508.095	89.5	4.5	69.8112973	38.810310	342.10	1.58
16	1180	12	0.215	42.564	0.439	10.739	610.764	89.1	4.9	70.5558552	42.729825	373.30	1.14
17	1200	12	0.126	21.672	0.239	5.319	323.232	89.2	2.4	72.5655524	44.744036	389.13	1.40
18	1240	12	0.205	37.635	0.412	9.513	592.749	89.1	4.3	70.4231121	46.774834	404.95	1.18
19	1400	12	0.418	71.685	0.752	18.113	1041.610	87.9	8.3	70.4500768	41.924958	366.94	1.28

Craig-University of Nevada, Las Vegas, MW14FM-36, Amphibole, 15.82 mg, J = 0.00556 ± 0.30%

4 amu discrimination = 0.5837 ± 0.06%, 40/39K = 0.040 ± 2.03%, 36/37Ca = 0.000243 ± 0.51%, 39/37Ca = 0.000555 ± 0.58%

step	T (C)	t (min.)	36Ar	37Ar	38Ar	39Ar	40Ar	%40Ar*	% 39Ar rlsd	Ca/K	40Ar*/39ArK	Age (Ma)	1s.d.
1	800	12	2.060	3.153	1.273	1.556	2079.70	50.2	1.6	36.4419048	575.979225	2590.05	10.54
2	850	12	0.097	1.615	0.131	0.777	118.642	64.1	0.8	37.3883681	80.687694	668.62	7.99
3	900	12	0.102	4.097	0.191	1.547	155.217	74.2	1.6	47.7569076	60.552593	523.51	9.49
4	950	12	0.133	8.173	0.370	2.713	302.270	82.7	2.8	54.4102871	77.091854	643.54	2.97
5	1000	12	0.224	21.762	0.728	7.561	641.309	86.1	7.8	51.953484	61.933237	533.84	2.05
6	1030	12	0.360	45.390	0.998	13.800	1144.090	87.6	14.3	59.4777132	62.033105	534.59	1.92
7	1050	12	0.222	26.898	0.520	8.026	643.460	86.8	8.3	60.6194429	59.177449	513.16	1.98
8	1070	12	0.100	13.411	0.251	4.105	256.624	87.6	4.2	59.0716653	45.625825	407.87	1.45
9	1090	12	0.080	9.988	0.181	2.925	217.306	89.1	3.0	61.7822695	57.103261	497.44	3.11
10	1110	12	0.122	14.509	0.288	4.416	323.916	88.4	4.6	59.4120861	53.374041	468.82	1.48
11	1120	12	0.099	12.864	0.240	3.869	279.182	90.4	4.0	60.1337433	53.328410	468.47	2.11
12	1130	12	0.117	13.615	0.219	3.871	272.891	86.8	4.0	63.6648941	50.024264	442.72	2.17
13	1140	12	0.094	13.354	0.245	4.014	307.940	92.3	4.2	60.1698138	58.196213	505.74	1.92
14	1150	12	0.117	15.360	0.299	4.658	388.873	91.2	4.8	59.6322036	63.203489	543.30	1.95
15	1160	12	0.151	15.730	0.319	4.457	411.888	87.5	4.6	63.8873082	67.305286	573.49	2.39
16	1180	12	0.159	13.672	0.298	3.870	405.711	85.9	4.0	63.9523188	74.955701	628.48	2.50
17	1200	12	0.153	14.502	0.326	4.285	464.919	88.5	4.4	61.2252759	80.281326	665.80	2.33
18	1240	12	0.236	22.652	0.528	6.953	730.666	87.7	7.2	58.9044711	77.802831	648.53	2.41
19	1400	12	0.451	44.334	1.004	13.237	1367.740	88.3	13.7	60.5807235	76.261430	637.70	2.74

Craig-University of Nevada, Las Vegas, MW13FM-16, Amphibole, 11.00 mg, J = 0.00564 ± 0.24%

4 amu discrimination = 0.5837 ± 0.06%, 40/39K = 0.040 ± 2.03%, 36/37Ca = 0.000243 ± 0.51%, 39/37Ca = 0.000555 ± 0.58%

step	T (C)	t (min.)	36Ar	37Ar	38Ar	39Ar	40Ar	%40Ar*	% 39Ar rlsd	Ca/K	40Ar*/39ArK	Age (Ma)	1s.d.
1	800	12	1.082	1.439	0.507	2.061	743.11	26.8	3.7	12.6294218	82.103305	686.51	3.28
2	850	12	0.087	0.756	0.080	1.143	81.079	52.1	2.0	11.9620745	29.435428	277.09	4.74
3	900	12	0.122	3.863	0.133	1.745	124.947	58.7	3.1	40.3099617	33.594846	313.03	5.67
4	950	12	0.141	5.058	0.174	1.347	202.691	70.7	2.4	68.8407239	88.231288	728.63	4.44
5	990	12	0.229	6.502	0.210	1.828	253.838	59.0	3.3	65.1515129	68.455748	589.01	7.40
6	1020	12	0.213	10.530	0.224	2.661	270.140	65.7	4.7	72.61164	55.880727	494.25	6.34
7	1040	12	0.242	37.680	0.402	8.273	549.870	84.1	14.7	83.7955496	47.665373	429.55	1.38
8	1060	12	0.187	27.269	0.300	6.159	388.233	82.8	11.0	81.4117631	44.206839	401.60	2.01
9	1080	12	0.054	4.496	0.054	1.241	70.915	78.8	2.2	66.3796483	34.247229	318.60	4.40
10	1100	12	0.066	6.715	0.086	1.644	89.164	82.9	2.9	74.9914914	32.656814	304.99	4.60
11	1120	12	0.083	11.750	0.140	2.819	146.500	86.4	5.0	76.5546277	35.039180	325.34	1.68
12	1130	12	0.088	11.920	0.134	2.730	149.927	85.0	4.9	80.2645615	36.543186	338.08	1.28
13	1140	12	0.088	11.952	0.146	2.842	167.870	86.7	5.1	77.2533025	40.555226	371.61	2.28
14	1150	12	0.077	10.997	0.133	2.516	162.608	89.6	4.5	80.3493813	45.753150	414.15	1.32
15	1170	12	0.097	13.526	0.170	2.948	205.397	87.5	5.3	84.4267001	49.197657	441.79	2.33
16	1200	12	0.136	17.539	0.227	3.805	292.845	85.3	6.8	84.8260195	54.158722	480.88	1.40
17	1230	12	0.142	14.207	0.193	3.127	258.909	81.1	5.6	83.5845304	55.028818	487.65	1.85
18	1270	12	0.121	9.577	0.129	2.055	172.591	75.6	3.7	85.7817133	50.539355	452.45	2.18
19	1400	12	0.259	22.374	0.323	5.159	446.738	82.1	9.2	79.7134627	56.007690	495.23	2.46

Appendix C: U-Pb Data

TC17FM-45

Analysis	U	206Pb	U/Th	206Pb*	±	Isotope Ratios 207Pb*	±	206Pb*	±	error	Apparent Ages 206Pb*	±	207Pb*	±	206Pb*	±	Best age	±	Conc
	(ppm)	204Pb		207Pb*	(%)	235U*	(%)	238U	(%)	corr.	238U*	(Ma)	235U	(Ma)	207Pb*	(Ma)	(Ma)	(Ma)	(%)
Spot 1	54	6076	1.3	10.3447	9.0	0.1825	9.1	0.0137	1.3	0.15	87.7	1.2	170.2	14.3	1560.0	169.4	87.7	1.2	NA
Spot 0	559	76999	10.1	20.5557	1.2	0.0960	1.7	0.0143	1.3	0.73	91.6	1.1	93.1	1.5	129.9	27.7	91.6	1.1	NA
Spot 20	49	3741	1.2	23.0653	4.6	0.0871	4.8	0.0146	1.4	0.28	93.3	1.3	84.8	3.9	NA	NA	93.3	1.3	NA
Spot 40	2957	381429	14.6	20.6599	0.9	0.0972	1.3	0.0146	1.0	0.77	93.3	0.9	94.2	1.2	118.0	20.1	93.3	0.9	NA
Spot 42	1042	750992	11.6	20.5436	1.0	0.0982	1.4	0.0146	1.1	0.74	93.7	1.0	95.1	1.3	131.3	22.8	93.7	1.0	NA
Spot 16	604	64627	5.9	20.7967	1.4	0.0976	2.0	0.0147	1.4	0.69	94.3	1.3	94.6	1.8	102.4	33.8	94.3	1.3	NA
Spot 27	80	7048	0.8	22.9836	2.5	0.0887	2.9	0.0148	1.4	0.49	94.7	1.3	86.3	2.4	NA	NA	94.7	1.3	NA
Spot 14	182	12724	0.6	21.1989	2.1	0.0965	2.5	0.0148	1.3	0.51	95.0	1.2	93.5	2.2	56.9	50.1	95.0	1.2	NA
Spot 35	5627	123369	13.5	17.1523	1.6	0.1200	1.8	0.0149	1.0	0.52	95.6	0.9	115.1	2.0	540.2	34.2	95.6	0.9	NA
Spot 41	1815	337654	11.1	20.9021	0.8	0.0991	1.4	0.0150	1.1	0.82	96.2	1.1	96.0	1.2	90.5	18.5	96.2	1.1	NA
Spot 19	131	20394	0.8	20.7662	2.3	0.0998	2.6	0.0150	1.2	0.45	96.3	1.1	96.6	2.4	105.9	55.3	96.3	1.1	NA
Spot 15	298	54884	0.7	21.6877	1.7	0.0961	2.0	0.0151	0.9	0.48	96.8	0.9	93.2	1.8	2.3	41.9	96.8	0.9	NA
Spot 30	204	86906	0.9	20.9430	1.5	0.0997	1.9	0.0151	1.2	0.63	96.9	1.2	96.5	1.7	85.8	34.9	96.9	1.2	NA
Spot 26	119	6358	0.6	21.2074	2.5	0.0988	2.7	0.0152	1.0	0.36	97.3	0.9	95.7	2.5	56.0	60.1	97.3	0.9	NA
Spot 21	140	14211	0.6	18.2338	3.2	0.1151	3.5	0.0152	1.2	0.35	97.4	1.2	110.6	3.6	404.8	72.6	97.4	1.2	NA
Spot 29	147	268579	0.7	17.7194	2.9	0.1185	3.1	0.0152	1.2	0.38	97.4	1.1	113.7	3.3	468.6	63.2	97.4	1.1	NA
Spot 28	115	9195	0.7	18.1612	2.8	0.1159	3.1	0.0153	1.3	0.43	97.7	1.3	111.4	3.3	413.8	62.6	97.7	1.3	NA
Spot 37	288	34303	0.7	20.5895	1.4	0.1026	1.8	0.0153	1.1	0.61	98.1	1.1	99.2	1.7	126.0	34.1	98.1	1.1	NA
Spot 3	434	105115	0.6	21.0517	1.4	0.1018	1.7	0.0155	0.9	0.54	99.5	0.9	98.4	1.6	73.5	34.3	99.5	0.9	NA
Spot 13	89	7451	0.7	20.6291	3.7	0.1043	3.9	0.0156	1.3	0.34	99.9	1.3	100.7	3.8	121.5	86.9	99.9	1.3	NA
Spot 43	63	40292	1.6	20.6641	3.8	0.1067	4.1	0.0160	1.4	0.34	102.3	1.4	102.9	4.0	117.5	90.2	102.3	1.4	NA
Spot 8	154	13469	0.7	15.7280	2.9	0.1440	3.1	0.0164	0.9	0.29	105.0	0.9	136.6	3.9	726.8	62.5	105.0	0.9	NA
Spot 10	95	400186	2.2	20.4589	3.0	0.1139	3.5	0.0169	1.8	0.51	108.0	1.9	109.5	3.7	141.0	71.2	108.0	1.9	NA
Spot 11	1943	5808223	2.8	19.9022	0.7	0.2339	1.1	0.0338	0.9	0.81	214.2	2.0	213.4	2.2	205.4	15.6	214.2	2.0	NA

Spot 44	1361	1335580	2.8	19.4542	0.6	0.2432	1.1	0.0343	0.9	0.81	217.5	1.9	221.0	2.2	258.0	14.6	217.5	1.9	NA
Spot 46	128	153906	3.6	12.5453	0.7	2.2364	1.0	0.2036	0.7	0.71	1194.5	8.1	1192.5	7.3	1189.0	14.4	1189.0	14.4	100.5
Spot 47	156	636872	3.5	12.3859	0.7	2.2423	1.2	0.2015	1.0	0.83	1183.5	10.5	1194.4	8.2	1214.2	12.9	1214.2	12.9	97.5
Spot 31	6327	3492113	10.7	9.6815	0.6	3.7732	1.0	0.2651	0.8	0.83	1515.7	11.3	1587.1	8.1	1683.2	10.5	1683.2	10.5	90.0
Spot 38	2416	13754998	3.8	9.5871	0.6	3.7753	1.1	0.2626	0.9	0.83	1503.2	12.2	1587.5	8.8	1701.3	11.1	1701.3	11.1	88.4
Spot 36	955	6305799	2.5	9.5428	0.6	3.8739	1.1	0.2682	1.0	0.86	1531.8	13.5	1608.3	9.3	1709.8	10.7	1709.8	10.7	89.6
Spot 12	807	1122788	3.3	9.5271	0.6	3.9386	1.3	0.2723	1.1	0.87	1552.3	15.3	1621.7	10.3	1712.9	11.6	1712.9	11.6	90.6
Spot 7	820	6031026	2.2	9.4460	0.6	4.4634	1.2	0.3059	1.0	0.86	1720.6	15.2	1724.2	9.8	1728.6	11.1	1728.6	11.1	99.5
Spot 24	729	890532	5.0	9.4452	0.6	4.0152	1.2	0.2752	1.1	0.88	1567.0	14.6	1637.3	9.7	1728.7	10.4	1728.7	10.4	90.6
Spot 5	5759	4758240	83.3	9.4201	0.7	4.2620	1.2	0.2913	1.0	0.84	1648.1	14.8	1686.1	9.9	1733.6	11.9	1733.6	11.9	95.1
Spot 23	1789	3384696	25.1	9.3211	0.7	4.1420	1.3	0.2801	1.1	0.86	1592.0	15.9	1662.6	10.7	1753.0	12.1	1753.0	12.1	90.8
Spot 34	1032	1635504	4.5	9.1933	0.7	4.3466	1.2	0.2899	1.0	0.84	1641.2	14.6	1702.3	9.9	1778.2	12.1	1778.2	12.1	92.3
Spot 49	322	941097	2.3	9.1380	0.6	4.5932	1.3	0.3045	1.1	0.87	1713.8	16.8	1748.0	10.6	1789.2	11.2	1789.2	11.2	95.8

REFERENCES CITED

Allmendinger, R.W., 2013, Stereonet 9, Program for stereographic projection, Department of Geology, Cornell University.

Anderson, E.M., 1951, The Dynamics of Faulting, 2nd edition. Oliver and Boyd, Edinburgh, p. 206.

Andrew, J.E., 2002, The Mesozoic and Tertiary Tectonics of the Panamint Range and Quail Mountains, California: Ph.D. Dissertation, 254 pp., University of Kansas.

Andrew, J.E., and Walker, J.D., 2009, Reconstructing late Cenozoic deformation in central Panamint Valley, California: Evolution of slip partitioning in the Walker Lane: Geosphere, v. 5, p. 172-198.

Applegate, J.D.R., Walker, J.D., and Hodges, K.V., 1992, Late Cretaceous extensional unroofing in the Funeral Mountains metamorphic core complex, California: Geology, v. 20, p. 519-522.

Applegate, J.D.R., 1995, Transform-normal extension on the Northern Death Valley fault system, California-Nevada: Basin Research, v. 7, p. 269-280.

Applegate, J.D.R., and Hodges, K.V., 1995, Mesozoic and Cenozoic extension recorded by metamorphism in the Funeral Mountains, California: Geological Society of America Bulletin, v. 107, p. 1063-1076.

Armstrong, R.L., 1982, Cordilleran Metamorphic Core Complexes – from Arizona to Southern Canada: Annual Review Earth and Planetary Science, v. 10, p. 129-154.

Atwater, T., and Stock, J., Pacific-North America Plate Tectonics of the Neogene Southwestern United States: An Update: International Geology Review, v. 40, p. 375-402.

Axen, G.J., 1992, Pore pressure, stress increase, and fault weakening in low-angle normal faulting: Journal of Geophysical Research, v. 97, p. 8979-8991.

———, 1993, Ramp-flat detachment faulting and low-angle normal reactivation of the Tule Springs thrust, southern Nevada: Geological Society of America Bulletin, v. 105, p. 1076-1090.

Axen, G.J., and Bartley, J.M., 1997, Field test of rolling hinges: Existence, mechanical types, and implications for extensional tectonics: Journal of Geophysical Research, v. 102, p. 20,515-20,537.

Axen, G.J., 1988, The geometry of planar domino-style normal faults above a dipping basal detachment: Journal of Structural Geology, v. 10., p. 405-411.

Barth, A.P., Wooden, J.L., Coleman, D.S., and Vogel, M.B., 2009, Assembling and disassembling California: a zircon and monazite geochonologic framework for Proterozoic crustal evolution in southern California: Geology, v. 117, p. 221-239.

Beyene, M.A., 2011, Mesozoic burial, Mesozoic and Cenozoic exhumation of the Funeral Mountains core complex, Death Valley, Southeastern California: Ph.D. Dissertation, 363 pp., University of Nevada, Las Vegas.

Bohannon, R.G., 1983, Mesozoic and Cenozoic tectonic development of the Muddy, North Muddy, and northern Black Mountains, Clark County, Nevada, *in* Miller, D.M., Todd, V.R., and Howard, K.A., eds., Tectonic and Stratigraphic Studies in the Eastern Great Basin: Geological Society of America Memoir 157, p. 125–148.

Bond, G.C., Christie-Blick, N., Kominz, M.A., and Devlin, W.J., 1985, An Early Cambrian rift to post-rift transition in the Cordillera of western North America: Nature, v. 316, p. 742-745.

Bradshaw, G.A., and Zoback, M.D., 1988, Listric normal faulting, stress refraction, and the state of stress in the Gulf Coast basin: Geology, v. 16, p. 271-274.

Bruhn, R.L., Yusas, M.R., and Huertas, F., Mechanics of low-angle normal faulting: An example from Roosevelt hot springs geothermal area, Utah: Tectonophysics, v. 86, p. 343-361.

Burchfiel, B.C., and Stewart, J.H., 1966, "Pull-Apart' origin of the central segment of Death Valley, California: Geological Society of America Bulletin, v.77, p.439-442.

Burchfiel, B.C., Wernicke, B., Willemin, J.H., Axen, G.J., and Cameron, S.C., 1982, A new type of decollement thrust: Nature, v. 300, p. 513-515.

Camilleri, P.A., and Chamberlain, K.R., 1997, Mesozoic tectonics and metamorphism in the Pequop Mountains and Wood Hills region, northeast Nevada: Implications for the architecture and evolution of the Sevier orogen: Geological of Society Bulletin, v. 109, p. 74-94.

Camilleri, P., Yonkee, W.A., Coogan, J.C., DeCelles, P.G., McGrew, A., and Wells, M., 1997, Hinterland to foreland transect through the Sevier orogen, NE Nevada to SW Wyoming: structural style, metamorphism, and kinematic history of a large contractional orogenic wedge, *in* Link, P.K., and Kowallis, B.J., editors, Proterozoic to Recent Stratigraphy, Tectonics, and Volcanology, Utah, Nevada, Southern Idaho and Central Mexico: Brigham Young University Geology Studies, v. 42, part 1, p. 297-309.

Camilleri, P., 1998, Prograde metamorphism, strain evolution, and collapse of footwalls of thick thrust sheets: a case study from the Mesozoic Sevier hinterland U.S.A.: Journal of Structural Geology, v. 20, p. 1023-1042.

Caskey, S.J., and Schweickert, R.A., 1992, Mesozoic deformation in the Nevada test site and vicinity: Implications for the structural framework of the Cordilleran fold and thrust belt and tertiary extension North of Las Vegas Valley: Tectonics, v. 11, p. 1314-1331.

Cemen, I., and Wright, L.A., 1990, Effect of Cenozoic extension on Mesozoic thrust surfaces in the central and southern Funeral Mountains, Death Valley, California, *in* Wernicke, B.P., ed., Basin and Range extensional tectonics near the latitude of Las Vegas, Nevada: Geological Society of America Memoir 176, p. 305-316.

Chen, J.H., and Moore, J.G., 1979, Late Jurassic Independence dike swarm in eastern California: Geology, v. 7, p. 129-133.

Coleman, D.S., Briggs, S., Glazner A.F., and Northrup, C.J., 2003, Timing of plutonism and deformation in the White Mountains of eastern California: Geological Society of America Bulletin, v. 115, p. 48-57.

Collettini, C., Niemeijer, A., Viti, C., and Marone, C., 2009, Fault zone fabric and fault weakness: Nature, v. 462, p. 907-911.

Collettini, C., 2011, The mechanical paradox of low-angle normal faults: Current understanding and open questions: Tectonophysics, v. 510, p. 253-268.

Coney, P.J., and Reynolds, S.J., 1977, Cordilleran Benioff zones: Nature, v. 270, pp. 403-406.

Coney, P.J., and Harms, T.A., 1984, Cordilleran metamorphic core complexes: Cenozoic extensional relics of Mesozoic compression: Geology, v. 12, p. 550-554.

Coney, P.J., 1987, The regional tectonic setting and possible causes of Cenozoic extension in the North American Cordillera, *from* Coward, M.P., Dewey J.F., and Hancock, P.L. (eds), 1987, *Continental Extensional Tectonics,* Geological Society Special publication, no. 28., p. 177-186.

Copeland, P., Currie, C.A., Lawton, T.F., and Murphy, M.A., 2017: Location, location, location: The variable lifespan of the Laramide orogeny: Geology, v. 45, pp. 223-226.

Craddock, S.D., Hoisch, T.D., Wells, M.L., Sauer, K.M., Beyene, M.A., and Vervoort, J.D., 2017, New pressure-temperature-time paths from the Funeral Mountains, California, recording Late Jurassic burial and exhumation during early Sevier Orogenesis: Geological Society of America Abstracts with Programs, v. 49, no. 6.

Czajkowski, J. (2002), Cretaceous contraction in the Lees Camp Anticline: Inyo Mine and vicinity, Funeral Mountains, Death Valley, California: MS thesis, 73 pp., University of Oregon, Eugene.

Davis, G.A., Lister, G.S., and Reynolds, S.J., 1986, Structural evolution of the Whipple and South mountains shear zones, southwestern United States: Geology, v.14, p. 7-10.

Davis, G.A., and Burchfiel, B.C., 1997, Comment on "The Butte Valley and Layton Well thrusts of eastern California: Distribution and regional significance" by Chester T. Wrucke, Calvin H. Stevens, and Joseph L. Wooden: Tectonics, v. 16, p. 182-183.

DeCelles, P.G., 2004, Late Jurassic to Eocene evolution of the Cordilleran thrust belt and foreland basin system, western U.S.A.: American Journal of Science, v. 304, pp. 105-168.

DeCelles, P.G., Ducea, M.N., Kapp, P., and Zandt, G., 2009, Cyclicity in Cordilleran orogenic systems: Nature Geoscience, v. 2, pp. 251-257.

DeCelles, P.G., and Graham, S.A., 2015, Cyclical processes in the North American Cordillera orogenic system: Geology, v. 43, p. 499-502.

DeCelles. P.G., and Mitra, G., 1995, History of the Sevier orogenic wedge in terms of critical taper models, northeast Utah and southwest Wyoming: Geological Society of America Bulletin, v. 107, p. 454-462.

Dokka, R.K., and Travis, C.J., 1990a, Late Cenozoic strike-slip faulting in the Mojave Desert, California: Tectonics, v. 9, p. 311-340.

——— ,1990b, Role of the Eastern California shear zone in accommodating Pacific-North American plate motion: Geophysical Research Letters, v.17, p. 1323-1326.

Donath, F.A., 1962, Analysis of Basin and Range structure, south-central Oregon: Bulletin of the Geological Society of America, v. 73, p. 1-16.

Dickinson, W. R., and Snyder, W. S., 1978, Plate tectonics of the Laramide orogeny, *in* Matthews, V., (*eds*), Laramide folding associated with block faulting in the western United States: Geological Society of America Memoir 151, p. 355–366.

Dickinson, W.R., Klute, M.A., Hayes., M.J., Janecke, S.U., Lundin, E.R., McKittrick, M.A., and Olivares, M.D., 1988, Paleogeographic and paleotectonic setting of Laramide sedimentary basins in the central Rocky Mountain region: Geological Society of America Bulletin, v. 100, p. 1023-1039.

Dickinson, W.R., 2009, Anatomy and global context of the North American cordillera, in Kay, S.M., Ramos, V.A., and Dickinson, W.R., eds., Backbone of the Americas: Shallow Subduction, Plateau Uplift, and Ridge and Terrane Collision: Geological Society of America Memoir 204, p. 1–29.

Druschke, P., Hanson, A.D., Wells, M.L., Rasbury, T., Stockli, D.F., and Gehrels, G., 2009, Synconvergent surface-breaking normal faults of Late Cretaceous age within the Sevier hinterland, east-central Nevada: Geology, v. 37, p. 447-450.

Dunne, G.C., and Walker, J.D., 1993, Age of Jurassic volcanism and tectonism, southern Owens Valley region, east-central California: Geological Society of America Bulletin, v. 105, p. 1223-1230.

———, 2004, Structure and evolution of the East Sierran thrust system, east central California: Tectonics, v. 23, TC4012.

Ebert, A., Herwegh, M., Berger, A., Pfiffner, A., 2008, Grain coarsening maps for polymineralic carbonate mylonites: a calibration based on data from different Helvetic napped (Switzerland): Tectonophysics, v. 457 (3-4), p. 128-142.

Engebretson, D.C., Cox, A., and Gordon, R.G., Relative Motions Between Oceanic and Continental Plates in the Pacific Basin: Geologic Society of America Special Papers, v. 206, p. 59.

Faulkner, D.R., Mitchell, T.M., Healy, D., and Heap, M.J., 2006, Slip on 'weak' faults by the rotation of regional stress in the fracture damage zone: Nature, v. 444, p. 922-925.

Fletcher, J.M., 2016, The role of a keystone fault in triggering the complex El Mayor-Cucapah earthquake rupture: Nature, v. 9, p. 303-309.

Fossen, H., 1992, The role of extensional tectonics in the Caledonides of south Norway: Journal of Structural Geology, v. 14, p. 1033-1046.

Fossen, H., 1992, Postcollisional extension of the Caledonide orogen in Scandinavia: Structural expressions and tectonic significance: Geology, v. 20, p. 737-740.

Frankel, K.L., et al., 2007, Cosmogenic [10]Be and [36]Cl geochronology of offset alluvial fans along the northern Death Valley fault zone: Implications for transient strain in the eastern California shear zone: Journal of Geophysical Research, v. 112, B06407.

Fridrich, C.J., and Thompson, R.A., 2011, Cenozoic Tectonic Reorganizations of the Death Valley Region, Southeast California and Southwest Nevada: United States Geological Survey Special Paper 1783, 36 p.

Gans, P.B., Miller, E.L., McCarthy, J., and Ouldcott, M.L., 1985, Tertiary extensional faulting and evolving ductile-brittle transition zones in the northern Snake Range and vicinity: New insights from seismic data: Geology, v. 13, p. 189-193.

Giallorenzo, M.A., Wells, M.L., Yonkee, W.A., Stockli, D.F., and Wernicke, B.P., 2018, Timing of exhumation, Wheeler Pass thrust sheet, southern Nevada and California: Late Jurassic to middle Cretaceous evolution of the southern Sevier fold-and-thrust belt: Geological Society of America Bulletin, v. 130, p. 558-579.

Glazner, A.F., Bartley, J.M., and Carl, B.S., 1999, Oblique opening and noncoaxial emplacement of the Jurassic Independence dike swarm, California: Journal of Structural Geology, v. 21, p. 1275-1283.

Hamilton, W.B., 1988, Detachment faulting in the Death Valley region, California and Nevada, U.S. Geological Survey Bulletin, v. 1790, p. 51-85.

Harrison, T.M., Célérier, J., Aikman, A.B., Hermann, J., and Heizler, M.T., 2009, Diffusion of 40Ar in muscovite: Geochimica et Cosmochimica Acta, v. 73, p. 1039–1051.

Healy, D., 2009, Anisotropy, pore fluid pressure and low angle normal faults: Journal of Structural Geology, v. 31, p. 561-574.

Heller, P.L., and Liu, L., 2015, Dynamic topography and vertical motion of the U.S. Rocky Mountain region prior to and during the Laramide orogeny: GSA Bulletin, v. 128, pp. 973-988.

Henderson, L.J., Gordon R.G., and Engebretsen D.C., 1984, Mesozoic aseismic ridges on the Farallon plate and southward migration of shallow subduction during the Laramide orogeny: Tectonics, v. 3., p. 121-131.

Hodges, K.V., and Walker, J.D., 1990, Petrologic Constraints on the Unroofing History of the Funeral Mountain Metamorphic Core Complex, California: Journal of Geophysical Research, v. 95, p. 8437-8445.

Hoisch, T.D., and Simpson, C., 1993, Rise and Tilt of Metamorphic Rocks in the Lower Plate of a Detachment Fault in the Funeral Mountains, Death Valley, California: Journal of Geophysical Research, v. 98, p. 6805-6827.

Hoisch, T.D., Heizler, M.T., and Zartman, R.E., 1997, Timing of detachment faulting in the Bullfrog Hills and Bare Mountain area, southwest Nevada: Inferences from [40]Ar/[39]Ar, K-Ar, U-Pb, and fission track thermochronology: Journal of Geophysical Research, v. 102, p. 2815-2833.

Hoisch, T.D., Wells, M.L., Beyene, M.A., Styger, S., and Vervoort, J.D., 2014, Jurassic Barrovian metamorphism in a western U.S. Cordilleran metamorphic core complex, Funeral Mountains, California: Geology, v. 42, p. 399-402.

Holdsworth, R.E., Butler, C.A., and Robers, A.B., 1997, The recognition of reactivation during continental deformation: Journal of the Geological Society of London, v. 154, p. 73-78.

Holm, D.K., and Dokka, R.K., 1991, Major Late Miocene cooling of the middle crust associated with extensional orogenesis in the Funeral Mountains, California: Geophysical Research Letters, v. 18, p. 1775-1778.

Humphreys, E.D., 1995, Post-Laramide removal of the Farallon slab, western United States: Geology, v. 23, p. 987-990.

Hunt, C.B., and Mabey, D.R., 1966, Stratigraphy and structure, Death Valley, California: U.S. Geological Survey Professional Papers, v. 494, 162 p.

Iriono, A., Premo, W.R., Martinez-Torres, L.M., Budahn, J.R., Atkinson Jr., W.R., Siems, D.F., and Guaras-Gonzales, B., 2004, Isotopic, geochemical and temporal characterization of Proterzoic basement rocks in the Quitovac region, northwestern Sonara, Mexico: implications for the reconstruction of the southwestern margin of Laurentia: Geological Society of America Bulletin, v. 116, p. 154-170.

Jackson, J.A., 1987, Active normal faulting and crustal extension, *From* Coward, M.P., Dewey, J.F., and Hancock, P.L., (eds), 1987, Continental Extensional Tectonics*:* Geological Society Special Publication, No. 28, p. 3-17.

James, E.W., 1989, Southern extension of the Independence dike swarm of eastern California: Geology, v. 17, p. 587-590.

Labotka, T.C., 1980, Petrology of a medium-pressure regional metamorphic terrane, Funeral Mountains, California: American Mineralogist, v. 65, p. 670-689.

Labotka, T.C., Warasila, R.L., and Spangler, R.R., 1985, Polymetamorphism in the Panamint Mountains, California; a ^{39}Ar/^{40}Ar study: Journal of Geophysical Research, v. 90, p. 10359-10371.

Lavier, L.L., Buck, W.R., Poliakov, A.N.B., 1999, Self-consistent rolling-hinge model for the evolution of large-offset low-angle normal faults: Geology, v. 27, p. 1127-1130.

Lister, G.S., and Davis, G.A., 1989, The origin of metamorphic core complexes and detachment faults formed during Tertiary continental extension in the northern Colorado River region, U.S.A.: Journal of Structural Geology, v. 11, p. 65-94.

Lister, G.S., and Baldwin, S.L., 1993, Plutonism and the origin of metamorphic core complexes: Geology, v. 21, p. 607-610.

Liu, L., Gurnis, M., Seton, M., Saleeby, J., Muller, R.D., and Jackson, J.M., 2010, The role of oceanic plateau subduction in the Laramide orogeny: Nature Geoscience, v. 3, pp. 353-357.

Liu, S., Nummendal, and D., Liu, L., 2011, Migration of dynamic subsidence across the Late Cretaceous United States Western Interior Basin in response to Farallon plate subduction: Geology, v. 39, pp. 555-558.

Ludwig K.R., Isoplot 3.00 user manual, Berkeley Geochronology Center Special Publication, vol. 4 (2003)

Macdonald, F.A., Prave, A.R., Petterson, R., Smith, E.F., Pruss, S.B., Oates, K., Waechter, F., Trotzuk, D., and Fallick, A.E., 2013, The Laurentian record of Neoproterozoic glaciation, tectonism, and eukaryotic evolution in Death Valley, California: Geological Society of America Bulletin, v. 125, p. 1203-1223.

MacLean, J.S., Sears, J.W., Chamberlain, K.R., Khudoley, A.K., Prokopiev, A.V., Kropachev, A.P., and Serkina, G.G., 2009, Detrital zircon geochronologic tests of the SE Siberia-SW Laurentia paleocontinental connection: Stephan Mueller Special Publication Series, v. 4, p. 111-116.

Mahon, R.C., Dehler, C.M., Link, P.K., Karlstrom, K.E., and Gehrels, G.E., 2014, Detrital zircon provenance and paleogeography of the Pahrump Group and overlying strata, Death Valley, California: Precambrian Research, v. 251, p. 102-117.

———, 2014, Geochronologic and stratigraphic constraints on the Mesoproterozoic and Neoproterozoic Pahrump Group, Death Valley, California: A record of the assembly, stability, and breakup of Rodinia: Geological Society of America Bulletin, v. 126, p. 619-638.

Maldonado, F., 1990, Structural geology of the upper plate of the Bullfrog Hills detachment fault system, southern Nevada: Geological Society of America Bulletin, v. 102, p. 992-1006.

Mattinson, C.G., Colgan, J.P., Metcalf, J.R., Miller, E.L., and Wooden, J.L., 2007, Late Cretaceous to Paleocene metamorphism and magmatism in the Funeral Mountains metamorphic core complex, Death Valley, California: Geological Society of America Special Papers, v. 419, p. 205-223.

Melosh, H.J., 1990, Mechanical basis for low-angle normal faulting in the Basin and Range province: Nature, v. 343, p. 331-335.

Miller, J.M.G., 1985, Glacial and syntectonic sedimentation: The Upper Proterozoic Kingston Peak Formation, southern Panamint Range, eastern California: Geological Society of America Bulletin, v. 96, p. 1537-1553.

Mitra, G., and Sussman, A.J., 1997, Structural evolution of connecting splay duplexes and their implication for critical taper: an example based on geometry and kinematics of the Canyon Range culmination, Sevier belt, central Utah: Journal of Structural Geology, v. 19, p. 503-521.

Morley, C.K., 1986, The Caledonian thrust front and palinspastic restorations in the southern Norwegian Caledonides: Journal of Structural Geology, v. 8, p. 753-765.

Niemi, N.A., 2002, Extensional Tectonics in the Basin and Range Province and the Geology of the Grapevine Mountains, Death Valley Region, California and Nevada [Ph.D Thesis]: California Institute of Technology, 343 p.

Oldow, J.S., 1983, Tectonic implications of a late Mesozoic fold and thrust belt in northwestern Nevada: Geology, v. 11, p. 542-546.

Pavlis, T.L., Rutkofske, J., Guerrero, F., and Serpa, L.F., 2014, Structural overprinting of Mesozoic thrust systems in eastern California and its importance to reconstruction of Neogene extension in the southern Basin and Range: Geosphere, v. 10, p. 732-756.

Prave, A.R., 1999, Two diamictites, two cap carbonates, two $\delta_{13}C$ excursions, two rifts: The Neoproterozoic Kingston Peak Formation, Death Valley, California: Geology, v. 27, p. 339-342.

Proffett, J.M., Jr., 1977, Cenozoic geology of the Yerington district, Nevada, and implications for the nature and origin of Basin and Range faulting: Geological Society of America Bulletin, v. 88, p. 247-266.

Reheis, M.C., and Dixon, T.H., 1996, Kinematics of the Eastern California shear zone: Evidence for slip transfer from Owens and Saline Valley fault zones to Fish Lake Valley fault zone: Geology, v. 24, p. 339-342.

Renik, B., and Christie-Blick, N., 2013, A new hypothesis for the amount and distribution of dextral displacement along the Fish Lake Valley – northern Death Valley – Furnace Creek fault zone, California-Nevada: Tectonics, v. 32, p. 123-145.

Reynolds, M.W., 1976, Geology of the Grapevine Mountains, Death Valley, California: A summary, *in* Geologic Features, Death Valley, California, edited by B.W. Troxel and L.A. Wright, Spec. Rep. Calif. Div. Mines Geol., p. 19-25.

Reynolds, S.J., and Lister, G.S., 1987, Structural aspects of fluid-rock interactions in detachment zones: Geology, v. 15, p. 362-366.

Ricketts, J.W., Karlstrom, K.E., and Kelley, S.A., 2015, Embryonic core complexes in narrow continental rifts: The importance of low-angle normal faults in the Rio Grande rift of central New Mexico: Geosphere, v. 11, p. 425-444.

Rykkelid, E., and Fossen, H., 1992, Composite fabrics in mid-crustal gneisses: Observations from the Øygarden Complex, West Norway Caledonides: Journal of Structural Geology, v. 14, p. 1-9.

Saleeby, J., 2003, Segmentation of the Farallon slab-Evidence from the southern Sierra Nevada region: GSA Bulletin, v. 115, pp. 655-668.

Sibson, R.H., 1985, A note on fault reactivation: Journal of Structural Geology, v. 7, p. 751-754.

Smith, G.I., Troxel, B.W., Gray Jr., C.H., and von Huene, R., 1968, Geologic reconnaissance of the Slate Range, San Bernardino and Inyo Counties, California, Special Report California Division of Mines Geology, v. 96, 33 p.

Smith, M.E., Carroll, A.R., Jicha, B.R., Cassel, E.J., and Scott, J.J., 2014, Paleogeographic record of Eocene Farallon slab rollback beneath western North America: Geology, v. 42, p. 1039-1042.

Snow, J.K., and Wernicke, B.P., 1989, Uniqueness of geological correlations: An example from the Death Valley extended terrain: Geological Society of American Bulletin, v. 101, p. 1351-1362.

Snow, J.K., Asmerom, Y., and Lux, D.R., 1991, Permian-Triassic plutonism and tectonics, Death Valley region, California and Nevada: Geology, v. 19, p. 629-632.

Snow, J.K., 1992, Large-magnitude Permian shortening and continental-margin tectonics in the southern Cordillera: Geological Society of America Bulletin, v. 104, p. 80-105.

Snow, J.K., and Wernicke, B.P., 2000, Cenozoic tectonism in the central Basin and Range; magnitude, rate, and distribution of upper crustal strain: American Journal of Science, v. 300, p. 659-719.

Spencer, J.E., 1984, Role of tectonic denudation in warping and uplift of low-angle normal faults: Geology, v. 12, p. 95-98.

Stevens, C.H., and Stone, P., 2005, Interpretation of the Last Chance thrust, Death Valley region, California, as an Early Permian decollement in a previously undeformed shale basin: *in*

Calzia, J.P., 2005, Fifty Years of Death Valley Research: A volume in honor of Lauren A. Wright and Bennie Troxel, v. 73, p. 79-101.

Stewart, J.H., Ross, D.C., Nelson, C.A., and Burchfiel, B.C., 1966, Last Chance thrust – a major fault in the eastern part of Inyo County, California: U.S. Geological Survey Professional Paper 550-D, D23-D34.

Stewart, J.H., 1971, Basin and Range Structure: A System of Horsts and Grabens Produced by Deep-Seated Extension: Geological Society of America Bulletin, v. 82, p. 1019-1044.

———, 1972, Initial deposits in the Cordilleran geosyncline; evidence of a late Precambrian (<850 m.y.) continental separation: Geological Society of America Bulletin, v. 83, p. 1345-1360.

———, 1976, Late Precambrian evolution of North America: plate tectonics implications: Geology, v. 4, p. 11-15.

Swanson, E., and Wernicke, B.P., 2017, Geologic map of the east-central Meadow Valley Mountains, and implications for reconstruction of the Mormon Peak detachment, Nevada: Geosphere, v. 13, p. 1234-1253.

Terzaghi, K., 1936, Simple tests determine hydrostatic uplift: Engineering News-record, v. 95, p. 987-996.

Tullis, J., and Yund, R.A., 1980, Hydrolytic weakening of experimentally deformed Westerly granite and Hale albite rock: Journal of Structural Geology, v. 2, p. 439-451.

Urai, J.L., Means, W.D., and Lister, G.S., 1986, Dynamic Recrystallization of Minerals, *in* Hobbs, B.E., and Heard, H.C., eds., Mineral and Rock Deformation: Laboratory Studies: The Paterson Volume: American Geophysical Union Geophysical Monograph 36, p. 161–199.

Walker, J.D., Martin, M.W., Bartley, J.M., and Coleman, D.S., 1990, Timing and kinematics of deformation in the Cronese Hills, California, and implications for Mesozoic structure of the southwestern Cordillera: Geology, v. 18, p. 554-557.

Wells, M.L., 1997, Alternating contraction and extension in the hinterlands of orogenic belts: An example from the Raft River Mountains, Utah: Geological Society of America, v. 109, p. 107-126.

Wells, M.L., 2000, Dating of major normal fault systems using thermochronology: An example from the Raft River detachment, Basin and Range, western United States: Journal of Geophysical Research, v. 105, p. 16,303-16,327.

Wells, M.L., Beyene, M.A., Spell, T.L., Kula, J.L., Miller, D.M., and Zanetti, K.A., 2005, The Pinto shear zone; a Laramide synconvergent extensional shear zone in the Mojave Desert region of the southwestern United States: Journal of Structural Geology, v. 27, p. 1697-1720.

Wells, M.L., Spell, T.L., Hoisch, T.D., Arriola, T., and Zanetti, K.A., 2008, Laser-probe 40Ar/39Ar dating of strain fringes: Mid-Cretaceous synconvergent orogen-parallel extension in the interior of the Sevier orogen: Tectonics, v. 27, TC3012.

Wells, M.L., Hoisch, T.D., Cruz-Uribe, A.M., and Vervoort, J.D., 2012, Geodynamics of synconvergent extension and tectonic mode switching: Constraints from the Sevier-Laramide orogen: Tectonics, v. 31, TC1002.

Wernicke, B., 1981, Low-angle normal faults in the Basin and Range Province: nappe tectonics in an extending orogen: Nature, v. 291, p. 645-648.

Wernicke, B., and Burchfiel, B.C., 1982, Modes of extensional tectonics, Journal of Structural Geology, v. 4, p. 105-115.

Wernicke, B., and Axen, G.J., 1988, On the role of isostasy in the evolution of normal fault systems: Geology, v.16, p. 848-851.

Wernicke, B., Axen, G.J., and Snow, J.K., 1988, Basin and Range extensional tectonics at the latitude of Las Vegas, Nevada: Geological Society of America Bulletin, v. 100, p. 1738-1757.

White, S.H., Bretan, P.G., and Rutter, E.H., 1986, Fault-zone reactivation: kinematics and mechanisms: Philosophical transactions of the Royal Society of London, v. A317, p. 81-97.

Wolfman, A., Mulligan, M.R., Wells, M.L., 2017, Resolving stratigraphic complexities of the Pahrump Group and migmatite protolith in the Funeral Mountains metamorphic core complex using U-Pb DZ geochronology: Geological Society of America Abstracts with Programs, v. 49, no. 6

Wright, L.A., and Troxel, B.W., 1993, Geologic Map of the central and northern Funeral Mountains and adjacent areas, Death Valley region, southern California: U.S. Geological Survey Misc. Inv. Series Map I-2305, scale 1:48000.

Wrucke, C.T., Stevens, C.H., and Wooden, J.L., 1995, The Butte Valley and Layton Well Thrusts of eastern California: Distribution and regional significance: Tectonics, v. 14, p. 1165-1171.

Yonkee, W.A., Dehler, C.D., Link, P.K., Balgord, E.A., Keeley, J.A., Hayes, D.S., Wells, M.L., Fanning, C.M., and Johnston, S.M., 2014, Tectono-stratigraphic framework of Neoproterozoic to Cambrian strata, west-central U.S.: Protracted rifting, glaciation, and evolution of the North American Cordilleran margin: Earth-Science Reviews, v. 136, pp. 59-95.

Yonkee, A.W., Weil, A.B., 2015, Tectonic evolution of the Sevier and Laramide belts within the North America Cordillera orogenic system: Earth-Science Reviews, v. 150, p.531-593.

CURRICULUM VITAE

Taylor D. Craig
craig@unlv.nevada.edu
Tcraig1992@gmail.com

Education

Anticipated Graduation: May 2019
University of Nevada – Las Vegas
M.S. in Geosciences
Funded by NSF grant
Advisor: Dr. Michael Wells, University of Nevada – Las Vegas

Graduation: December 2015
Appalachian State University, GPA: 3.35
B.S. in Geology
Undergraduate Thesis: Microstructural analysis of the Tallulah Falls Dome: Deformation conditions and kinematics associated with Alleghanian-aged dome formation
Funded by NSF grant
Advisor: Dr. Jamie Levine, Appalachian State University

Research Experience

Fall 2017-Present:
Field researcher
University of Nevada – Las Vegas
Independent study conducting structural and sedimentological mapping of the Bird Springs syncline, a syntectonic basin along the leading edge of the Sevier fold-thrust belt.
Advisor: Dr. Michael Wells, Geoscience Department, Las Vegas, NV

Fall 2016-Present:
Graduate Assistant
University of Nevada – Las Vegas
Detailed Structural mapping, thermochronology and geochronology of the Chloride Cliff region of the Funeral Mountains. Providing timing and geometric constraints on the evolution of the Funeral Mountains metamorphic core complex.
Advisor: Dr. Michael Wells, Geosciences Department, Las Vegas, NV

Spring 2014-Fall 2015:
Undergraduate Research Assistant
Appalachian State University
Performed detailed petrographic analysis of quartz deformation microstructures and kinematic fabrics to constrain deformation conditions associated with doming in the Southern Appalachians.
Advisor: Dr. Jamie Levine, Geology Department: Boone, NC

Teaching Experience

Fall 2016 and Fall 2017
Teaching Assistant, Structural Geology Lab
University of Nevada – Las Vegas
Advisor: Dr. Michael Wells, Geosciences Department: Las Vegas, NV
Responsible for the teaching and grading the undergraduate Structure Lab at UNLV.

Fall 2015
McKinney Geology Teaching Museum Tutor (Answerspherian)
Appalachian State University
Advisor: Dr. Andrew B. Heckert, Geology Department: Boone, NC, heckertab@appstate.edu
Tutored introductory geology students with lab and class work.

Spring 2015
Teaching Assistant, Introduction to Environmental Geology
Appalachian State University
Advisor: Lauren Waterworth, waterworthlh@appstate.edu
My responsibilities were to assist students with their labs and help them understand the material.

Honors and Rewards:

Spring 2018
UNLV Geosymposium Best Oral Presentation – 1st Place
Spring 2017
UNLV Geosymposium Best Graduate Poster – 2nd Place
Spring 2017
2017 GSA Student Research Grant – Partial funding
Fall 2014-Fall 2015
Undergraduate Research Assistant ($2000 per year)
Spring 2014-Fall 2015; Fall 2012; Fall 2011
Appalachian State Universities Dean's List (GPA requirements: 3.25 for 15 hours or more of coursework)

Professional Societies and Other Activities

Fall 2016-present
Association of American Petroleum Geologists – UNLV chapter
Fall 2013-present
Geologic Society of America Member
Fall 2014-Spring 2015
Appalachian Geological Society Secretary
Spring 2013-Fall 2015
Appalachian Geological Society Member

Publications

Casale, G., Levine, J.S.F., **Craig, T.D.,** Stewart, C., 2017, Timing and deformation conditions of the Tallulah Falls Dome, NE Georgia; Implications for the Alleghanian Orogeny: Geological Society of America Bulletin, v. 129, p. 1195 – 1208.

Abstracts and Conference Presentations

Craig, T.D., Wells, M.L., Craddock, S.D., Hoisch, T.D., Timing and Kinematics of Mesozoic Burial and contractional deformation in the Funeral Mountains metamorphic core complex, Death Valley National Park, CA: Geological Society of America Abstrasts with Programs, Vol. 50, No. 5.

Craig, T.D., Wells, M.L., Hoisch, T.D., 2017, Structural and kinematic history of the Chloride Cliff region: Implications for tectonic inheritance in the formation of the Funeral Mountains metamorphic core complex, Death Valley, CA: Geological Society of America Abstracts with Programs, Vol. 49, No. 7.

Levine, J.S.F., Casale, G., Rahl, J.M., **Craig, T.D.,** 2016, Alleghanian-aged high-temperature deformation conditions associated with formation of the Tallulah Falls Dome, Northeastern Georgia: Geological Society of America Abstracts with Programs, Vol. 48, No. 7.

Casale, G., Levine, J.S.F., **Craig, T.D.,** Stewart, C., 2016, Timing and deformation conditions of the Tallulah Falls Dome, NE Georgia; Implications for the Alleghanian orogeny, Vol. 48, No. 7.

Craig, T.D., Levine, J.S.F., Casale, G., Rahl, J.M., Stewart, C., 2015, Microstructural analysis of the Tallulah Falls Dome: Deformation conditions and kinematics associated with Alleghanian dome formation: Geological Society of America Abstracts with Programs, Vol 47, No.7.

Casale, G., Levine, J.S.F., **Craig, T.D.,** Stewart, C., Rahl, J.M., 2015, Timing and conditions of dome formation in the southern Appalachians; Implications for internal deformation of the Blue Ridge thrust sheet: Geological Society of America Abstracts with Programs, Vol 47, No.7.

Stewart, C., Casale, G., Levine, J.S.F., **Craig, T.D.,** 2015, Field based structural observation of dome geometry and kinematics, Tallulah Falls Dome, Georgia: Geological Society of America Abstracts with Programs, Vol 47, No.7.

Craig, T.D., Levine, J.S.F., Casale, G., Stewart, C., 2015, Microstructural and kinematic analysis of deformation conditions within the Tallulah Falls Dome: Geological Society of America Abstracts with Programs, Vol. 47, No.2, p.84.

Stewart, C., Casale, G., Levine, J.S.F., **Craig, T.D.,** 2015, Field based structural interpretation of the Tallulah Falls Dome in the southern Appalachians: Geological Society of America Abstracts with Programs, Vol 47, No.2, p.78.

Technical/Computational Skills

MATLAB, ArcMap, Adobe Illustrator, Adobe Photoshop
Petrographic Microscopes
Mineral Separation
LA-ICPMS

References

Dr. Michael Wells, Professor of Geosciences, University of Nevada – Las Vegas, michael.wells@unlv.edu, (702) 895-0828

Dr. Jamie Levine, Assistant Professor of Geology, Appalachian State University, levinejs@appstate.edu, (828) 262-2166

Dr. Gabriele Casale, Assistant Professor of Geology, Appalachian State University, casalegm@appstate.edu, (828) 262-2746